2020

Improved characterization of pure and formulated active pharmaceutical ingredients by fast magic angle spinning solid-state NMR spectroscopy

Anuradha Viraj Wijesekara
Iowa State University

Improved characterization of pure and formulated active pharmaceutical ingredients by fast magic angle spinning solid-state NMR spectroscopy

by

Anuradha V. Wijesekara

A thesis submitted to the graduate faculty

in partial fulfillment of the requirements for the degree of

MASTER OF SCIENCE

Major: Physical Chemistry

Program of Study Committee:
Aaron J. Rossini, Major Professor
Vincenzo Venditti
Robbyn K. Anand

The student author, whose presentation of the scholarship herein was approved by the program of study committee, is solely responsible for the content of this thesis. The Graduate College will ensure this thesis is globally accessible and will not permit alterations after a degree is conferred.

Iowa State University

Ames, Iowa

2020

DEDICATION

To my parents and teachers

TABLE OF CONTENTS

Page

NOMENCLATURE

API	Active Pharmaceutical Ingredient
SSNMR	Solid-State Nuclear Magnetic Resonance
MAS	Magic Angle Spinning
FS	Frequency Selective
HMQC	Heteronuclear Multiple Quantum Coherence
RESPDOR	Resonance Echo Saturation Pulse Double Resonance
SOFAST	Selective Optimized Flip-Angle Short Transient
SCXRD	Single Crystal X-ray Diffraction
PXRD	Powder X-ray Diffraction
IR	Infrared
ASD	Amorphous Solid Dispersions
DNP	Dynamic Nuclear Polarization
CSA	Chemical Shift Anisotropy
CP	Cross Polarization
HSQC	Heteronuclear Single Quantum Coherence
RDC	Residual Dipolar Coupling
HETCOR	Heteronuclear Correlation
CSP	Crystal Structure Predication
DFT	Density Function Theory
GIPAW	Gauge Including Projector Augmented Wave
EFG	Electric Field Gradient

LIST OF SYMBOLS

B_o	Static applied magnetic field
γ	Gyromagnetic ratio
I	Nuclear spin quantum number
ν_0	Larmor frequency
C_Q	Quadrupolar coupling constant

ACKNOWLEDGMENTS

First and foremost, I would like to thank Professor Aaron Rossini for allowing me to work in his research laboratory. I found Aaron very helpful and understanding and was very energetic in seeing improvement in the projects. Working with Aaron gave me great opportunities to attend many conferences and get to know especially people in the pharmaceutical industry which I assume would be very helpful to me in the long run of my career.

I would also like to thank my committee members; Professor Vincenzo Venditti and Professor Robbyn Anand and all the department faculty and staff for helping me in various ways during my stay at Iowa State University. I am especially grateful to all the members in the Rossini group for the help and advice given to me throughout the program. My special gratitude goes to Dr. David Hirsh who helped and guided me in my inaugural project. I also would like to thank Amrit Venkatesh for all the help and support given in my projects and for making a positive work atmosphere in the lab. Finally, I would like to thank Scott Carnahan for showing me how to pack samples into rotors to do NMR experiments.

I am also thankful to Dr. Ivan Hung at the National High Magnetic Field Laboratory at Tallahassee for helping to acquire high field NMR measurements for both the projects I was engaged in. I would also extend my gratitude to Joseph W. Lubach and Karthik Nagapudi of Genentech Inc. for the great collaboration and providing us the necessary pharmaceutical compounds.

Finally, I must thank my parents, all my family members and my colleagues for the immense support and love given to me. I would also like to say thank you to Eranga Gamage for all the good memories cherished at the Iowa State University.

ABSTRACT

This thesis describes improved methods for the characterization of pure and formulated solid active pharmaceutical ingredients (APIs) by solid-state nuclear magnetic resonance (SSNMR) spectroscopy. APIs can be prepared in many different solid forms and phases that affect their physicochemical properties and suitability for oral dosage forms. The development and commercialization of dosage forms require analytical techniques that can determine and quantify the API phase in the final drug product. ^{13}C solid-state NMR spectroscopy is widely employed to characterize pure and formulated solid APIs; however, ^{13}C SSNMR experiments on dosage forms with low API loadings are often challenging due to low sensitivity and interference from excipients. Here, fast magic angle spinning (MAS) ^{1}H SSNMR experiments are shown to be applicable for the rapid characterization of low drug load formulations. Diagnostic ^{1}H SSNMR spectra of APIs within tablets are obtained by using combinations of frequency-selective saturation and excitation pulses, 2D experiments, and ^{1}H spin diffusion periods. ^{1}H SSNMR provides a one to three orders of magnitude reduction in experiment time compared to standard ^{13}C SSNMR experiments, enabling diagnostic SSNMR spectra of dilute APIs within tablets to be obtained within a few minutes.

We introduce fast MAS $^{1}H\{^{14}N\}$ Frequency Selective (FS)-HMQC experiments, analogous to solution SOFAST HMQC experiments, which provides a factor 2-3 improvement in sensitivity which corresponds to a factor 4 to 9 reductions in experiment times compared to conventional HMQC SSNMR experiments. Using this method ^{1}H-^{14}N through bond and through space correlation spectra can be acquired in minutes on model compounds and a few hours from more challenging samples. The $^{1}H\{^{14}N\}$ FS RESPDOR experiments were then used to measure the N-H interatomic distances for two pharmaceutically important compounds. These

measurements were used to determine the protonation states of APIs and assign them as salts or cocrystals.

CHAPTER 1. GENERAL INTRODUCTION

This thesis describes the use of SSNMR spectroscopy to characterize pure and formulated APIs. In chapter 2, pure APIs and commercial dosage forms are characterized using fast MAS ^{1}H SSNMR. Fast MAS improves the resolution of the ^{1}H SSNMR spectra, enabling the direct detection of ^{1}H NMR signals from the API signals within commercial tablets. It is shown how fast MAS ^{1}H SSNMR confirms the presence of the desired form of the API in the dosage form. A thorough comparison between the advantages of using fast MAS ^{1}H SSNMR over ^{13}C SSNMR is presented under this chapter. Furthermore, it was possible to detect dilute polymorphic of APIs within model formulations using ^{1}H SSNMR.

In chapter 3, ^{1}H{^{14}N} FS HMQC and FS RESPDOR experiments are used to characterize multicomponent APIs. Here, modified pulse sequences are used for frequency selective dipolar HMQC (FS D-HMQC) experiments which can be acquired in a few minutes. It is also shown here that the FS HMQC experiments can be performed on other nuclei such as ^{17}O and ^{35}Cl, which are often found in pharmaceutical compounds. Furthermore, FS RESPDOR experiments are used to determine the NH bond lengths of two APIs and distinguish them as salt and cocrystal.

Introduction to solid APIs

A significant portion of all APIs is small organic molecules which are typically formulated as solid drugs. Solid APIs may exist in many different physical forms.[1] These different physical forms include salts, polymorphs, hydrates, solvates, amorphous forms, and cocrystals. A detailed schematic of the most common polymorphic forms of APIs is shown in Figure 1.

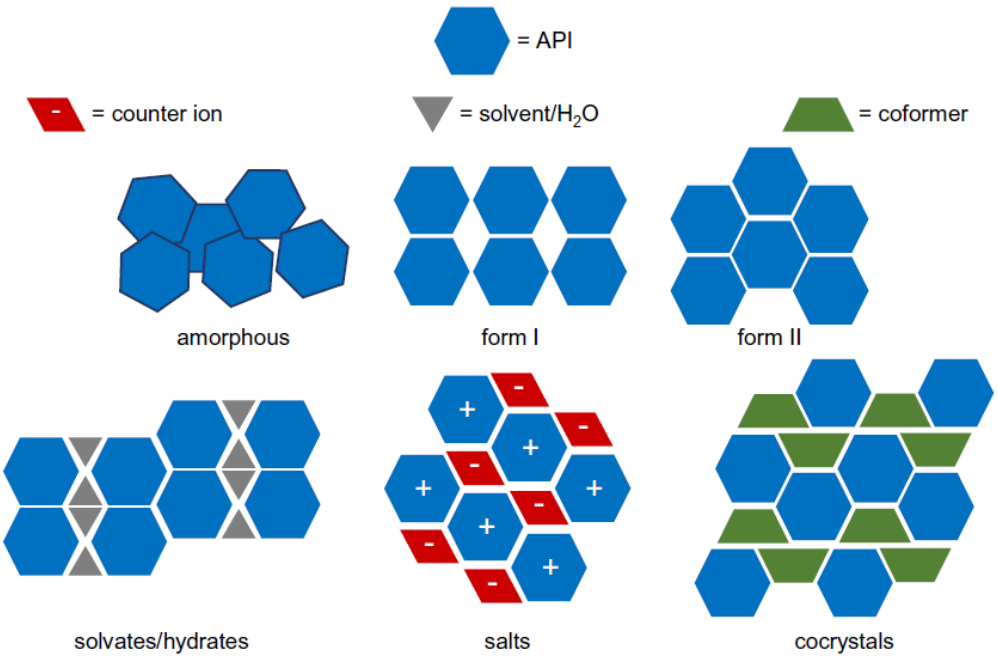

Figure 1. Different possible solid-state forms of APIs reproduced from *Adv. Drug Deliv. Rev.* **2017**,117, 86–110

Unique solid forms are synthesized by changing crystallization/precipitation conditions (solvents, anti-solvents, temperature, heating, grinding, cooling, etc.) and/or reacting the APIs with acids, bases or other coformers. Different polymorphic forms of APIs have unique arrangements of their three-dimensional molecular structure within the crystallographic lattice.[2] The different placement of the molecules within a lattice alters the intermolecular interactions and strongly impacts the physical properties such as stability, melting point, solubility and bioavailability. For these reasons solid-state chemists and formulation scientists extensively search for methods to crystalize or precipitate different solid forms of APIs with suitable physicochemical properties required in dosage forms.[3] The objective is to find a solid form of an API that will be stable over long time periods and offers the required water solubility and bioavailability. Note that unique solid API forms are also patentable, hence, intellectual property considerations also drive the discovery and characterization of solid APIs.

Polymorph screening

Salts and cocrystals are found to be the very commonly analyzed polymorphs.[4] Therefore, they need to be discovered before performing any characterization or detailed analysis. For the early discovery of new solid forms of the APIs, a validated screening process of salts/cocrystals must be implemented. The main goal of the screening strategy is to find salts/cocrystals or other polymorphs with desirable physical and chemical properties such as solubility, crystallinity, hygroscopicity, and bioavailability before issuing the patents for the new forms.[5]

Solid forms of APIs

Currently, salt formation is one of the main methods of modifying APIs to enhance physical properties. Approximately half of commercial medicines found in the market are administered as salts and one-third of the APIs that are used in tablet formulation are found to be in the solid form.[6–8] Salt formation involves acid-base chemistry where there is a complete proton transfer from the acid to the API. Salt formation often improves the solubility and bioavailability of API molecules and by using different acids the physical properties such as the melting point, stability, release kinetics, and hygroscopicity can be altered. This approach has been routinely used when a drug candidate shows low solubility and release rates.[9] Crystalline salts can also exist in multiple forms such as anhydrous, hydrated and solvate forms.[10] However, a major drawback of salts is that the API molecules must possess acid or basic ionizable groups to favor the proton transfer. Cocrystal formation is an alternative method to improve the pharmacokinetic properties of APIs.[11] In this process of co-crystallization hydrogen bonding motifs are involved instead of proton transfer between the free base and the counterions. In cocrystals, the interaction between the API and the counterion is freely reversible and covalent. In literature, there are multiple definitions for a cocrystal. A general definition for a cocrystal as

mentioned in literature can be quoted as, “an API, neutral or ionic form or a zwitterion, along with a neutral coformer, held together through noncovalent, freely reversible interactions”.[1] The complete proton transfer between GDC-0022, which is an API developed at Genetech Inc. and Tosylic acid to form a salt is shown in Figure 2A below. The formation of hydrogen bonding between GDC-0022 and Fumaric acid to form a cocrystal is shown in Figure 2B.

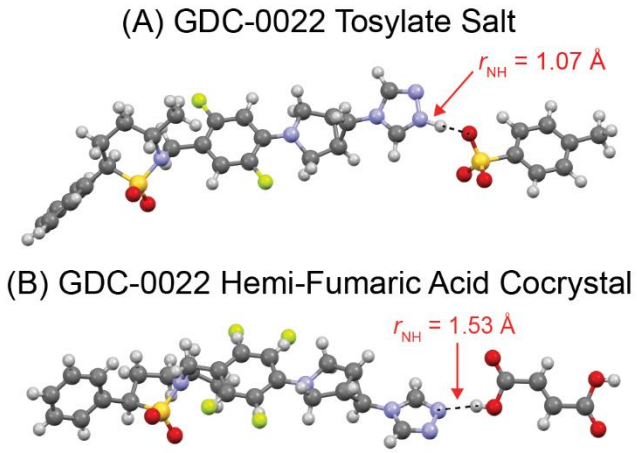

Figure 2. Crystal structures of (A) GDC-0022 Tosylate salt and (B) GDC-0022 Hemi-Fumaric acid cocrystal.

Generally, acid coformers have a range of acid dissociation constants (pK_a) which may be used to predict cocrystal or salt formation. The counterion is selected based upon the pK_a rule which takes into account the degree of ionization of the acidic or the basic functional groups in the drugs.[12] When the difference in the pK_a of the API and the coformer (ΔpK_a) is greater than 2-3, a proton transfer between the API molecule and acid coformer takes place to form a salt. If the ΔpK_a is lesser than 2, a cocrystal should almost always form. However, when the $0 \leq \Delta pK_a \leq 3$ the prediction of salt/cocrystal formation is ambiguous and either a cocrystal or a motif with intermediate proton transfer could form. Therefore, ΔpK_a alone is not an accurate way to predict the formation of a salt or a cocrystal.[13,14]

A significant proportion of the APIs used in formulations is small organic molecules. These molecules can be crystallized in different forms to produce another important class of multicomponent APIs known as polymorphs.[15] Polymorphism could be defined as the ability of a compound to exist in two or more crystalline forms in which the molecule has different packing or conformational arrangements.[16] Polymorphs of a given API have unique crystal structures with different special atomic arrangements. A given polymorphic form of an API shows different physical and chemical properties due to the differences in the crystal structure. Sulfathiazole and theophylline are classic examples of molecules exhibiting polymorphism.[17,18] Different polymorphs of a compound are typically obtained by varying crystallization conditions and/or by heating solid phases. For all these reasons, it is crucial to identify all the possible solid forms of an API to identify the phase most suitable for the commercial formulation. As described below, SSNMR spectroscopy is a commonly applied tool to identify, quantify, and characterize the structure of different solid API forms.

Once the formulation scientists have identified the most suitable solid form of an API (salt, cocrystal or polymorph) that will be used in a formulation it is crucial to ensure that the desired solid form of the API remains in the final drug product. Different API forms can form because the API may be subjected to elevated temperatures, pressures and come in contact with different solvents during the manufacturing process, all of which could induce a phase transformation to a new polymorph, or result in dissociation of the API from the acids used to make salts or cocrystals.[19]

Characterization of solid APIs

Accurate characterization of solid forms of APIs such as salts, cocrystals, and polymorphs is a critical part of the drug development process. Specifically, characterization techniques are required to determine the molecular structures of solid APIs, detect API-excipient

interactions, quantify API loads, and identify the existence of other solid forms of the API. If large single crystals (edge lengths > 100 μm) are available, then single-crystal x-ray diffraction (SCXRD) is the preferred technique for determination of the molecular structure of solid APIs.[20] However, widespread use of SCXRD is hindered by the difficulty of producing diffraction quality crystals. Powder X-ray diffraction (PXRD) is often used to "fingerprint" different solid forms of APIs, however, determining the molecular structure from PXRD is very challenging. However, both of these diffraction techniques do not assist in locating the atomic positions responsible for hydrogen bonding.[21] They are also generally inapplicable to formulated APIs since the excipients often make up the bulk of a tablet and will interfere or obscure diffraction peaks from the API. Infrared (IR) spectroscopy is widely applied to probe covalent and hydrogen bonding in APIs.[22] However, the resolution of IR spectra is often insufficient and there is not enough information available from this technique to determine a molecular structure. SSNMR is an important analytical tool that is extensively used to characterize pharmaceutical compounds, which will be discussed in the next section.

Application of SSNMR to drug formulations

The primary use of SSNMR spectroscopy in the pharmaceutical field is to fingerprint and quantify solid drug substances. SSNMR spectroscopy can answer various important questions related to pharmaceutical compounds such as is the material crystalline or amorphous? What crystalline form (polymorph) is present? How many different solid forms are present in a mixture? Questions related to mobility and dynamics can also be addressed with the help of SSNMR.[23] SSNMR spectroscopy is a non-destructive method and non-invasive technique that is both quantitative and selective. SSNMR spectroscopy is quantitative because the NMR signal is proportional to the number of nuclei present in the sample. Therefore, quantification of different

crystalline forms such as polymorphs, solvates, and also mixtures of crystalline and amorphous components can be performed.[24] Furthermore, the ability to selectively label compounds with favorable nuclei is useful for looking at drug excipient interactions and changes taking place in a formulation.

Polymorph identification and amorphous form characterization

SSNMR is recognized for its capability to identify different crystalline forms of drug molecules. ^{1}H, ^{13}C, ^{15}N and ^{17}O isotropic chemical shifts are very sensitive to even slight structural differences that occur in different solid forms. Therefore, different solid forms of formulations and commercial drug products will have different SSNMR spectra.[25,26] Two-dimensional SSNMR has been routinely used to characterize amorphous pharmaceuticals such as ASDs. These experiments give important information related to the interaction between the APIs and polymer molecules that are used for the stabilization of the ASDs.[27]

Quantification of drug loads

Several examples have been reported in literature where SSNMR is used to quantify the drug load of an API. Recent studies have used ^{1}H, ^{13}C and ^{19}F SSNMR to quantify both crystalline and amorphous forms of API in bulk and dosage forms.[28–30] In addition, studies have shown that APIs at levels low as 1 % w/w can be detected using NMR.[31] Also, SSNMR is used to quantify important phenomena such as the disproportionation of APIs in commercial tablets.[32]

Dynamics

SSNMR has been extensively used to look at the dynamics of amorphous materials and lyophilized systems. Generally, the relaxation times of different species in the APIs are used to understand the mobility and phase separations taking place within the system.[33]

Information from SSNMR spectra and SSNMR techniques

An important piece of information from NMR spectra is the isotropic chemical shift. The isotropic chemical shift depends on the surrounding electronic environment. The chemical shift is a very sensitive parameter to conformational electronic changes at various sights of a molecule, which is useful to identify different forms of molecules depending on the type of interactions and bonding patterns. The NMR linewidths also provide valuable information about the nature of the system analyzed. Generally, the NMR linewidths of amorphous materials are order magnitude broader than those of crystalline materials due to the distribution of chemical shifts. The line widths and line shapes of crystalline materials can provide information about the morphology.[34] Relaxation time is also another important parameter that reports on correlations between various parameters such as dynamics and temperature dependence.[35] Also, relaxation times have been exploited to predict the particle size distributions and other properties such as chemical stability and dissolution rates.[36] Multi-dimensional NMR experiments on pharmaceutical drug molecules are useful to identify the connectivity between the APIs and excipients as well as the assignment of peaks which helps determination of miscibility in multicomponent APIs such amorphous solid dispersions.[37]

SSNMR and X-ray crystallography are two techniques of choice for the characterization of structural properties of commercial synthetic drugs or novel supramolecular complexes. The implementation of SSNMR techniques on pharmaceutical compounds relies not only on the pulse sequence schemes but also on technological developments in probes, high field magnets, and high-power sources. Sensitivity is often a critical factor when analyzing pharmaceutical compounds with dilute APIs. Each nucleus has its own advantages and disadvantages regarding the sensitivity of the NMR experiment. Various techniques such as selective isotropic

enrichment and dynamic nuclear polarization (DNP)[38,39] are used to improve the sensitivity of the NMR experiment and to widen the applications of SSNMR on pharmaceutical compounds.

Magic angle spinning

In solution NMR the linewidths are typically narrow because the molecules isotopically tumble in the liquid medium. However, for most of the compounds in the solid-state, there is no such tumbling or negligible mobility of the molecules. Therefore in the solid-state basically two main interactions that are averaged out in solution NMR are present. They are the dipole-dipole couplings and chemical shift anisotropy (CSA).[40] Also, other factors that contribute to broad NMR signals are structural disorder and strong homonuclear dipolar interactions. Magic angle spinning (MAS) is a technique that is commonly used in the field of SSNMR nowadays.[41–43] MAS averages anisotropic interactions that broaden the NMR spectra of powdered samples. By far, fast MAS has been the primary and most efficient resolution enhancement technique in SSNMR.

The magic angle is tilted from the axis of the principal magnetic field B_o by 54.73°, which corresponds to the orientation of the body diagonal of a cube. Mechanical rotation of the powdered samples around this axis at a frequency exceeding the magnitude of the interactions (in kHz), averages out the anisotropic interactions that have a dependence of the $(3\cos^2\theta - 1)/2$ term, that is the second-order Legendre polynomial which gives the dependency towards the orientation θ with respect to the applied external magnetic field B_o. A schematic of the orientation of the sample at the magic angle with respect to B_o is given in figure 3. Figure 3 also contains the 400 MHz (B_0 = 9.4 T) Bruker Avance III HD spectrometer equipped with broadband double resonance HX 1.3 mm fast MAS and 4 mm HX probes.

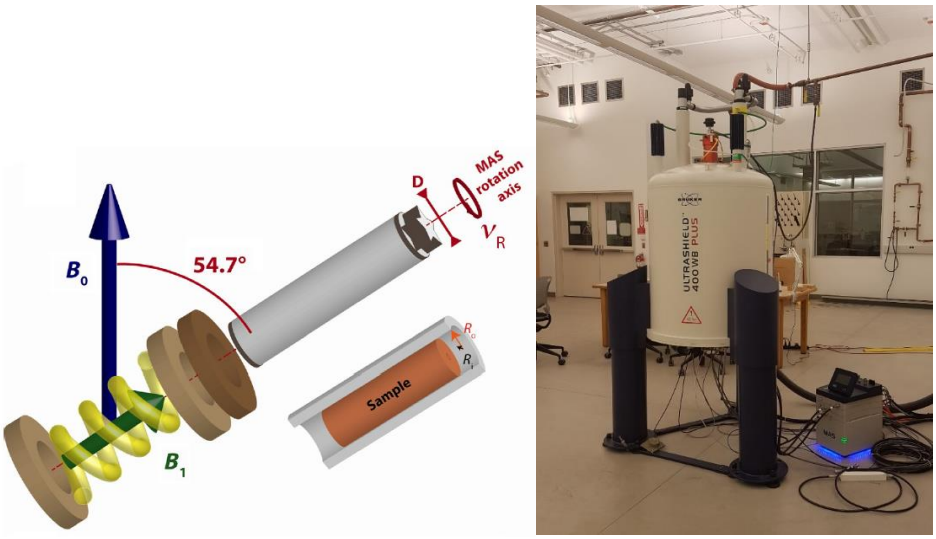

Figure 3. Schematic of the magic angle (left) reproduced from *Annu. Reports NMR Spectrosc.* **2014**, *81*, 109–144 and 400 MHz (B_0 = 9.4 T) magnet (right)

Solid-state NMR distance measurements

The development of NMR methods for accurately measuring bond distances between nuclei pairs is a significant application of SSNMR in the structural analysis of pharmaceutical compounds. The RESPDOR[44] technique is one of the common ways of measuring distances between a spin ½ nucleus such as ^{1}H or ^{13}C and a quadrupolar nucleus such as ^{14}N.[45] One of the main applications of the NMR experiments used to determine the bond lengths is the determination of the protonation state of an API and discrimination of different polymorphic forms.

High resolution ^{1}H NMR experiments

Due to the high natural abundance (~100 %), high sensitivity due to high γ and its ubiquitous nature in many organic solids, ^{1}H NMR plays a crucial role in structural analysis of small pharmaceutical compounds. Due to the rapid isotropic tumbling of molecules in the liquid state, very narrow ^{1}H NMR line widths are observed. However, in the solid-state, as a result of the strong homonuclear dipolar couplings on the order of 10 – 40 kHz, broad ^{1}H SSNMR spectra

(around tens of kHz) are observed.[46] Therefore, in most cases ^{1}H SSNMR gives rise to featureless spectra, making the peak assignments hard. For ^{1}H MAS NMR experiments the proton line width is usually inversely proportional to the sample spinning frequency. Moderate spinning frequencies (below 10 kHz) are insufficient to average out strong dipolar couplings, resulting in poor resolution and limited structural information.[47] Introduction of faster MAS rates (up to 50 kHz) has been extensively used to obtain well-resolved ^{1}H NMR spectra of solid compounds. However, recent advancements in the probes, high field magnets, and manufacture of smaller diameter rotors (0.7 mm) have enabled the use of ultra-fast MAS frequencies (up to 110 kHz) and have opened up a wider range of applications for ^{1}H SSNMR in comparison to other analytical or diffraction-based techniques.[48,49]

^{13}C SSNMR experiments

The ^{13}C isotope is a dilute spin with a natural abundance of ~1.1% and a moderate γ (*ca.* 1/4 of ^{1}H). Consequently, the relative NMR receptivity of the ^{13}C nucleus is *ca.* 6000 times lower than that of ^{1}H. In the recent developments of pharmaceutical research, one of the most common experiments is the ^{13}C cross-polarization CP/MAS.[50] Although, this makes ^{13}C SSNMR experiments time consuming, one advantage of using ^{13}C over ^{1}H is that the strong homonuclear dipolar couplings that broaden in the NMR spectra will be absent, which makes the peak assignments easier due to the higher resolution. The sensitivity of a ^{13}C NMR experiment is usually improved by polarization transfer from the ^{1}H spins during the CP step. This phenomenon involves the application of two RF fields to both the nuclei to fulfill the Hartmann-Hahn condition during the contact time.[51] Sample rotation at moderate MAS frequencies (~10 kHz) averages out the chemical shift anisotropy, providing SSNMR spectra with resolution comparable to solution ^{13}C NMR spectra. To remove heteronuclear dipolar interactions with

protons, high power heteronuclear decoupling with a ^{1}H RF field above 80 kHz is applied during acquisition.[52]

^{14}N SSNMR experiments

Due to the ubiquity of nitrogen in organic solids, nitrogen NMR is widely applied for the characterization of pharmaceuticals and other organic molecules. The two NMR active nuclei of nitrogen are ^{15}N and ^{14}N where ^{15}N (I = ½) has a natural isotopic abundance of ~0.37% while ^{14}N (I = 1) is ~99% abundant. ^{14}N has a lower gyromagnetic ratio and it being a spin-1 quadrupolar nucleus, is very sensitive to the electric field gradients (EFG), which is determined by the symmetry at the nuclear site, through the quadrupolar interaction.[53] The quadrupolar nature of ^{14}N makes the acquisition and analysis of ^{14}N NMR spectra difficult. ^{14}N SSNMR spectra are broadened by the first order quadrupolar interaction, often resulting in spectra that have breadths on the order of several MHz. However, indirect detection of ^{14}N can be achieved using experiments such as heteronuclear multiple quantum coherence (HMQC) or heteronuclear single quantum coherence (HSQC) where the coherence transfer from neighboring ^{1}H or ^{13}C to ^{14}N is achieved thorough J or residual dipolar coupling (RDCs).[54–57] These sequences offer improved sensitivity and resolution as compared to the direct detection of ^{14}N SSNMR signals.

SSNMR experiments on APIs with other NMR active nuclei

^{19}F is also a very suitable nucleus to do SSNMR experiments on because it is 100 % naturally abundant and has large γ providing receptivity only lower to that of ^{1}H. Another advantage of using ^{19}F NMR to look at pharmaceutical drug molecules is that the most common excipients do not contain any fluorine atoms. Therefore, ^{19}F SSNMR experiments can be used to obtain characteristic fingerprint spectra of the APIs within dosage forms. In the literature ^{13}C-^{19}F and ^{1}H-^{19}F heteronuclear correlation (HETCOR) SSNMR experiments have been shown to be

very useful to identify API forms and probe interactions between amorphous APIs and polymers in tablets.[58–60]

^{35}Cl SSNMR is also a good probe of the chloride anion environments in APIs that exist as HCl salts. ^{35}Cl SSNMR has been extensively used to distinguish polymorphs.[61] In the literature studies have shown that ^{35}Cl SSNMR experiments can be helpful for the structural characterization of HCl salts of APIs.[62] ^{17}O SSNMR is also another nucleus that has gained close attention currently in the fields of pharmaceuticals. Recent studies have shown that O-H bond distances can be probed on ^{17}O labeled APIs.[63]

DFT-based crystal structure prediction

Theoretical methods are nowadays commonly used to predict the crystal structures, physical properties and SSNMR spectra of solid APIs. Computational crystal structure prediction (CSP) is used to predict all the possible solid structures of APIs. Recent studies have shown how SSNMR can be combined with plane-wave density functional theory (DFT) calculations to validate the crystal structures of potential pharmaceutical compounds and differentiate polymorphs based on the chemical shift.[64,65] These DFT calculations are generally supported by gauge including projected augmented wave (GIPAW) approach to get a clear comparison between the experimental and theoretical chemical shift values and has enabled the rapid development of chemical shift-based NMR crystallography. Plane-wave DFT GIPAW calculations can accurately predict the slight differences in chemical shifts that occur between different API forms. However, the computational cost when analyzing larger crystal structures is one downside in this approach. To overcome this issue, the development of machine learning models has emerged as an efficient method for crystal structure validation and predicting the accurate crystal structures of pharmaceutically important compounds.[66]

References

(1) Schultheiss, N.; Newman, A. Pharmaceutical Cocrystals and Their Physicochemical Properties. *Cryst. Growth Des* **2009**, *9* (6), 2950–2967.

(2) Cerreia Vioglio, P.; Chierotti, M. R.; Gobetto, R. Pharmaceutical Aspects of Salt and Cocrystal Forms of APIs and Characterization Challenges. *Advanced Drug Delivery Reviews*. **2017**, pp 86–110.

(3) Huang, L. F.; Tong, W. Q. Impact of Solid State Properties on Developability Assessment of Drug Candidates. *Adv. Drug Deliv. Rev.* **2004**, *56* (3), 321–334.

(4) Morissette, S. L.; Almarsson, Ö.; Peterson, M. L.; Remenar, J. F.; Read, M. J.; Lemmo, A. V.; Ellis, S.; Cima, M. J.; Gardner, C. R. High-Throughput Crystallization: Polymorphs, Salts, Co-Crystals and Solvates of Pharmaceutical Solids. *Adv. Drug Deliv. Rev.* **2004**, *56* (3), 275–300.

(5) Capes, J. S.; Cameron, R. E. Contact Line Crystallization To Obtain Metastable Polymorphs. *Cryst. Growth Des.* **2007**, *7* (1), 108–112.

(6) Skořepová, E.; Bím, D.; Hušák, M.; Klimeš, J.; Chatziadi, A.; Ridvan, L.; Boleslavská, T.; Beránek, J.; Šebek, P.; Rulíšek, L. Increase in Solubility of Poorly-Ionizable Pharmaceuticals by Salt Formation: A Case of Agomelatine Sulfonates. *Cryst. Growth Des.* **2017**, *17* (10), 5283–5294.

(7) Paulekuhn, G. S.; Dressman, J. B.; Saal, C. Trends in Active Pharmaceutical Ingredient Salt Selection Based on Analysis of the Orange Book Database. *J. Med. Chem.* **2007**, *50* (26), 6665–6672.

(8) He, Y.; Orton, E.; Yang, D. The Selection of a Pharmaceutical Salt-The Effect of the Acidity of the Counterion on Its Solubility and Potential Biopharmaceutical Performance. *Pharmaceutics* **2018**, *107* (1), 419–425.

(9) Gupta, D.; Bhatia, D.; Dave, V.; Sutariya, V.; Gupta, S. V. Salts of Therapeutic Agents: Chemical, Physicochemical, and Biological Considerations. *Molecules*. **2018**, pp 1719–1734.

(10) Petrova, R. I.; Peresypkin, A.; Mortko, C. J.; Mckeown, A. E.; Lee, J.; Williams, J. M. Rapid Conversion of API Hydrates to Anhydrous Forms in Aqueous Media. *J. Pharm. Sci.* **2009**, *98* (11), 4111–4118.

(11) Karimi-Jafari, M.; Padrela, L.; Walker, G. M.; Croker, D. M. Creating Cocrystals: A Review of Pharmaceutical Cocrystal Preparation Routes and Applications. *Crystal Growth and Design*. **2018**, pp 6370–6387.

(12) Childs, S. L.; Stahly, G. P.; Park, A. The Salt-Cocrystal Continuum: The Influence of Crystal Structure on Ionization State. *Mol. Pharm.* **2007**, *4* (3), 323–338.

(13) Bhogala, B. R.; Basavoju, S.; Nangia, A. Tape and Layer Structures in Cocrystals of Some Di-and Tricarboxylic Acids with 4,49-Bipyridines and Isonicotinamide. From Binary to Ternary Cocrystals. *CrystEngComm* **2005**, *7*, 551–562.

(14) Vishweshwar, P.; McMahon, J. A.; Bis, J. A.; Zaworotko, M. J. Pharmaceutical Co-Crystals. *J. Pharm. Sci.* **2006**, *95* (3), 499–516.

(15) Lu, J.; Rohani, S. Polymorphism and Crystallization of Active Pharmaceutical Ingredients (APIs). *Curr. Med. Chem.* **2009**, *16* (7), 884–905.

(16) Datta, S.; Grant, D. J. W. Crystal Structures of Drugs: Advances in Determination, Prediction and Engineering. *Nature Reviews Drug Discovery*. **2004**, pp 42–57.

(17) Anwar, J.; Tarling, S. E.; Barnes, P. Polymorphism of Sulfathiazole. *J. Pharm. Sci.* **1989**, *78* (4), 337–342.

(18) Seton, L.; Khamar, D.; Bradshaw, I. J.; Hutcheon, G. A. Solid State Forms of Theophylline: Presenting a New Anhydrous Polymorph. *Cryst. Growth Des* **2010**, *10*, 3879–3886.

(19) Baumann, M.; Baxendale, I. R. The Synthesis of Active Pharmaceutical Ingredients (APIs) Using Continuous Flow Chemistry. *Beilstein J. Org. Chem.* **2015**, *11*, 1194–1219.

(20) Aitipamula, S.; Vangala, V. R. X-Ray Crystallography and Its Role in Understanding the Physicochemical Properties of Pharmaceutical Cocrystals. In *Journal of the Indian Institute of Science*; **2017**; Vol. 97, pp 227–243.

(21) Guzmán-Afonso, C.; Hong, Y.-L.; Colaux, H.; Iijima, H.; Yonekura, K.; Nishiyama, Y. Understanding Hydrogen-Bonding Structures of Molecular Crystals via Electron and NMR Nanocrystallography. *Nat. Commun.* **2019**, *10*, 3537.

(22) Bhavana, V.; Chavan, R. B.; Mannava, M. K. C.; Nangia, A.; Shastri, N. R. Quantification of Niclosamide Polymorphic Forms – A Comparative Study by Raman, NIR and MIR Using Chemometric Techniques. *Talanta* **2019**, *199*, 679–688.

(23) Wenslow, R. M. ^{19}F Solid-State NMR Spectroscopic Investigation of Crystalline and Amorphous Forms of a Selective Muscarinic M 3 Receptor Antagonist, in Both Bulk and Pharmaceutical Dosage Form Samples. *Drug Dev. Ind. Pharm.* **2002**, *28* (5), 555–561.

(24) Holzgrabe, U. Quantitative NMR Spectroscopy in Pharmaceutical Applications. *Progress in Nuclear Magnetic Resonance Spectroscopy*. **2010**, pp 229–240.

(25) Griffin, J. M.; Martin, D. R.; Brown, S. P. Distinguishing Anhydrous and Hydrous Forms of an Active Pharmaceutical Ingredient in a Tablet Formulation Using Solid-State NMR Spectroscopy. *Angew. Chemie - Int. Ed.* **2007**, *46* (42), 8036–8038.

(26) Hirsh, D. A.; Wijesekara, A. V.; Carnahan, S. L.; Hung, I.; Lubach, J. W.; Nagapudi, K.; Rossini, A. J. Rapid Characterization of Formulated Pharmaceuticals Using Fast MAS ^{1}H Solid-State NMR Spectroscopy. *Mol. Pharm.* **2019**, *16* (7), 3121–3132.

(27) Newman, A.; Knipp, G.; Zografi, G. Assessing the Performance of Amorphous Solid Dispersions. *Journal of Pharmaceutical Sciences*. **2012**, pp 1355–1377.

(28) Zielińska-pisklak, M.; Pisklak, D. M.; Wawer, I. Application of ^{13}C CPMAS NMR for Qualitative and Quantitative Characterization of Carvedilol and Its Commercial Formulations. *J. Pharm. Sci.* **2012**, *101* (5), 1763–1772.

(29) Tinmanee, R.; Larsen, S. C.; Morris, K. R.; Kirsch, L. E. Quantification of Gabapentin Polymorphs in Gabapentin/Excipient Mixtures Using Solid State ^{13}C NMR Spectroscopy and X-Ray Powder Diffraction. *J. Pharm. Biomed. Anal.* **2017**, *146*, 29–36.

(30) Brus, J.; Urbanova, M.; Sedenkova, I.; Brusova, H. New Perspectives of ^{19}F MAS NMR in the Characterization of Amorphous Forms of Atorvastatin in Dosage Formulations. *Int. J. Pharm.* **2011**, *409* (1–2), 62–74.

(31) Maruyoshi, K.; Iuga, D.; Watts, A. E.; Hughes, C. E.; Harris, K. D. M.; Brown, S. P. Assessing the Detection Limit of a Minority Solid-State Form of a Pharmaceutical by ^{1}H Double-Quantum Magic-Angle Spinning Nuclear Magnetic Resonance Spectroscopy. *J. Pharm. Sci.* **2017**, *106* (11), 3372–3377.

(32) Hirsh, D. A.; Su, Y.; Nie, H.; Xu, W.; Stueber, D.; Variankaval, N.; Schurko, R. W. Quantifying Disproportionation in Pharmaceutical Formulations with ^{35}Cl Solid-State NMR. **2018**, *15*, 4038–4048.

(33) Schanda, P.; Ernst, M. Studying Dynamics by Magic-Angle Spinning Solid-State NMR Spectroscopy: Principles and Applications to Biomolecules. *Progress in Nuclear Magnetic Resonance Spectroscopy*. **2016**, pp 1–46.

(34) Paudel, A.; Geppi, M.; Van Den Mooter, G. Structural and Dynamic Properties of Amorphous Solid Dispersions: The Role of Solid-State Nuclear Magnetic Resonance Spectroscopy and Relaxometry. *Journal of Pharmaceutical Sciences*. **2014**, pp 2635–2662.

(35) Sanchez, S.; Ziarelli, F.; Viel, S.; Delaurent, C.; Caldarelli, S. Improved Solid-State NMR Quantifications of Active Principles in Pharmaceutical Formulations. *J. Pharm. Biomed. Anal.* **2008**, *47* (4–5), 683–687.

(36) Rossini, A. J.; Zagdoun, A.; Hegner, F.; Der, M. S.; Gajan, D.; Lesage, A.; Emsley, L. Dynamic Nuclear Polarization NMR Spectroscopy of Microcrystalline Solids. *J. Am. Chem. Soc* **2012**, *134*, 16899–16908.

(37) Brown, S. P. Probing Proton-Proton Proximities in the Solid State. *Prog. Nucl. Magn. Reson. Spectrosc.* **2007**, *50* (4), 199–251.

(38) Zhao, L.; Pinon, A. C.; Emsley, L.; Rossini, A. J. DNP-Enhanced Solid-State NMR Spectroscopy of Active Pharmaceutical Ingredients. *Magn. Reson. Chem.* **2018**, *56* (7), 1–27.

(39) Rossini, A. J. Materials Characterization by Dynamic Nuclear Polarization-Enhanced Solid-State NMR Spectroscopy. *J. Phys. Chem. Lett* **2018**, *9*, 5150–5159.

(40) Liang, L.; Hou, G.; Bao, X. Measurement of Proton Chemical Shift Anisotropy in Solid-State NMR Spectroscopy. *Solid State Nuclear Magnetic Resonance*. September **2018**, pp 16–28.

(41) Polenova, T.; Gupta, R.; Goldbourt, A. Magic Angle Spinning NMR Spectroscopy: A Versatile Technique for Structural and Dynamic Analysis of Solid-Phase Systems. *Anal. Chem* **2015**, *87*, 2020.

(42) Samoson, A.; Tuherm, T.; Gan, Z. High-Field High-Speed MAS Resolution Enhancement in ^{1}H NMR Spectroscopy of Solids. *Solid State Nucl. Magn. Reson.* **2001**, *20* (3–4), 130–136.

(43) Andrew, E. R. Magic Angle Spinning. *Int. Rev. Phys. Chem.* **1981**, *1* (2), 195–224.

(44) Chen, L.; Wang, Q.; Hu, B.; Lafon, O.; Trébosc, J.; Deng, F.; Amoureux, J. P. Measurement of Hetero-Nuclear Distances Using a Symmetry-Based Pulse Sequence in Solid-State NMR. *Phys. Chem. Chem. Phys.* **2010**, *12* (32), 9395–9405.

(45) Pope, G. M.; Hung, I.; Gan, Z.; Mobarak, H.; Widmalm, G.; Harper, J. K. Exploiting ^{13}C/^{14}N Solid-State NMR Distance Measurements to Assign Dihedral Angles and Locate Neighboring Molecules. *Chem. Commun.* **2018**, *54* (49), 6376–6379.

(46) Brown, S. P. Applications of High-Resolution ^{1}H Solid-State NMR. *Solid State Nuclear Magnetic Resonance*. **2012**, pp 1–27.

(47) Sternberg, U.; Witter, R.; Kuprov, I.; Lamley, J. M.; Oss, A.; Lewandowski, J. R.; Samoson, A. ^{1}H Line Width Dependence on MAS Speed in Solid State NMR – Comparison of Experiment and Simulation. *J. Magn. Reson.* **2018**, *291*, 32–39.

(48) Yazawa, K.; Suzuki, F.; Nishiyama, Y.; Ohata, T.; Aoki, A.; Nishimura, K.; Kaji, H.; Shimizu, T.; Asakura, T. Determination of Accurate 1H Positions of an Alanine Tripeptide with Anti-Parallel and Parallel β-Sheet Structures by High Resolution ^{1}H Solid State NMR and GIPAW Chemical Shift Calculation. *Chem. Commun.* **2012**, *48* (91), 11199–11201.

(49) Zhang, R.; Mroue, K. H.; Ramamoorthy, A. Proton-Based Ultrafast Magic Angle Spinning Solid-State NMR Spectroscopy. *Acc. Chem. Res.* **2017**, *50* (4), 1105–1113.

(50) Pisklak, D. M.; Zielińska-Pisklak, M. A.; Szeleszczuk, Ł.; Wawer, I. ^{13}C Solid-State NMR Analysis of the Most Common Pharmaceutical Excipients Used in Solid Drug Formulations, Part I: Chemical Shifts Assignment. *J. Pharm. Biomed. Anal.* **2016**, *122*, 81–89.

(51) Hartmann, S. R.; Hahn, E. L. Nuclear Double Resonance in the Rotating Frame. *Phys. Rev.* **1962**, *128* (5), 2042–2053.

(52) Fung, B. M.; Khitrin, A. K.; Ermolaev, K. An Improved Broadband Decoupling Sequence for Liquid Crystals and Solids. *J. Magn. Reson.* **2000**, *142* (1), 97–101.

(53) Dib, E.; Mineva, T.; Alonso, B. Recent Advances in ^{14}N Solid-State NMR. In *Annual Reports on NMR Spectroscopy*; **2016**; Vol. 87, pp 175–235.

(54) Tatton, A. S.; Pham, T. N.; Vogt, F. G.; Iuga, D.; Edwards, A. J.; Brown, S. P. Probing Hydrogen Bonding in Cocrystals and Amorphous Dispersions Using ^{14}N-^{1}H HMQC Solid-State NMR. *Mol. Pharm.* **2013**, *10* (3), 999–1007.

(55) Nishiyama, Y.; Lu, X.; Trébosc, J.; Lafon, O.; Gan, Z.; Madhu, P. K.; Amoureux, J. P. Practical Choice of 1H- 1H Decoupling Schemes in through-Bond ^{1}H-{X} HMQC Experiments at Ultra-Fast MAS. *J. Magn. Reson.* **2012**, *214*, 151–158.

(56) Manjunatha Reddy, G. N.; Malon, M.; Marsh, A.; Nishiyama, Y.; Brown, S. P. Fast Magic-Angle Spinning Three-Dimensional NMR Experiment for Simultaneously Probing HH and NH Proximities in Solids. *Anal. Chem.* **2016**, *88* (23), 11412–11419.

(57) Venkatesh, A.; Hanrahan, M. P.; Rossini, A. J. Proton Detection of MAS Solid-State NMR Spectra of Half-Integer Quadrupolar Nuclei. *Solid State Nucl. Magn. Reson.* **2017**, *84*, 171–181.

(58) Yu, J. X.; Hallac, R. R.; Chiguru, S.; Mason, R. P. New Frontiers and Developing Applications in ^{19}F NMR. *Progress in Nuclear Magnetic Resonance Spectroscopy*. **2013**, pp 25–49.

(59) Urbanova, M.; Brus, J.; Sedenkova, I.; Policianova, O.; Kobera, L. Characterization of Solid Polymer Dispersions of Active Pharmaceutical Ingredients by ^{19}F MAS NMR and Factor Analysis. In *Spectrochimica Acta - Part A: Molecular and Biomolecular Spectroscopy*; **2013**; Vol. 100, pp 59–66.

(60) Vogt, F. G.; Strohmeier, M. 2D Solid-State NMR Analysis of Inclusion in Drug-Cyclodextrin Complexes. *Mol. Pharm.* **2012**, *9* (11), 3357–3374.

(61) Namespetra, A. M.; Hirsh, D. A.; Hildebrand, M. P.; Sandre, A. R.; Hamaed, H.; Rawson, J. M.; Schurko, R. W. ^{35}Cl Solid-State NMR Spectroscopy of HCl Pharmaceuticals and Their Polymorphs in Bulk and Dosage Forms. *CrystEngComm* **2016**, *18* (33), 6213–6232.

(62) Hamaed, H.; Pawlowski, J. M.; Cooper, B. F. T.; Fu, R.; Holger Eichhorn, S.; Schurko, R. W. Application of Solid-State ^{35}Cl NMR to the Structural Characterization of Hydrochloride Pharmaceuticals and Their Polymorphs. *J. Am. Chem. Soc* **2008**, *130*, 11056–11065.

(63) Carnahan, S. L.; Lampkin, B. J.; Naik, P.; Hanrahan, M. P.; Slowing, I. I.; Vanveller, B.; Wu, G.; Rossini, A. J. Probing O−H Bonding through Proton Detected ^{1}H− ^{17}O Double Resonance Solid-State NMR Spectroscopy. *J. Am. Chem. Soc* **2019**, *141*, 441–450.

(64) Mathew, R.; Uchman, K. A.; Gkoura, L.; Pickard, C. J.; Baias, M. Identifying Aspirin Polymorphs from Combined DFT-Based Crystal Structure Prediction and Solid-State NMR. **2020**, 1–8.

(65) Baias, M.; Widdifield, C. M.; Dumez, J. N.; Thompson, H. P. G.; Cooper, T. G.; Salager, E.; Bassil, S.; Stein, R. S.; Lesage, A.; Day, G. M.; et al. Powder Crystallography of Pharmaceutical Materials by Combined Crystal Structure Prediction and Solid-State ^{1}H NMR Spectroscopy. *Phys. Chem. Chem. Phys.* **2013**, *15* (21), 8069–8080.

(66) Ryan, K.; Lengyel, J.; Shatruk, M. Crystal Structure Prediction via Deep Learning. *J. Am. Chem. Soc.* **2018**, *140* (32), 10158–10168.

CHAPTER 2. RAPID CHARACTERIZATION OF FORMULATED PHARMACEUTICALS USING FAST MAS ^{1}H SOLID-STATE NMR SPECTROSCOPY

Modified from a manuscript published in Mol. Pharm.

Reprinted with permission from Mol. Pharm. 2019, 16 (7), 3121–3132

David A. Hirsh,[1#] Anuradha V. Wijesekara,[1#] Scott L. Carnahan,[1] Ivan Hung,[2] Joseph W. Lubach,[3] Karthik Nagapudi,[3] and Aaron J. Rossini[1*]

[1]Iowa State University, Department of Chemistry, Ames, IA, USA, 50011.

[2]Center of Interdisciplinary Magnetic Resonance, National High Magnetic Field Laboratory, 1800 East Paul Dirac Drive, Tallahassee, FL 32310, USA.

[3]Genentech Inc., South San Francisco, CA, USA, 94080.

Abstract

Active pharmaceutical ingredients (APIs) can be prepared in many different solid forms and phases that affect their physicochemical properties and suitability for oral dosage forms. The development and commercialization of dosage forms require analytical techniques that can determine and quantify the API phase in the final drug product. ^{13}C solid-state NMR (SSNMR) spectroscopy is widely employed to characterize pure and formulated solid APIs; however, ^{13}C SSNMR experiments on dosage forms with low API loading are often challenging due to low sensitivity and interference from excipients. Here, fast MAS ^{1}H SSNMR experiments are shown to be applicable for the rapid characterization of low drug load formulations. Diagnostic ^{1}H SSNMR spectra of APIs within tablets are obtained by using combinations of frequency-selective saturation and excitation pulses, 2D experiments and ^{1}H spin diffusion periods. Selective saturation pulses efficiently suppress the broad ^{1}H SSNMR signals from the most

commonly encountered excipients such as lactose and cellulose, allowing observation of high-frequency API ^{1}H NMR signals. ^{1}H SSNMR provides a one to three orders of magnitude reduction in experiment time compared to standard ^{13}C SSNMR experiments, enabling diagnostic SSNMR spectra of dilute APIs within tablets to be obtained within a few minutes. The ^{1}H SSNMR spectra can be used for quantification provided calibrations are performed on a standard sample with known API loading.

Introduction

Active pharmaceutical ingredients (APIs) exist in numerous distinct solid phases (*e.g.*, polymorphs, cocrystals, salts, amorphous dispersions, *etc.*) and their physicochemical properties determine the performance of the API within solid dosage forms such as tablets.[1–3] ^{13}C cross-polarization magic angle spinning (CPMAS) solid-state NMR (SSNMR) spectroscopy is widely applied for the identification, characterization, and quantification of pure and formulated solid APIs.[4–7] However, the intrinsically poor sensitivity of natural isotopic abundance ^{13}C SSNMR spectroscopy and the low concentration of APIs (typically 2 to 35 wt.%) often make it challenging to detect and characterize APIs in dosage forms. Prior ^{13}C SSNMR studies of formulated drug products have shown that ^{13}C SSNMR spectra diagnostic of the API phase can be acquired even for API loadings down to *ca.* 1 wt.% in favorable cases.[7–11] However, it is well known that APIs and organic solids can have long ^{1}H longitudinal relaxation times (T_1) on the order of hundreds of seconds.[12–16] APIs with long ^{1}H T_1 will have substantially reduced sensitivity for ^{13}C SSNMR and it is challenging or impossible to study such APIs by ^{13}C SSNMR in formulations with low drug loads. Additionally, excipient materials in the formulation give rise to NMR signals that overlap/interfere with those from the API. Interference is especially problematic for ^{1}H and ^{13}C SSNMR experiments because most excipients are organic materials.[17,18] Alternatively, NMR signals from the API can be selectively detected by

probing NMR-active elements such as fluorine,[19,20] nitrogen,[17,21] sodium,[22] and chlorine[18,23] that are exclusive to the API. Unfortunately, these NMR experiments are often infeasible because of poor sensitivity and/or absence of these elements in the API.

Dynamic nuclear polarization (DNP)[24–26] and fast magic angle spinning (MAS)[27] are often employed to enhance the sensitivity of SSNMR experiments by orders of magnitude. DNP has enabled ^{13}C, ^{15}N, and ^{35}Cl SSNMR experiments on a range of pure and formulated APIs.[17,23,26,28,29] DNP is especially helpful for NMR experiments on APIs with long ^{1}H T_1.[30,31] In addition to requiring specialized hardware, DNP typically involves cryogenic sample temperatures and methods for doping the sample with stable radicals, which may cause unanticipated changes in the solid form of an API.[32] The achievable DNP sensitivity enhancements are also highly sample dependent.[17,23,26,28]

Fast MAS increases the sensitivity of SSNMR by providing access to high resolution ^{1}H SSNMR spectra and/or enabling proton detection of heteronuclei.[27,33,34] Fast MAS and/or homonuclear decoupling (*i.e.*, CRAMPS) are routinely used to obtain ^{1}H SSNMR spectra of pure APIs.[4,5,34–40] Brown and co-workers applied CRAMPS double-quantum single-quantum (DQ-SQ) ^{1}H-^{1}H 2D NMR experiments to differentiate hydrated and anhydrous forms of an API in a dosage form of unspecified API loading.[41] They also showed fast MAS DQ-SQ experiments can detect and resolve minor polymorphic forms within mixtures of pure APIs down to a loading of 1 wt.%.[42] Zhou and Rienstra have previously applied fast MAS and proton detection to obtain 2D ^{1}H-^{13}C HETCOR spectra of an ibuprofen tablet with high API loading (*ca.* 65 wt.%).[43] However, proton detected 2D $^{1}H\{^{13}C\}$ SSNMR experiments are unlikely to provide significant gains in sensitivity as compared to direct detection 1D ^{13}C CPMAS SSNMR with large diameter rotors.

Here, we investigate the feasibility of using fast MAS ^{1}H SSNMR experiments ($\nu_{rot} \geq 50$ kHz) to rapidly detect and characterize dilute APIs in commercial and model dosage forms. To the best of our knowledge, fast MAS ^{1}H SSNMR spectroscopy has not been demonstrated as a method to detect APIs in realistic dosage forms with low drug loads. ^{1}H NMR experiments exploiting combinations of selective excitation (SE) pulses, selective saturation pulses (SSPs) and spin diffusion (SD) elements effectively suppress ^{1}H NMR signals from the abundant excipients and allow ^{1}H NMR signals from the APIs in the formulations to be selectively detected. Comparison of fast MAS ^{1}H and traditional ^{13}C CPMAS SSNMR spectra shows that ^{1}H SSNMR typically provides an order of magnitude reduction in experiment time. ^{1}H solid-state NMR experiments on polymorphs and model formulations demonstrate that ^{1}H solid-state NMR experiments can be used to detect different solid drug forms. The enhanced NMR sensitivity provided by ^{1}H SSNMR is shown to be useful for experiments on formulations with low API loading and APIs that have long ^{1}H longitudinal relaxation times (T_1).

Experimental

Sample preparation

Pure API samples, lactose monohydrate, magnesium stearate, and microcrystalline cellulose (MCC) were purchased from Sigma-Aldrich and used without further purification. Commercial tablets of mecl (All Day Less Drowsy Dramamine-brand, 25 mg API dose, manufactured by Medtech Products Inc.), phenaz (Azo-brand, 97.5 mg API dose, manufactured by i-Health Inc.), phenyl (Sudafed PE-brand, 10 mg API dose, manufactured by McNeil Consumer Healthcare) were purchased from CVS Pharmacy. The API wt.% in the commercial tablets was determined by dividing the reported API dose by the total measured mass of the tablet. (Table S1) Polymorphs of mexi were prepared from the as received mexi-I according to previously reported syntheses,[18,44] with some slight modifications. Mexi-II: 100 mg of mexi-I

dissolved in *ca.* 2 mL of methanol and mexi-II was slowly recrystallized over a period of 5 days. Mexi-III: 100 mg of mexi-I was heated at 160 °C in an oven for 2 hours. Model formulations were prepared for pheny (20.8 mg pheny, 276.8 mg MCC) and mexi (29.8 mg mexi-I, 5.81 mg mexi-III, 75.9 mg MCC) by thoroughly mixing the constituent powders in a vortex mixer for 5 minutes. Polymorphs of theo were prepared from the as received commercial sample of theo-II according to previously reported syntheses.[32,45] theo-M was synthesized by slowly recrystallizing 100 mg of theo-II in an excess of water. theo-I was obtained by a modified procedure. Normally, theo-I is obtained by holding theo-II at 270°C for 2 hours,[45] however, with this procedure theo-II was typically obtained. Instead, theo-I was synthesized by holding theo-M at 270 °C for 2 hours. A model formulation of theo was prepared by thoroughly mixing 5 mg of theo-I, 9.8 mg of theo-II and 84.9 mg of MCC. 2 wt. %, 4 wt. % and 6.1 wt. % mixtures of theo-II in MCC were prepared by using the following masses for each component. 2 wt. % theo-II (2 mg theo-II in 97.8 mg MCC). 4 wt. % theo-II (4 mg theo-II in 96.2 mg MCC). 6.1 wt. % theo-II (6.1 mg theo-II in 93.8 mg MCC).

Solid-state NMR spectroscopy

All samples were gently ground into a powder using a motor and pestle prior to packing into 1.3 mm or 4 mm zirconia rotors for solid-state NMR experiments. ^{1}H and all ^{13}C SSNMR experiments were performed on a 400 MHz (B_0 = 9.4 T) Bruker Avance III HD spectrometer equipped with broadband double resonance HX 1.3 mm fast MAS and 4 mm HX probes. Additional ^{1}H solid-state NMR (SSNMR) experiments were performed on a 800 MHz (B_0 = 18.8 T) Bruker Avance III spectrometer at the National High Field Magnetic Laboratory (NHFML) in Tallahassee, Florida equipped with a Bruker triple resonance HCN 1.3 mm fast MAS probe. ^{1}H SSNMR spectra were indirectly referenced to neat tetramethylsilane (δ_{iso} = 0 ppm) using adamantane (δ_{iso} = 1.82 ppm) and the unified scale in the IUPAC standard.[46] ^{13}C chemical shifts

were referenced to neat tetramethylsilane (δ_{iso} = 0 ppm) by setting the high frequency peak of adamantane to 38.48 ppm. All SSNMR spectra were processed using the TopSpin v3.5 software package.

^{1}H SSNMR experiments at both fields were performed with MAS frequencies of 50 kHz. See Figure S1 for the pulse sequences used in this work. Rotor-synchronized ^{1}H spin echo (400 MHz) or DEPTH[47] (800 MHz) experiments were used to minimize background signals from the probes and rotor caps in 1D NMR spectra. ^{1}H longitudinal relaxation time constants (T_1) were measured with saturation recovery spin echo pulse sequences. The recycle delay for 1D NMR experiments was typically set to 1.3 or 5 times the ^{1}H T_1 measured for the pure API.

2D ^{1}H–^{1}H spin diffusion (SD) NMR spectra were collected with (or without) selective saturation pulses (SSPs) and a spin diffusion period (Figure S1). 2D SD NMR spectra were typically obtained with 4 scans per increment, t_1 was incremented in steps of 40 μs (25 kHz indirect dimension spectral width). Typically 130 to 160 t_1 increments were acquired, corresponding to respective acquisition times of 2.6 to 3.2 ms in the indirect dimension. Total experiment times are indicated on the various Figures. SSPs were applied on resonance with common excipient molecules (at *ca.* 3.5 ppm) saturated nearly all of the excipient ^{1}H NMR signals with minimal effect on the high frequency NMR signals of the APIs (Figure S2). The SSP pulse length was 6 ms in all cases and the power and z-filter delay following the SSP (τ_{ZF}) was directly optimized on each sample. τ_{ZF} was between 0.020 ms and 20 ms depending on the sample. The SSP typically used RF fields of less than 1 kHz. The SSP was typically applied at an offset of 3 – 4.5 ppm, near to the peak maximum of MCC. However, at lower field, the SSP offset needs to be carefully optimized because ^{1}H spin diffusion is likely more rapid at lower field (see Figure S19 for an example of optimization of the SSP offset). For 9.4 T experiments on

mexi an alternative SSP condition was used: three 6 ms saturation pulses were separated by SSP diffusion periods (τ_{SSP}) of 20 ms were applied at a transmitter frequency of *ca.* 2.9 ppm. The 1D and 2D SD NMR experiments typically used spin diffusion delays between 5 and 70 ms. 1D selective-excitation spin diffusion (SE-SD) experiments were conducted at B_0 = 18.8 T with a 600 μs low-power rectangular selective excitation pulse (*ca.* 400 Hz RF field) applied on resonance with high frequency API signals. The 1D SE-SD NMR spectra were obtained with the same pulse sequence as the 2D ^{1}H–^{1}H NOE experiments except without any evolution in t_1 (Figure S1C). For experiments on theo at 9.4 T DANTE pulse trains[48,49] were used for frequency-selective excitation. The DANTE excitation pulses consisted of a train of 15 0.2 μs pulses each separated by two rotor cycles (40 μs). The rf field of the 0.2 μs pulses was 85 kHz.

All ^{13}C MAS (ν_{rot} = 8 kHz) SSNMR experiments were performed at 9.4 T with a triple resonance Bruker HXY probe configured in double resonance mode to maximize sensitivity. MAS ^{13}C SSNMR spectra were obtained with cross-polarization to enhance sensitivity.[50] ^{13}C SSNMR spectra were acquired with the CP-TOSS sequence with a 243-step phase cycle.[51,52] The ^{1}H CP spin lock pulse was linearly ramped between 90% and 100% of the spin lock RF field to broaden the Hartmann-Hahn match condition.[53] The length of the contact pulse was between 1.5 and 2.5 ms and was optimized on each sample. SPINAL-64 heteronuclear decoupling[54] with an RF field of *ca.* 80 kHz was used for all ^{13}C NMR experiments

Powder X-ray diffraction

Powder X-ray diffraction was used to confirm that the mexi polymorph synthesis was successful (Figure S3). Powder X-ray Diffraction (PXRD) patterns of all of the samples were obtained using a Rigaku Ultima U4 XRD, with a CuKα source (λ = 1.540562 Å). A 2θ range of

5º to 50º was scanned in stepwise fashion (step size = 0.05º, dwell = 2 seconds) for a total acquisition time of *ca.* 20 mins per sample.

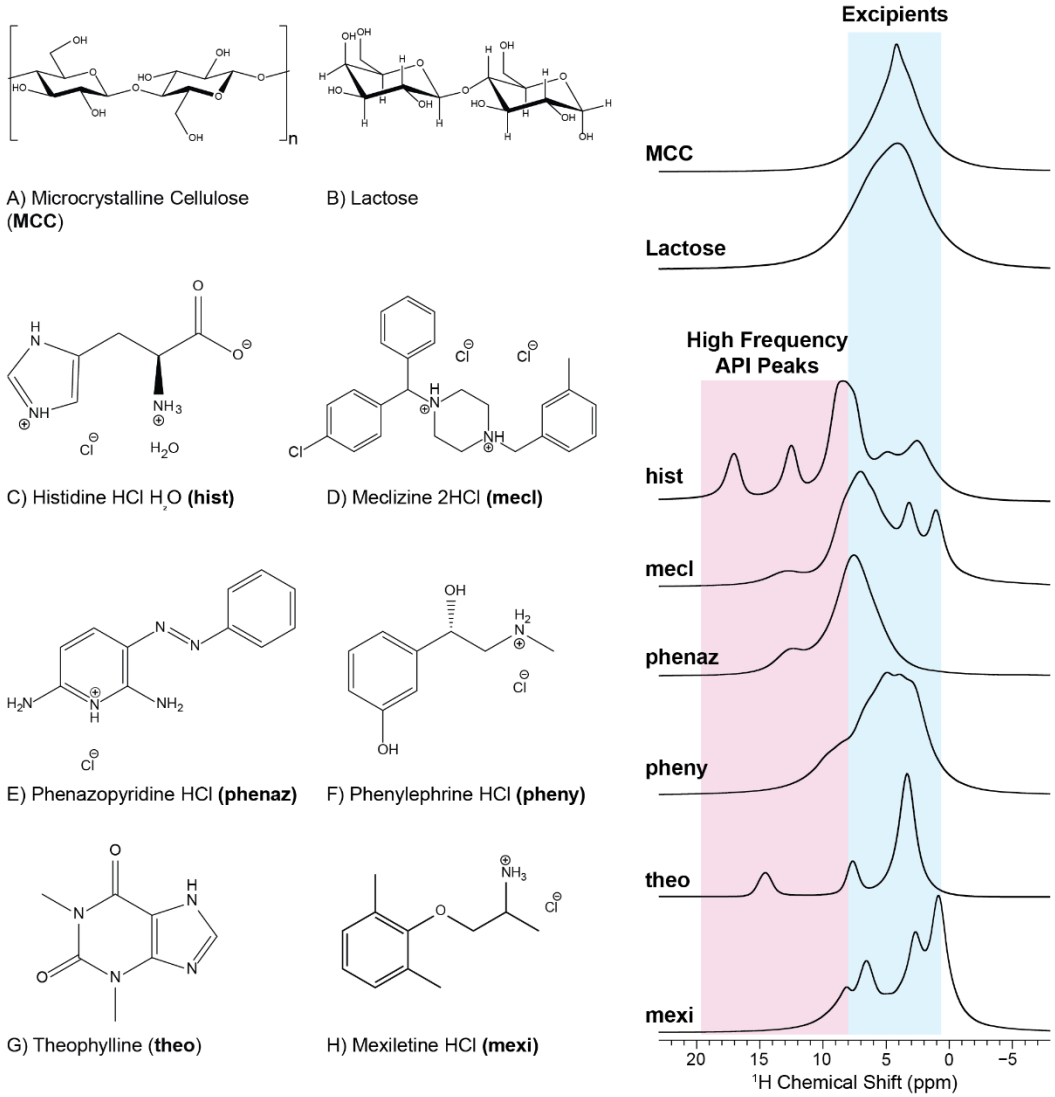

Figure 1. Molecular structures of (A-B) common excipient molecules and (C-H) representative small molecules/APIs used in this work. 1D ^{1}H SSNMR spectra of each compound are shown in the right column. All ^{1}H SSNMR spectra were obtained with a 50 kHz MAS frequency at B_0 = 9.4 T.

Results and discussion

Fast MAS ^{1}H SSNMR spectra of representative APIs and typical excipients

Figure 1 shows the molecular structures of representative APIs investigated in this study. Molecular structures are also shown for commonly encountered excipients such as microcrystalline cellulose (MCC) and lactose. These excipients are the major components of many tablets. Figure 1 and Figure S4 shows ^{1}H SSNMR spectra of the APIs and excipients obtained with a MAS frequency (ν_{rot}) of 50 kHz and B_0 = 9.4 T (400 MHz ^{1}H Larmor frequency). Inspection of Figure 1 shows that MCC and lactose give rise to relatively broad and featureless ^{1}H NMR spectra that span a frequency range of *ca.* 0 to 7 ppm. The ^{1}H SSNMR spectra of MCC and lactose are relatively featureless because the hydroxyl protons and alkyl protons have similar chemical shifts. On the other hand, many of the APIs have well-resolved high frequency ^{1}H NMR signals that are well separated from the excipient ^{1}H NMR signals. These high-frequency ^{1}H NMR peaks typically arise from hydrogen atoms in amine, ammonium, and carboxylic acid functional groups.[33,37,40–42] The high frequency ^{1}H NMR signals can be used to observe the ^{1}H SSNMR spectra of the APIs within formulations.

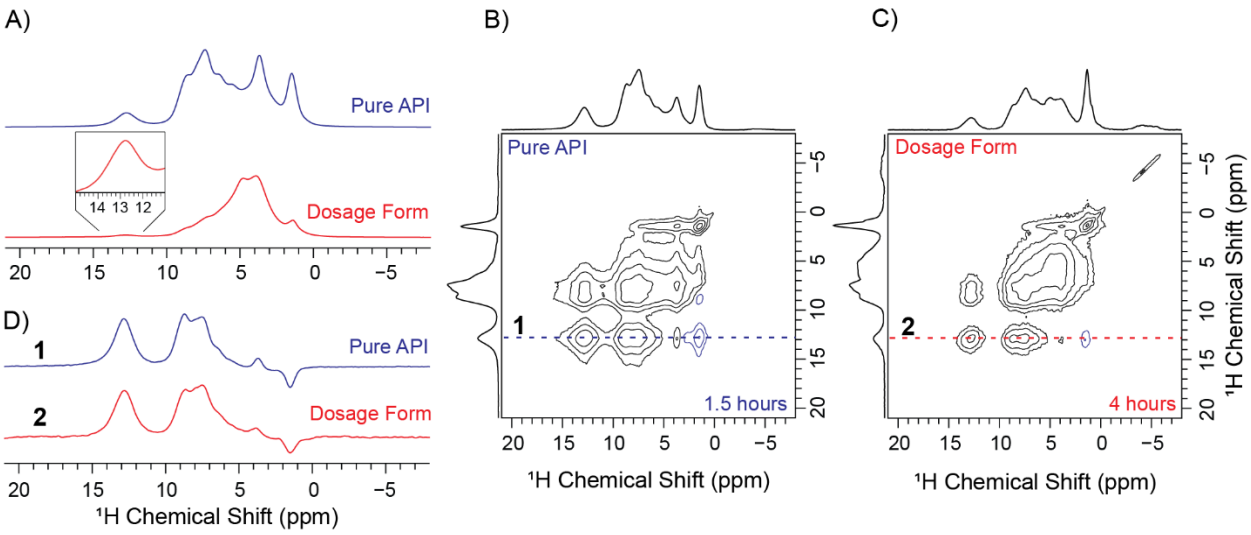

Figure 2. MAS ^{1}H SSNMR spectra of pure mecl and a commercial 12.5 wt.% mecl tablet acquired at B_0 = 18.8 T with ν_{rot} = 50 kHz. A) 1D DEPTH NMR spectra. B), C) 2D ^{1}H SD NMR spectra acquired with a selective saturation pulse applied at 3.5 ppm and a 20 ms spin diffusion time. D) ^{1}H NMR spectra extracted from rows of the 2D NMR spectra (dashed lines in B and C).

Fast MAS ^{1}H SSNMR spectra of commercial Dramamine® tablets

1D ^{1}H SSNMR experiments on the antihistamine API meclizine dihydrochloride (mecl, Figure 1) and a commercial Dramamine® Less Drowsy tablet with 12.5 wt.% mecl loading illustrate the challenges of obtaining ^{1}H SSNMR spectra of an API within a low drug load formulation (Figure 2A). A MAS frequency of 50 kHz is sufficient to provide a high resolution ^{1}H SSNMR spectrum of the pure mecl at B_0 = 18.8 T. The 1D ^{1}H NMR spectra were obtained with a DEPTH pulse sequence[47] to suppress probe background NMR signals. The 18.8 T ^{1}H SSNMR spectrum of the mecl tablet is dominated by the intense NMR signals from the excipient molecules, namely MCC. The intense MCC signals obscure most of the mecl signals; however, the ^{1}H NMR signal of the ammonium group of mecl is resolved at 12.7 ppm (Figure 2A, inset). Protons with high chemical shifts are often involved in hydrogen bonding and are diagnostic of the solid form.[33,37,40–42,55] The chemical shift of the ammonium group is identical in the tablet and pure API, immediately suggesting the same polymorph is present in both samples. Additional ^{1}H

NMR signals from the API may be required for phase identification, especially for APIs that could form additional phases.

Combinations of frequency-selective saturation and excitation pulses, 2D NMR spectra, and spin diffusion periods can be used to eliminate NMR signals from the excipients and obtain diagnostic ^{1}H SSNMR spectra of the API in formulations. Under fast MAS, homonuclear ^{1}H spin diffusion is slowed and different ^{1}H chemical shifts can be suppressed with selective saturation pulses (SSPs), typically low-power, long duration pulses (1 to 30 ms).[56–58] The most commonly encountered excipient molecules have similar ^{1}H chemical shifts in the solid-state, centered around 3-5 ppm (Figure 1). SSPs applied in this region will eliminate signals from most excipients. Note that the broad, overlapped ^{1}H SSNMR signals of MCC will lead to rapid ^{1}H spin diffusion amongst the ^{1}H spins in MCC, allowing the SSP to efficiently saturate the entire MCC signal. High frequency acid or amine peaks from APIs are typically between 8 and 20 ppm[33,37,40–42] and are minimally affected by SSPs targeting the excipient resonances (Figure S2 and S4). Note that most APIs are marketed as free acids, salts, or cocrystals;[59] therefore, APIs will usually possess amine, ammonium, or acid functional groups that give rise to high frequency ^{1}H chemical shifts.

2D ^{1}H spin diffusion experiments

1D and 2D ^{1}H spin diffusion (SD) NMR experiments[36,60] enhance resolution and provide access to additional ^{1}H chemical shifts of the API (see Figure S1 for pulse sequences). 2D ^{1}H SD NMR experiments with SSPs were performed on pure mecl and the mecl tablet (Figures 2B and 2C). 2D ^{1}H SD NMR spectra of the mecl tablet could also be obtained without SSPs because the ammonium peak is well resolved (Figures S6 and S7). However, SSPs are required to reduce excipient signals in most tablets. ^{1}H spin diffusion occurs during the delay (τ_{SD}) between the last two $\pi/2$ pulses, producing additional API peaks in the rows of the 2D NMR spectra. Spin

diffusion only occurs between ^{1}H nuclei that are proximate,[61,62] therefore, the NMR spectrum of the mecl tablet extracted from the ammonium peak row at 12.7 ppm will only show ^{1}H NMR signals from the API (dashed lines in Figure 2). Figure 2D clearly shows that the same API phase is present in pure mecl and the mecl tablet, in agreement with ^{13}C SSNMR experiments (see below). The ^{1}H SSNMR spectra obtained from the rows of the 2D spin diffusion spectra are distinct from the ^{1}H spin echo NMR spectra because peak intensities depend upon the spin diffusion rates between the high frequency peak and the lower frequency peaks (*cf.* Figures 2A and 2D). For isolated spins, spectral spin diffusion rates are determined by the strength of the dipolar coupling of the two coupled spins and the peak overlap integral evaluated at zero frequency. The peak overlap integral is approximately inversely proportional to the square of the frequency difference.[63,64] For example, the ammonium peak shows rapid spin diffusion to the positively shifted aromatic ^{1}H NMR signals because the peaks have similar shifts and partially overlap at their baseline. On the other hand, the methyl and ammonium cross-peak have a low intensity and the cross-peak is negative. ^{1}H spin diffusion between the methyl protons and ammonium groups is likely slow because methyl and ammonium peaks are well separated ($\Delta\delta \approx$ 11 ppm = 8.8 kHz at 18.8 T). Conventional ZQ spin diffusion (^{1}H-^{1}H flip-flop) causes positive cross-peaks. We therefore speculate that the negative ammonium-methyl cross-peak could be caused by a double-quantum nuclear Overhauser effect (DQ-NOE) and this will be the subject of future study.

Notably, the 2D SD ^{1}H NMR spectra were obtained in a few hours and experiment times could be further accelerated by reducing the spin diffusion time to focus the observed direct dimension signal into fewer API peaks or by acquiring fewer increments in the 2D experiment (which will cause reduced resolution in the indirect dimension). The data shown in Figure 2 were

acquired at B_0 = 18.8 T, but 2D ^{1}H SD NMR experiments with SSPs were also successful at B_0 = 9.4 T (Figure S8). The selectivity of the SSPs for excipient saturation is generally better at high field because ^{1}H spin diffusion is slowed by improved ^{1}H shift dispersion.

1D spin diffusion experiments

If the chemical shift of a resolved API ^{1}H NMR signal is known from prior characterization of pure API forms or from 1D ^{1}H NMR experiments on the tablet, 1D selective excitation spin diffusion (SE-SD) NMR experiments can be performed (Figure S1C). In the 1D SE-SD NMR experiments on mecl, the ammonium peak at 12.7 ppm was selectively excited with a low-power 600 μs π/2 pulse. The transverse ^{1}H ammonium magnetization was then reconverted to longitudinal magnetization by a high-power broadband π/2 pulse, which simultaneously saturates the other ^{1}H NMR signals. The longitudinal ^{1}H ammonium magnetization then undergoes spin diffusion for a fixed period of time, leading to the appearance of additional ^{1}H chemical shifts, which can then be read by a final broadband π/2 excitation pulse.

The 1D SE-SD method produces a high quality ^{1}H SD NMR spectrum of the mecl tablet in only 30 minutes (Figure 3A). The 1D ^{1}H SE-SD NMR spectrum of the mecl in the tablet obtained with a 70 ms spin diffusion time has a high signal-to-noise (SNR) ratio of *ca.* 44 for the characteristic ammonium peak, corresponding to a sensitivity (S) of 8.1 min$^{-1/2}$ (S = SNR × $t^{-1/2}$). Different pulse shapes or excitation schemes[57,58,65] could likely improve the selectivity and efficiency of the SE pulses. For example, in later experiments on theo, simple DANTE schemes[48,49] were used for efficient frequency-selective excitation.

Comparison to ^{13}C solid-state NMR spectroscopy

^{1}H SSNMR experiments provide much better sensitivity than conventional ^{13}C CPMAS NMR experiments. A ^{13}C CPMAS spectrum of the mecl tablet was obtained with a 4 mm rotor and had a SNR of 17 after 2 hours of signal averaging (Figure 3C and Figure S9). In comparison, a 1D SE-SD ^{1}H SSNMR spectrum with comparable SNR could theoretically be obtained 16 times faster (in 7.5 mins). For the ^{13}C SSNMR experiments S = 1.6 min$^{-1/2}$, while the 1D ^{1}H SSNMR spectrum of the mecl tablet had a S of 63 min$^{-1/2}$ and the 1D ^{1}H SE-SD spectrum had a S of 8.1 min$^{-1/2}$ (Figure 3A and Figure S9). Therefore, 1D ^{1}H SSNMR offers 5– to 39–fold higher sensitivity for mecl, corresponding to 1 to 3 orders of magnitude reductions in experiment time as compared to ^{13}C CPMAS. Note that the sensitivity of 1D SE-SD experiments could be further increased by reducing the ^{1}H spin diffusion time to focus the NMR signal into fewer peaks, however, this would come at the expense of loss of intensity at other ^{1}H chemical shifts.

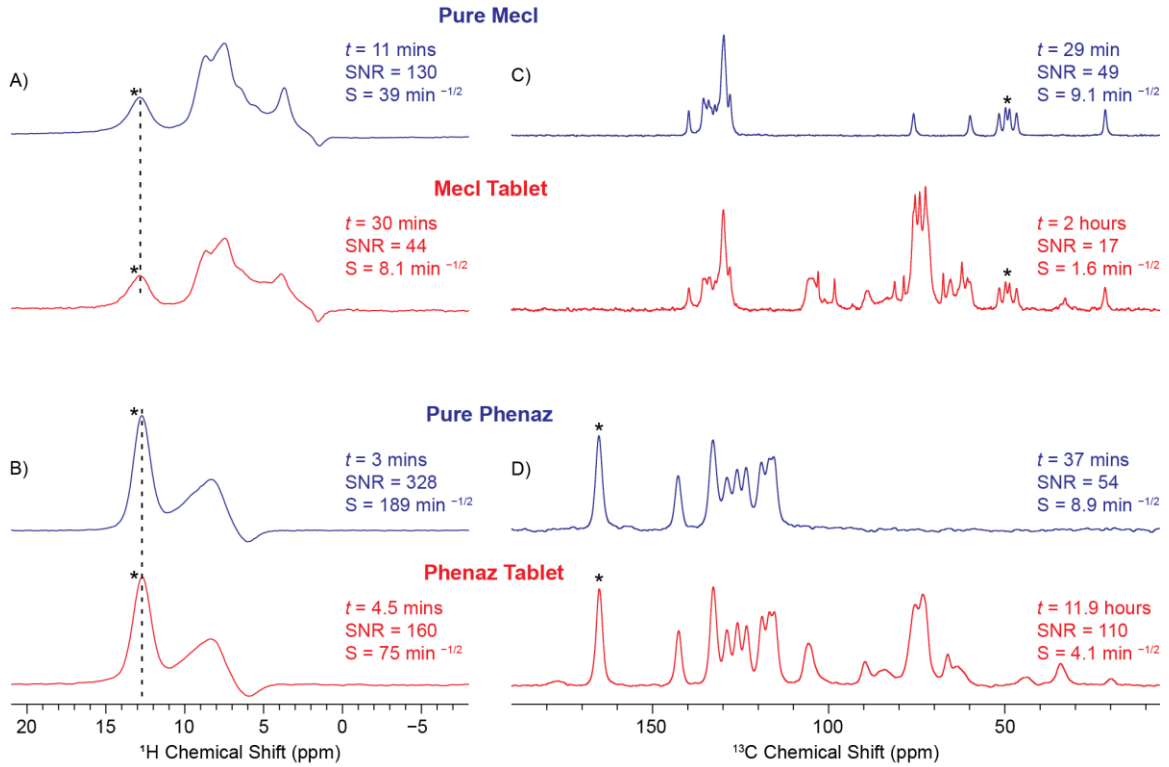

Figure 3. 1D ^{1}H SE-SD and ^{13}C CPMAS SSNMR spectra of A), C) pure mecl and a mecl tablet and B), D) pure phenaz and a phenaz tablet. The dashed line indicates the offset of the SE excitation

pulse. Total experiment times are indicated. Spin diffusion times were 70 ms and 20 ms for mecl and phenaz, respectively. The ^{1}H SSNMR spectra were acquired at B_0 = 18.8 T with ν_{rot} = 50 kHz and 1.3 mm rotors. ^{13}C CPMAS spectra were obtained at B_0 = 9.4 T with ν_{rot} = 8 kHz and 4 mm rotors. Experiment time (t), signal-to-noise ratio (SNR) and sensitivity (S) are indicated for each spectrum. The asterisks denote the peaks used for determination of (SNR) and calculation of *S*.

Characterization of other commercial formulations

Fast MAS ^{1}H SSNMR experiments were performed on other commercial API formulations to investigate the generality of our approach. ^{1}H and ^{13}C SSNMR experiments on the API phenazopyridine hydrochloride (phenaz) and a commercial tablet with 68 wt.% API loading are summarized in Figures 3B and 3D (also Figures S10 and S11). Diagnostic ^{1}H SSNMR spectra of phenaz in the tablet were obtained in a few minutes with the 1D SE-SD pulse sequence (Figure 3B). The similarity of the 1D SE-SD spectra of the pure phenaz and the phenaz tablet suggests the same API phase is present in both. The 1D SE-SD spectrum of phenaz in the tablet showed a SNR of 160 after 4.5 minutes of signal averaging (S = 75 min$^{-1/2}$), demonstrating the high sensitivity provided by ^{1}H SSNMR spectroscopy. Comparing the 1D ^{1}H SE-SD spectrum and the ^{13}C CPMAS spectrum of the phenaz tablet shows that ^{1}H SSNMR provides an order of magnitude improvement in sensitivity, corresponding to a 100-fold reduction in experiment time. For example, consider a hypothetical 2 wt.% phenaz tablet: only 20 minutes would be required to obtain a 1D SE-SD ^{1}H SSNMR spectrum with a SNR of *ca.* 10, while *ca.* 4.5 days would be required to obtain a ^{13}C CPMAS with similar SNR.

The tablet Sudafed® PE containing 7 wt.% of the API phenylephrine hydrochloride (pheny) was also studied (Figure S12-S15). This tablet is challenging to characterize because it has a low API loading, pure pheny has a relatively long ^{1}H T_1 of 18 s, and the API protons are present in a secondary ammonium group ($C_2NH_2^+$) containing ^{1}H nuclei that are strongly dipolar coupled, leading to broadening of the high frequency API ^{1}H NMR signals. The secondary ammonium protons also have chemical shifts at *ca.* 10 ppm, close to the ^{1}H shifts of many

excipients. The overlapped ^{1}H NMR signals make it challenging to selectively saturate the excipients, resulting in reduced intensity of the high-frequency API signals. Despite these challenges, 2D ^{1}H SSNMR spectra of the pheny tablet were obtained in 7 hours at B_0 = 9.4 T, while a ^{13}C SSNMR spectrum of similar quality was obtained after 16 hours of signal averaging (Figures S15). Comparison of the ^{13}C SSNMR spectra of pure pheny and the tablet suggest that the API is likely amorphous in the tablet. This is reflected in the distinct appearance of the ^{1}H SSNMR spectra of the pheny tablet and pure pheny. In contrast, a model 7 wt.% pheny formulation made of a physical mixture of crystalline pheny and MCC yielded ^{1}H SSNMR spectra consistent with the crystalline phase (Figure S14). The experiments on pheny illustrate that ^{1}H SSNMR experiments are challenging when the ^{1}H NMR spectrum of the API suffers from overlap of many ^{1}H NMR signals and does not possess a well-resolved, high-frequency ^{1}H NMR signal. In such cases ^{13}C CPMAS will likely be the preferred NMR method for interrogating the API phase within the tablet.

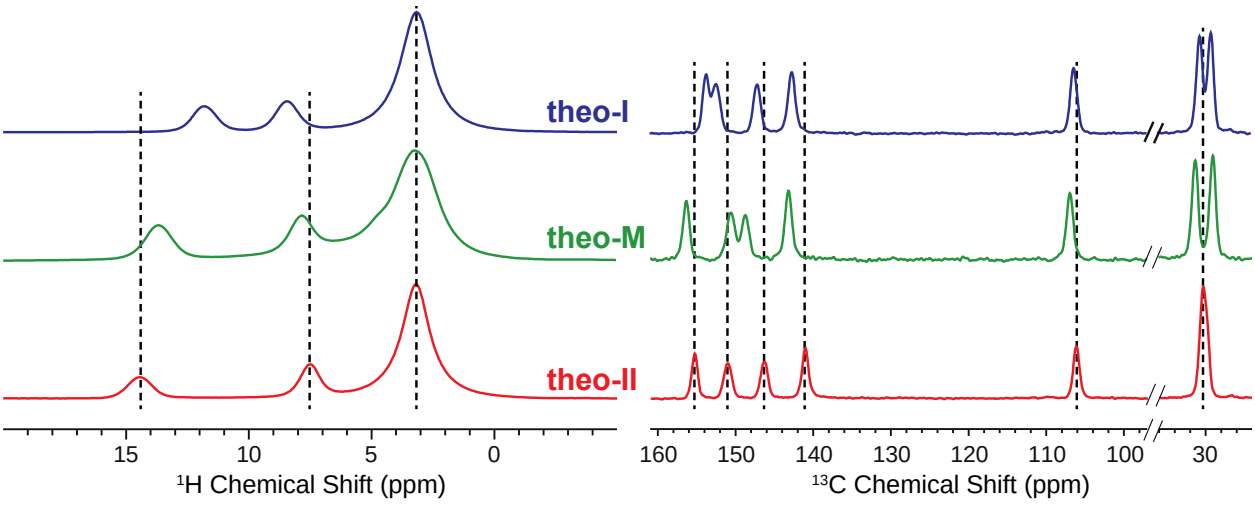

Figure 4. ^{1}H and ^{13}C CPMAS SSNMR spectra of theophylline form I (theo-I), theophylline monohydrate (theo-m), and theophylline form II (theo-II). ^{1}H SSNMR spectra were obtained with a 50 kHz MAS frequency at B_0 = 9.4 T. ^{13}C SSNMR spectra were obtained with an 8 kHz MAS frequency at B_0 = 9.4 T. Vertical dashed lines are guides for the eye to illustrate the differences in isotropic chemical shifts.

Detection of polymorphic forms

It is well known that both ^{1}H chemical shifts[37,39,40,55,66,67] and SD rates[33,35,66] are very sensitive to differences in structure. Therefore, ^{1}H SSNMR should be an ideal technique to detect different API phases within formulations. To test this hypothesis, polymorphs of theophylline (theo) and mexiletine hydrochloride (mexi) and model formulations were characterized by ^{1}H SSNMR. In addition to demonstrating the utility of our techniques to detect distinct solid phases in formulations, a critical aspect of pharmaceutical product development, these case studies provide examples of potential challenges for ^{1}H SSNMR (*i.e.*, slow ^{1}H longitudinal relaxation and poor separation of the high frequency API peaks from the excipients), and methods that can be used to overcome them.

Characterization of Theophylline polymorphs

Theo has several stable crystal forms and a monohydrate form, all of which are readily accessible by simple recrystallization procedures.[32,45] MAS ^{1}H and ^{13}C SSNMR spectra of theophylline form II (theo-II), theophylline form I (theo-I) and theophylline monohydrate (theo-m) are shown in Figure 4. The similarity of the ^{1}H and ^{13}C SSNMR spectra to those previously reported for the different polymorphs confirms the identity and purity of each polymorph.[32] The 1D ^{1}H SSNMR spectra of the different theo forms illustrates that all forms are easily distinguished on the basis of the distinct ^{1}H chemical shifts observed for the amine (12-15 ppm) and methine (CH) protons (7.5-8.5 ppm). Baias *et al.* have noted that the differences in amine ^{1}H chemical shift occurs because of the distinct hydrogen bonding motifs encountered in the different crystal forms.[39] The single crystal X-ray structure of theo-II shows the NH group forms a hydrogen bond to the nitrogen atom in the five-membered purine ring of an adjacent theophylline molecule.[45] The single crystal X-ray structures of theo-m and theo-I both show the NH group forms a hydrogen bond to a carbonyl group of an adjacent theophylline molecule.[45]

^{1}H T_1 measurements were performed on the different pure theo forms with both slow (ν_{rot} = 8 kHz) and fast MAS (ν_{rot} = 50 kHz) frequencies. Under slow MAS each ^{1}H NMR signal showed a similar mono-exponential T_1 because ^{1}H spin diffusion is rapid between all ^{1}H spins (Figure S16). The ^{1}H T_1 was *ca.* 53 s for theo-I and 64 s for theo-II (Table S2). Under fast MAS each ^{1}H NMR signal had a distinct T_1; for both theo forms the T_1 of the methyl ^{1}H was on the order of 60 s, while the T_1 of the high-frequency amine was much longer and between 300 – 460 s for the different forms (Table S3). The long ^{1}H T_1 for the amine ^{1}H of theo arises with fast MAS because ^{1}H spin diffusion has been slowed and there are likely no dynamic motions at the correct frequencies to cause longitudinal relaxation. Note that for the other compounds examined there were only slight differences in T_1 measured for the different ^{1}H NMR signals. Fast MAS could reduce the sensitivity of SD ^{1}H SSNMR experiments where the amine signal will be excited because the amine ^{1}H T_1 of several hundred seconds will dictate the recycle delay.

Previously, Taulelle and Nishiyama showed that RFDR recoupling can be applied to accelerate ^{1}H spin diffusion under fast MAS and reduce the differences in ^{1}H T_1 between resolved ^{1}H NMR signals.[68] Alternatively, spin-lock pulses can also be used to accelerate spin diffusion when there is a large frequency difference between peaks.[69] Here a low power ^{1}H spin-lock pulse ($\nu_1(^1H) \approx 15$ kHz) with a duration of a 1.8 ms was used to enable ^{1}H spin diffusion across the entire theo ^{1}H NMR spectrum and transfer magnetization from the methyl ^{1}H to the amine and methine ^{1}H. The spin-lock pulse shortens the effective T_1 of high frequency theo amine ^{1}H NMR signals from several hundred seconds to less than 90 seconds (Table S3). Therefore, a ^{1}H broadband $\pi/2$ pulse, spin-lock pulse, flip-back $\pi/2$ pulse block was inserted prior to any SE pulses in the subsequent ^{1}H SSNMR experiments on theo (Figure S1). For 1D SE-SD experiments on theo a spin-lock pulse was used to promote ^{1}H spin diffusion in lieu of

the usual longitudinal magnetization storage period (Figure S1E). Spin-lock pulses used to accelerate ^{1}H spin diffusion in theo were between 600 μs and 1.8 ms in duration.

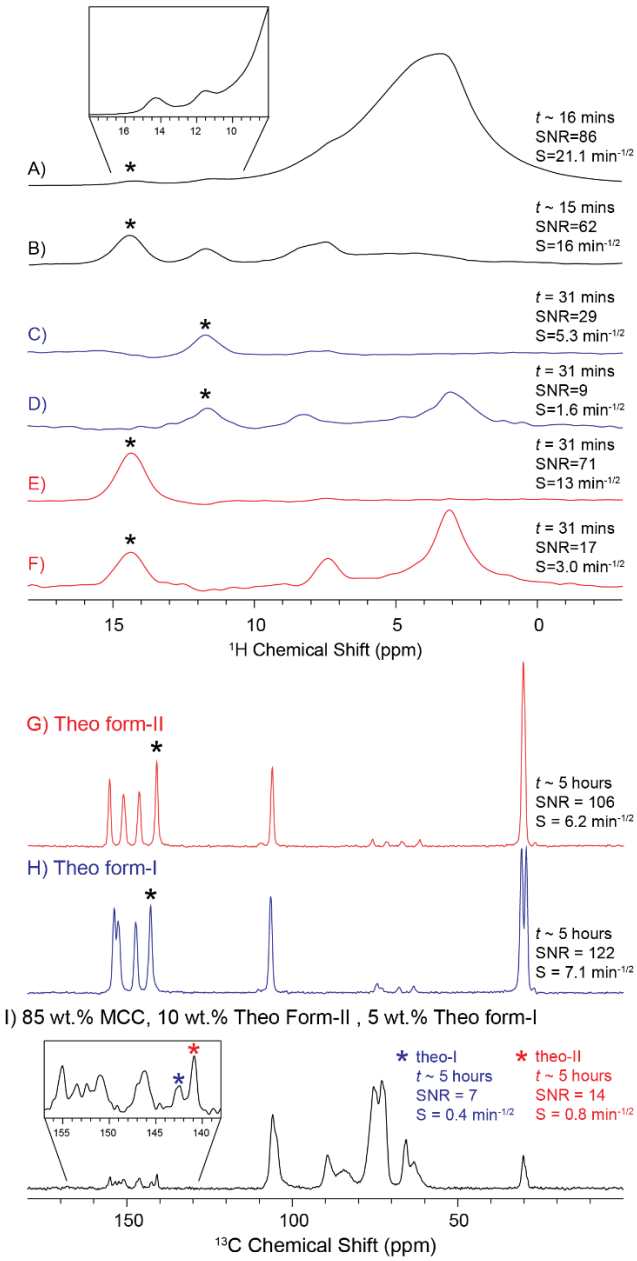

Figure 5. ^{1}H and ^{13}C SSNMR spectra of a physical mixture of 85 wt.% MCC, 10 wt.% theo-II and 5 wt.% theo-I. ^{1}H spin echo spectra recorded A) without and B) with SSP on resonance with MCC. (C-F) 1D SE-SD ^{1}H SSNMR spectra with the SE pulse on resonance with the high frequency amine ^{1}H NMR signal of (C, D) theo-I or (E, F) theo-II. ^{1}H SSNMR spectra in D) and F) were obtained with a 1.8 ms spin-lock pulse following the SE pulse to promote ^{1}H spin diffusion. Spectra in C) and E) were recorded with a 20 μs spin-lock pulse to minimize ^{1}H spin diffusion. ^{1}H SSNMR

spectra were obtained with a 50 kHz MAS frequency at B_0 = 9.4 T. ^{13}C SSNMR spectra were obtained with an 8 kHz MAS frequency at B_0 = 9.4 T. Experiment times (*t*), signal-to-noise ratios (SNR) and sensitivity (S) are indicated. The asterisks denote the peaks used for determination of (SNR) and calculation of *S.*

NMR experiments were performed on mixtures of theo solid forms and MCC to demonstrate the potential of fast MAS ^{1}H SSNMR to rapidly detect different solid API forms when they are dilute within a formulation. A mixture consisting of 85 wt.% MCC, 10 wt.% theo-II and 5 wt.% theo-I was used in these experiments. This mixture mimics a scenario where there is a total drug load of 15 wt.% in the formulation and one-third of the API (theo-II) has undergone a transition to a secondary API phase (theo-I). In the 1D ^{1}H SSNMR spectrum obtained without SSPs, the high frequency amine signals of both theo-I and theo-II are obscured (Figure 5A). Acquisition of a 1D ^{1}H SSNMR spectrum with SSPs helps suppress the MCC signals and clearly shows both amine and methine ^{1}H NMR signals for both theo forms (Figure 5B).

1D SE-SD NMR experiments were also performed with DANTE SE pulses on resonance with the amine signal of theo-I or theo-II (Figures 5C-5F). The 1D SE-SD ^{1}H SSNMR spectra obtained with a minimal spin diffusion time only show the respective amine chemical shifts (Figures 5C and 5E), while those recorded with a 1.8 ms spin-lock pulse to promote ^{1}H spin diffusion show additional chemical shifts from the methine and methyl groups (Figures 5D and 5F). The ^{1}H chemical shifts observed in the 1D SE-SD NMR spectra exactly match those observed in the ^{1}H NMR spectra of the corresponding pure phases (Figure 4), confirming the identity of the theo phases in the mixture.

Comparing the sensitivity of ^{13}C and ^{1}H SSNMR experiments on the theo-MCC mixture shows that ^{1}H SSNMR once again provides far superior sensitivity. After 5 hours of signal

averaging the ^{13}C CPMAS spectrum of the mixture shows SNR of about 14 and 7 for characteristic ^{13}C peaks of theo-II and theo-I, respectively. These SNR values correspond to a sensitivity of 0.8 $min^{-1/2}$ and 0.4 $min^{-1/2}$ for theo-II and theo-I, respectively. Note that the low sensitivity of ^{13}C CPMAS for theo primarily arises because of its relatively long ^{1}H T_1 which requires a long recycle delay over 1 minute to be used for optimal sensitivity. Despite the long ^{1}H T_1, ^{1}H SSNMR spectra of both theo forms within the mixture can be obtained in 15 – 30 minutes with a SNR of over 30. The sensitivity of the ^{1}H SSNMR spectra recorded without any spin diffusion is 13 $min^{-1/2}$ and 5 $min^{-1/2}$ for theo-II and theo-I, respectively. The sensitivity provided by ^{1}H SSNMR is about 16 times better than ^{13}C CPMAS, corresponding to a two order of magnitude reduction in experiment time. This is why high quality ^{1}H NMR spectra are obtained in only 15-30 minutes each, while the ^{13}C CPMAS spectrum required hours of signal averaging.

The SSNMR experiments on the theo-MCC mixture illustrate why it is challenging to characterize formulations with low API loading by conventional ^{13}C CPMAS. For example, consider a scenario where the theo-II loading is only around 2 wt.%, then ~2.5 days of signal averaging would be required to obtain a ^{13}C SSNMR spectrum with a SNR of 10. On the other hand, in only 30 minutes a ^{1}H SSNMR spectrum of a 2 wt.% mixture of theo-II in MCC with a SNR of about 18 was obtained (Figure S17). This example demonstrates the advantages of fast MAS ^{1}H SSNMR for probing formulations with very low API loading and/or when the API possesses a long ^{1}H T_1.

Detection of Mexiletine polymorphs

Three polymorphic forms of mexiletine hydrochloride (mexi), referred to as mexi-I, mexi-II, and mexi-III, were also prepared and characterized by ^{1}H SSNMR. These polymorphs have previously been characterized with X-ray diffraction as well as ^{13}C and ^{35}Cl SSNMR.[18,44]

The distinct 1D ^{1}H SSNMR spectra of the mexi polymorphs at B_0 = 9.4 T suggests that ^{1}H NMR should be useful to distinguish and quantify the different forms (Figure 6 and Figure S18). A model mexi formulation was prepared by mixing 5.2 wt.% mexi-III, 26.7 wt.% mexi-I, and 68.0 wt.% MCC (total API load of 32 wt.%). The model mexi formulation mimics the composition of a tablet with 16% of the API converted to a secondary phase (mexi-III).

The mexi formulation is challenging to study by ^{1}H SSNMR because the primary ammonium protons of mexi have chemical shifts of *ca.* 8 ppm, near to the ^{1}H shifts of MCC. Therefore, SSP conditions that can completely saturate MCC signals and minimally perturb the mexi signals are required. Optimization of the SSP offset for mexi-I, mexi-III and MCC at B_0 = 9.4 T showed that with a single SSP, the MCC signals can only be saturated when the SSP is applied at offsets of *ca.* 4.7 to 3.7 ppm, which falls within the MCC lineshape (Figure S19A). However, at these offsets the ^{1}H NMR signals from mexi-I and mexi-III are also partially saturated, likely because the mexi ^{1}H SSNMR spectra are poorly resolved at 9.4 T and ^{1}H spin diffusion rapidly equilibrates polarization across the spectrum.

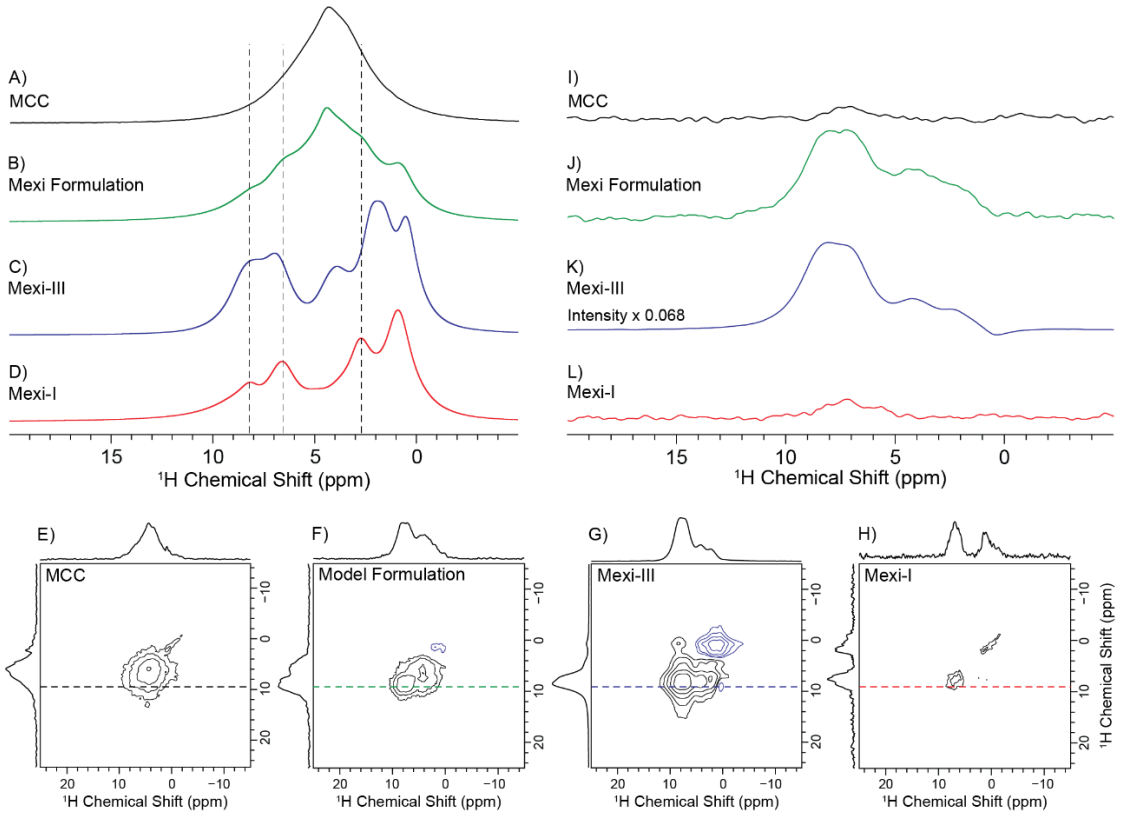

Figure 6. (A-D) 1D ^{1}H spin echo SSNMR spectra of MCC, the model mexi formulation, mexi-III and mexi-I. The mexi formulation consists of a physical mixture of 5.2 wt.% mexi-III, 26.7 wt.% mexi-I, and 68.0 wt.% MCC. Vertical dashed lines are guides for the eye to illustrate differences in ^{1}H chemical shifts for the two mexi polymorphs. (E-H) 2D ^{1}H SD NMR spectra of of MCC, the model mexi formulation, mexi-III and mexi-I. All spectra were recorded with a 20 ms spin diffusion mixing time and three SSPs applied at an offset of 2.8 ppm. (I-L) ^{1}H SSNMR spectra extracted from the indicated rows of the 2D ^{1}H SD NMR spectra. Only ^{1}H NMR signals from mexi-III are visible from the formulation.

Alternatively, application of three SSPs, each separated by a 20 ms *z*-filter/spin diffusion period, enables MCC signals to be saturated completely with SSP offsets of 2.0 to 5.0 (Figure S19B). 2D ^{1}H SD NMR spectra acquired with SSP offsets below 3.0 ppm saturates the mexi-I and MCC signals, while mexi-III signals are still observable. 2D SD ^{1}H NMR spectra with three SSPs applied at 2.9 ppm were acquired at B_0 = 9.4 T from mexi-I, mexi-III, MCC and the model formulation (Figure 6E-H). The rows extracted from the 2D SD ^{1}H NMR spectra at an indirect

dimension shift of 9.7 ppm are shown in Figure 6I-L. As expected, only NMR signals from mexi-III are visible in the formulation because the SSPs efficiently saturate both MCC and mexi-I NMR signals. These results illustrate that ^{1}H SSNMR could be useful to selectively detect different polymorphic forms on the basis of their response to SSPs. However, a clear drawback of the ^{1}H SSNMR experiments that mexi-I NMR signals could not be observed in this case because they are attenuated by the SSPs required to eliminate MCC NMR signals. This limitation could likely be overcome by increasing the static magnetic field and/or MAS frequency to increase ^{1}H resolution, reduce spin diffusion and improve the selectivity of SSPs.

Quantification of API loading by ^{1}H SSNMR

Finally, the ability of ^{1}H SSNMR to quantify API loading in a formulation was also tested. It has previously been demonstrated that ^{13}C CPMAS can be used to quantify API loading within a formulation based upon the comparison of peak intensities.[7–11] ^{1}H SSNMR experiments were performed on physical mixtures of theo-II and MCC with variable loading of theo-II from 2 wt.% to 9.8 wt.% to investigate the possibility of using ^{1}H SSNMR for quantification of APIs in formulations. Figure 7A shows a plot of the integrated intensity of the amine ^{1}H NMR signal of theo-II measured with 1D SE-SD experiments as a function of the theo-II wt.%. For the calibration experiments the recycle delay was fixed to 95 s which corresponds to 1.3 times the signal build-up time constant of 73 s measured for the theo-II amine signal. The SE pulse was placed on resonance with the theo-II amine signal and the spin diffusion spin-lock pulse was set to 20 μs in duration to maximize sensitivity by focusing signal into the amine peak. Figure 7A shows that there is a linear correlation between the theo-II ^{1}H NMR signal intensity and the theo-II wt.% within the mixtures. Using the measured integrated intensities and the calibration equation, the average absolute error in the API loading was 0.36 wt.% and the average relative

error was 9.9% of the expected API loading (Table S4). These experiments demonstrate fast MAS ^{1}H SSNMR should be quantitative, provided the ^{1}H NMR signal response to the SSP and SE pulses are first calibrated on standards with known API loading.

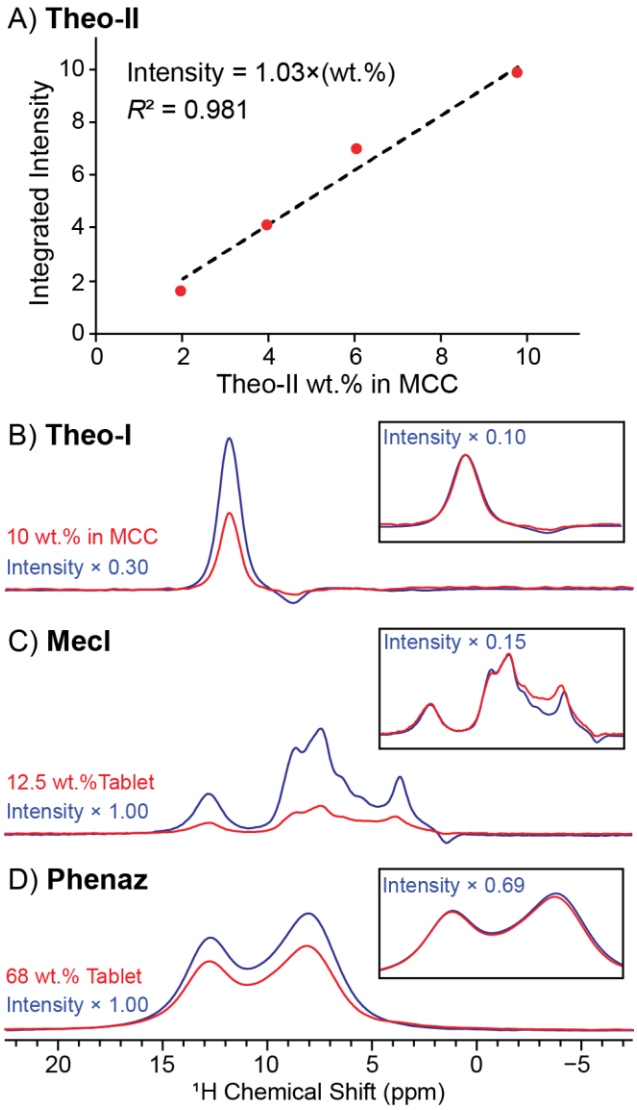

Figure 7. A) Plot of integrated intensity of the amine ^{1}H NMR signal of theo-II on different mixtures with MCC. Comparison of the 1D SE-SD ^{1}H NMR signal intensities for the corresponding pure APIs and for B) 10 wt.% theo-I in MCC, C) a 12.5 wt.% mecl tablet, D) a 68 wt.% phenaz tablet. The insets show the intensity scaling required to match the integrated intensity of high frequency API signals of the formulation to those of the pure API. The spectra are normalized for differences in number of scans. Data for A), B) and D) was obtained at B_0 = 9.4 T and C) was obtained at B_0 = 18.8 T.

Signal intensities were also used to estimate the loading of other APIs within formulations. 1D SE-SD ^{1}H NMR integrated signal intensities were compared for samples of pure theo-I and a 10 wt.% theo I – MCC physical mixture (Figure 7B). Based upon the integrated signal intensity the theo-I wt.% in the mixture was determined to be 11 wt.%, which is within 1 wt.% of the expected value. Comparison of the mexi-III signal intensity in 2D ^{1}H SD experiments yields a 6.8 wt.% loading of mexi-III in the formulation, which is close to the expected value of 5.2 wt.% mexi-III (Figure 6K). Quantification was also attempted with 1D SE-SD ^{1}H SSNMR experiments on pure and formulated mecl and phenaz (Figure 7). For the commercial mecl tablet an API loading of 15.0 wt.% was determined, which is within 2.5 wt.% of the stated mecl loading of 12.5 wt.%. Note that different ^{1}H T_1 values were measured for mecl in bulk and dosage forms (Table S5). All NMR spectra of mecl were obtained with recycle delays of 1.3×T_1 for optimal sensitivity. However, there is likely some uncertainty in the measured T_1 values and this will affect the accuracy of quantification. Quantification could be improved by using longer recycle delays to minimize contributions of longitudinal relaxation to signal differences. For the commercial phenaz tablet the API loading was measured to be 69 wt. % which is within 1 wt.% of the expected value of 68 wt.%. The phenaz quantification was performed with 1D SE-SD experiments that used recycle delays of 5×T_1. We anticipate that the accuracy of API quantification by ^{1}H SSNMR could be further improved by using common practices such as adding an internal standard to the sample,[7] weighing the amount of sample packed into the rotor and/or limiting the sample to the central portion of the rotor to minimize rf homogeneity effects.

Conclusions

In summary, straightforward and highly sensitive 1D and 2D fast MAS ^{1}H SSNMR experiments can be used to rapidly identify the solid forms of dilute APIs within dosage forms. The sensitivity of ^{1}H SSNMR greatly exceeds that of ^{13}C SSNMR, typically enabling one to three order of magnitude reductions in experiment times. Diagnostic ^{1}H SSNMR spectra of dilute APIs within formulations can typically be obtained in minutes, even when the API has unfavorable T_1 relaxation times and low API loading, whereas ^{13}C SSNMR spectra would require hours or days of signal averaging to obtain NMR spectra of similar SNR. ^{1}H SSNMR can permit the routine detection of many APIs that have a long ^{1}H T_1 and/or APIs that are very dilute in a formulation. For theo and mexi the ^{1}H SSNMR spectra of different crystalline forms are distinct, allowing polymorphic forms to be identified and detected on the basis of ^{1}H chemical shifts or on the basis of different responses to saturation and excitation pulses. Experiments on theo mixtures demonstrate that ^{1}H SSNMR spectra are quantitative after calibration on the individual components of the formulation.

While many pharmaceutical samples are amenable to characterization using ^{1}H SSNMR experiments, such methods may not be applicable or useful for all APIs, as was observed for pheny and mexi-I. In cases where the API lacks high frequency ^{1}H NMR signals and/or has a poorly resolved ^{1}H NMR spectrum, both SSPs and SE pulses will be inefficient, and it will be challenging to detect API ^{1}H NMR signals from the formulation and/or obtain meaningful structural information about the API. However, these limitations could be overcome by improving ^{1}H SSNMR resolution and reducing SD rates by using higher magnetic fields and/or faster MAS frequencies. Probes capable of MAS frequencies greater than 100 kHz are becoming widespread and should allow APIs with ^{1}H chemical shifts below 10 ppm to be studied.[27,34] Alternatively, DQ NMR experiments can provide improved resolution and shift

discrimination,[41,42] at the expense of reduced sensitivity. While the focus of the current work has been on pharmaceuticals, the methods described here should also be applicable to study other complex mixtures of organic solids.

Acknowledgments

This material is based upon work supported by the National Science Foundation under Grant No. 1709972 to AJR. We thank Genentech, Inc. and its Innovation Fund, for providing additional financial support for this work. AJR also thanks Iowa State University for additional support. A portion of this work was performed at the National High Magnetic Field Laboratory, which is supported by the National Science Foundation Cooperative Agreement No. DMR-1644779 and the State of Florida.

References

(1) Hörter, D.; Dressman, J. B. Influence of physicochemical properties on dissolution of drugs in the gastrointestinal tract. *Adv. Drug Deliv. Rev.* **1997**, *25*, 3–14.

(2) Huang, L.-F.; Tong, W.-Q. Impact of solid state properties on developability assessment of drug candidates. *Adv. Drug Deliv. Rev.* **2004**, *56*, 321–334.

(3) Hilfiker, R. *Polymorphism*; Hilfiker, R., Ed.; Wiley-VCH: Weinheim, FRG, **2006**.

(4) Berendt, R. T.; Sperger, D. M.; Munson, E. J.; Isbester, P. K. Solid-state NMR spectroscopy in pharmaceutical research and analysis. *TrAC Trends Anal. Chem.* **2006**, *25*, 977–984.

(5) Monti, G. A.; Chattah, A. K.; Linck, Y. G. In *Annual Reports on NMR Spectroscopy*; Elsevier Ltd., **2014**; Vol. 83, pp 221–269.

(6) Skorupska, E.; Jeziorna, A.; Kazmierski, S.; Potrzebowski, M. J. Recent progress in solid-state NMR studies of drugs confined within drug delivery systems. *Solid State Nucl. Magn. Reson.* **2014**, *57–58*, 2–16.

(7) Harris, R. K.; Hodgkinson, P.; Larsson, T.; Muruganantham, A. Quantification of bambuterol hydrochloride in a formulated product using solid-state NMR. *J. Pharm. Biomed. Anal.* **2005**, *38*, 858–864.

(8) Sanchez, S.; Ziarelli, F.; Viel, S.; Delaurent, C.; Caldarelli, S. Improved solid-state NMR quantifications of active principles in pharmaceutical formulations. *J. Pharm. Biomed. Anal.* **2008**, *47*, 683–687.

(9) Virtanen, T.; Maunu, S. L. Quantitation of a polymorphic mixture of an active pharmaceutical ingredient with solid state ^{13}C CPMAS NMR spectroscopy. *Int. J. Pharm.* **2010**, *394*, 18–25.

(10) Zielińska-Pisklak, M.; Pisklak, D. M.; Wawer, I. Application of ^{13}C CPMAS NMR for Qualitative and Quantitative Characterization of Carvedilol and its Commercial Formulations. *J. Pharm. Sci.* **2012**, *101*, 1763–1772.

(11) Tinmanee, R.; Larsen, S. C.; Morris, K. R.; Kirsch, L. E. Quantification of gabapentin polymorphs in gabapentin/excipient mixtures using solid state ^{13}C NMR spectroscopy and X-ray powder diffraction. *J. Pharm. Biomed. Anal.* **2017**, *146*, 29–36.

(12) Ganapathy, S.; Naito, A.; McDowell, C. A. Paramagnetic doping as an aid in obtaining high-resolution carbon-13 NMR spectra of biomolecules in the solid state. *J. Am. Chem. Soc.* **1981**, *103*, 6011–6015.

(13) Brown, C. E. Effects of chemical modification and cobalt(II) chloride addition on the carbon-13 NMR spectra of carnosine as a solid powder. *J. Am. Chem. Soc.* **1982**, *104*, 5608–5610.

(14) Alemany, L. B.; Grant, D. M.; Pugmire, R. J.; Alger, T. D.; Zilm, K. W. Cross polarization and magic angle sample spinning NMR spectra of model organic compounds. 1. Highly protonated molecules. *J. Am. Chem. Soc.* **1983**, *105*, 2133–2141.

(15) Nelson, B. N.; Schieber, L. J.; Barich, D. H.; Lubach, J. W.; Offerdahl, T. J.; Lewis, D. H.; Heinrich, J. P.; Munson, E. J. Multiple-sample probe for solid-state NMR studies of pharmaceuticals. *Solid State Nucl. Magn. Reson.* **2006**, *29*, 204–213.

(16) Lou, X.; Shen, M.; Li, C.; Chen, Q.; Hu, B. Reduction of the ^{13}C cross-polarization experimental time for pharmaceutical samples with long T_1 by ball milling in solid-state NMR. *Solid State Nucl. Magn. Reson.* **2018**, *94*, 20–25.

(17) Rossini, A. J.; Widdifield, C. M.; Zagdoun, A.; Lelli, M.; Schwarzwälder, M.; Copéret, C.; Lesage, A.; Emsley, L. Dynamic Nuclear Polarization Enhanced NMR Spectroscopy for Pharmaceutical Formulations. *J. Am. Chem. Soc.* **2014**, *136*, 2324–2334.

(18) Namespetra, A. M.; Hirsh, D. A.; Hildebrand, M. P.; Sandre, A. R.; Hamaed, H.; Rawson, J. M.; Schurko, R. W. ^{35}Cl solid-state NMR spectroscopy of HCl pharmaceuticals and their polymorphs in bulk and dosage forms. *CrystEngComm* **2016**, *18*, 6213–6232.

(19) Wenslow, R. M. ^{19}F Solid-State NMR Spectroscopic Investigation of Crystalline and Amorphous Forms of a Selective Muscarinic M 3 Receptor Antagonist, in Both Bulk and Pharmaceutical Dosage Form Samples. *Drug Dev. Ind. Pharm.* **2002**, *28*, 555–561.

(20) Brus, J.; Urbanova, M.; Sedenkova, I.; Brusova, H. New perspectives of ^{19}F MAS NMR in the characterization of amorphous forms of atorvastatin in dosage formulations. *Int. J. Pharm.* **2011**, *409*, 62–74.

(21) Patel, J. R.; Carlton, R. A.; Yuniatine, F.; Needham, T. E.; Wu, L.; Vogt, F. G. Preparation and Structural Characterization of Amorphous Spray-Dried Dispersions of Tenoxicam with Enhanced Dissolution. *J. Pharm. Sci.* **2012**, *101*, 641–663.

(22) Burgess, K. M. N.; Perras, F. A.; Lebrun, A.; Messner-Henning, E.; Korobkov, I.; Bryce, D. L. Sodium-23 Solid-State Nuclear Magnetic Resonance of Commercial Sodium Naproxen and its Solvates. *J. Pharm. Sci.* **2012**, *101*, 2930–2940.

(23) Hirsh, D. A.; Rossini, A. J.; Emsley, L.; Schurko, R. W. ^{35}Cl dynamic nuclear polarization solid-state NMR of active pharmaceutical ingredients. *Phys. Chem. Chem. Phys.* **2016**, *18*, 25893–25904.

(24) Maly, T.; Debelouchina, G. T.; Bajaj, V. S.; Hu, K.-N.; Joo, C.-G.; Mak–Jurkauskas, M. L.; Sirigiri, J. R.; van der Wel, P. C. a; Herzfeld, J.; Temkin, R. J.; Griffin, R. G. Dynamic nuclear polarization at high magnetic fields. *J. Chem. Phys.* **2008**, *128*, 052211.

(25) Ni, Q. Z.; Daviso, E.; Can, T. V; Markhasin, E.; Jawla, S. K.; Swager, T. M.; Temkin, R. J.; Herzfeld, J.; Griffin, R. G. High Frequency Dynamic Nuclear Polarization. *Acc. Chem. Res.* **2013**, *46*, 1933–1941.

(26) Zhao, L.; Pinon, A. C.; Emsley, L.; Rossini, A. J. DNP-enhanced solid-state NMR spectroscopy of active pharmaceutical ingredients. *Magn. Reson. Chem.* **2018**, 1–27.

(27) Deschamps, M. Ultrafast Magic Angle Spinning Nuclear Magnetic Resonance. *Annu. Reports NMR Spectrosc.* **2014**, *81*, 109–144.

(28) Ni, Q. Z.; Yang, F.; Can, T. V.; Sergeyev, I. V.; D'Addio, S. M.; Jawla, S. K.; Li, Y.; Lipert, M. P.; Xu, W.; Williamson, R. T.; Leone, A.; Griffin, R. G.; Su, Y. In Situ Characterization of Pharmaceutical Formulations by Dynamic Nuclear Polarization Enhanced MAS NMR. *J. Phys. Chem. B* **2017**, *121*, 8132–8141.

(29) Zhao, L.; Hanrahan, M. P.; Chakravarty, P.; DiPasquale, A. G.; Sirois, L. E.; Nagapudi, K.; Lubach, J. W.; Rossini, A. J. Characterization of Pharmaceutical Cocrystals and Salts by Dynamic Nuclear Polarization-Enhanced Solid-State NMR Spectroscopy. *Cryst. Growth Des.* **2018**, *18*, 2588–2601.

(30) Rossini, A. J.; Zagdoun, A.; Hegner, F.; Schwarzwälder, M.; Gajan, D.; Copéret, C.; Lesage, A.; Emsley, L. Dynamic nuclear polarization NMR spectroscopy of microcrystalline solids. *J. Am. Chem. Soc.* **2012**, *134*, 16899–16908.

(31) Pinon, A. C.; Schlagnitweit, J.; Berruyer, P.; Rossini, A. J.; Lelli, M.; Socie, E.; Tang, M.; Pham, T.; Lesage, A.; Schantz, S.; Emsley, L. Measuring Nano- to Microstructures from Relayed Dynamic Nuclear Polarization NMR. *J. Phys. Chem. C* **2017**, *121*, 15993–16005.

(32) Pinon, A. C.; Rossini, A. J.; Widdifield, C. M.; Gajan, D.; Emsley, L. Polymorphs of Theophylline Characterized by DNP Enhanced Solid-State NMR. *Mol. Pharm.* **2015**, *12*, 4146–4153.

(33) Brown, S. P. Applications of high-resolution ^{1}H solid-state NMR. *Solid State Nucl. Magn. Reson.* **2012**, *41*, 1–27.

(34) Nishiyama, Y. Fast magic-angle sample spinning solid-state NMR at 60–100 kHz for Natural Abundance Samples. *Solid State Nucl. Magn. Reson.* **2016**.

(35) Elena, B.; Pintacuda, G.; Mifsud, N.; Emsley, L. Molecular Structure Determination in Powders by NMR Crystallography from Proton Spin Diffusion. *J. Am. Chem. Soc.* **2006**, *128*, 9555–9560.

(36) Brown, S. P. Probing proton–proton proximities in the solid state. *Prog. Nucl. Magn. Reson. Spectrosc.* **2007**, *50*, 199–251.

(37) Salager, E.; Stein, R. S.; Pickard, C. J.; Elena, B.; Emsley, L. Powder NMR crystallography of thymol. *Phys. Chem. Chem. Phys.* **2009**, *11*, 2610.

(38) Vogt, F. G.; Clawson, J. S.; Strohmeier, M.; Edwards, A. J.; Pham, T. N.; Watson, S. A. Solid-State NMR Analysis of Organic Cocrystals and Complexes. *Cryst. Growth Des.* **2009**, *9*, 921–937.

(39) Baias, M.; Widdifield, C. M.; Dumez, J.-N.; Thompson, H. P. G.; Cooper, T. G.; Salager, E.; Bassil, S.; Stein, R. S.; Lesage, A.; Day, G. M.; Emsley, L. Powder crystallography of pharmaceutical materials by combined crystal structure prediction and solid-state ^{1}H NMR spectroscopy. *Phys. Chem. Chem. Phys.* **2013**, *15*, 8069.

(40) Widdifield, C. M.; Robson, H.; Hodgkinson, P. Furosemide's one little hydrogen atom: NMR crystallography structure verification of powdered molecular organics. *Chem. Commun.* **2016**, *52*, 6685–6688.

(41) Griffin, J. M.; Martin, D. R.; Brown, S. P. Distinguishing Anhydrous and Hydrous Forms of an Active Pharmaceutical Ingredient in a Tablet Formulation Using Solid-State NMR Spectroscopy. *Angew. Chemie Int. Ed.* **2007**, *46*, 8036–8038.

(42) Maruyoshi, K.; Iuga, D.; Watts, A. E.; Hughes, C. E.; Harris, K. D. M.; Brown, S. P. Assessing the Detection Limit of a Minority Solid-State Form of a Pharmaceutical by ^{1}H Double-Quantum Magic-Angle Spinning Nuclear Magnetic Resonance Spectroscopy. *J. Pharm. Sci.* **2017**, *106*, 3372–3377.

(43) Zhou, D. H.; Rienstra, C. M. Rapid Analysis of Organic Compounds by Proton-Detected Heteronuclear Correlation NMR Spectroscopy with 40 kHz Magic-Angle Spinning. *Angew. Chemie Int. Ed.* **2008**, *47*, 7328–7331.

(44) Hildebrand, M.; Hamaed, H.; Namespetra, A. M.; Donohue, J. M.; Fu, R.; Hung, I.; Gan, Z.; Schurko, R. W. ^{35}Cl solid-state NMR of HCl salts of active pharmaceutical ingredients: structural prediction, spectral fingerprinting and polymorph recognition. *CrystEngComm* **2014**, *16*, 7334.

(45) Fucke, K.; McIntyre, G. J.; Wilkinson, C.; Henry, M.; Howard, J. A. K.; Steed, J. W. New Insights into an Old Molecule: Interaction Energies of Theophylline Crystal Forms. *Cryst. Growth Des.* **2012**, *12*, 1395–1401.

(46) Harris, R. K.; Becker, E. D.; Cabral de Menezes, S. M.; Granger, P.; Hoffman, R. E.; Zilm, K. W. Further conventions for NMR shielding and chemical shifts (IUPAC Recommendations 2008). *Pure Appl. Chem.* **2008**, *80*, 59–84.

(47) Cory, D. .; Ritchey, W. . Suppression of signals from the probe in bloch decay spectra. *J. Magn. Reson.* **1988**, *80*, 128–132.

(48) Bodenhausen, G.; Freeman, R.; Morris, G. A. A Simple Pulse Sequence for Selective Excitation in Fourier-Transform Nmr. *J. Magn. Reson.* **1976**, *23*, 171–175.

(49) Morris, G. A.; Freeman, R. Selective excitation in Fourier transform nuclear magnetic resonance. *J. Magn. Reson.* **1978**, *29*, 433–462.

(50) Pines, A.; Gibby, M. G.; Waugh, J. S. Proton-Enhanced Nuclear Induction Spectroscopy. A Method for High Resolution NMR of Dilute Spins in Solids. *J. Chem. Phys.* **1972**, *56*, 1776–1777.

(51) Song, Z.; Antzutkin, O. N.; Feng, X.; Levitt, M. H. Sideband suppression in magic-angle-spinning NMR by a sequence of 5 π pulses. *Solid State Nucl. Magn. Reson.* **1993**, *2*, 143–146.

(52) Antzutkin, O. N. Sideband manipulation in magic-angle-spinning nuclear magnetic resonance. *Prog. Nucl. Magn. Reson. Spectrosc.* **1999**, *35*, 203–266.

(53) Peersen, O. B.; Wu, X. L.; Kustanovich, I.; Smith, S. O. Variable-Amplitude Cross-Polarization MAS NMR. *J. Magn. Reson. Ser. A* **1993**, *104*, 334–339.

(54) Fung, B. M.; Khitrin, A. K.; Ermolaev, K. An Improved Broadband Decoupling Sequence for Liquid Crystals and Solids. *J. Magn. Reson.* **2000**, *142*, 97–101.

(55) Santos, S. M.; Rocha, J.; Mafra, L. NMR Crystallography: Toward Chemical Shift-Driven Crystal Structure Determination of the β-Lactam Antibiotic Amoxicillin Trihydrate. *Cryst. Growth Des.* **2013**, *13*, 2390–2395.

(56) Robertson, A. J.; Pandey, M. K.; Marsh, A.; Nishiyama, Y.; Brown, S. P. The use of a selective saturation pulse to suppress t 1 noise in two-dimensional ^{1}H fast magic angle spinning solid-state NMR spectroscopy. *J. Magn. Reson.* **2015**, *260*, 89–97.

(57) Brinkmann, A.; Kentgens, A. P. M. Proton-Selective ^{17}O− ^{1}H Distance Measurements in Fast Magic-Angle-Spinning Solid-State NMR Spectroscopy for the Determination of Hydrogen Bond Lengths. *J. Am. Chem. Soc.* **2006**, *128*, 14758–14759.

(58) Mithu, V. S.; Tan, K. O.; Madhu, P. K. Selective inversion of ^{1}H resonances in solid-state nuclear magnetic resonance: Use of double-DANTE pulse sequence. *J. Magn. Reson.* **2013**, *237*, 11–16.

(59) Paulekuhn, G. S.; Dressman, J. B.; Saal, C. Trends in Active Pharmaceutical Ingredient Salt Selection based on Analysis of the Orange Book Database. *J. Med. Chem.* **2007**, *50*, 6665–6672.

(60) Caravatti, P.; Neuenschwander, P.; Ernst, R. R. Characterization of Heterogeneous Polymer Blends by Two-Dimensional Proton Spin Diffusion Spectroscopy. *Macromolecules* **1985**, *18*, 119–122.

(61) Schmidt-Rohr, K.; Spiess, H. W. *Multidimensional Solid-State NMR and Polymers*; Academic Press Ltd.: London, UK, **1994**.

(62) Peter Cheung, T. T. In *Encyclopedia of Magnetic Resonance*; John Wiley & Sons, Ltd: Chichester, UK, **2007**; Vol. 84, pp 83–121.

(63) Suter, D.; Ernst, R. R. Spectral spin diffusion in the presence of an extraneous dipolar reservoir. *Phys. Rev. B* **1982**, *25*, 6038–6041.

(64) Ernst, M.; Meier, B. H. In *Solid State NMR of Polymers*; Ando, I., Asakura, T., Eds.; Elsevier B.V., **1998**; pp 83–121.

(65) Freeman, R. Selective excitation in high-resolution NMR. *Chem. Rev.* **1991**, *91*, 1397–1412.

(66) Elena, B.; Emsley, L. Powder Crystallography by Proton Solid-State NMR Spectroscopy. *J. Am. Chem. Soc.* **2005**, *127*, 9140–9146.

(67) Oikawa, T.; Okumura, M.; Kimura, T.; Nishiyama, Y. Solid-state NMR meets electron diffraction: determination of crystalline polymorphs of small organic microcrystalline samples. *Acta Crystallogr. Sect. C Struct. Chem.* **2017**, *73*, 219–228.

(68) Ye, Y. Q.; Malon, M.; Martineau, C.; Taulelle, F.; Nishiyama, Y. Rapid measurement of multidimensional ^{1}H solid-state NMR spectra at ultra-fast MAS frequencies. *J. Magn. Reson.* **2014**, *239*, 75–80.

(69) Robyr, P.; Meier, B. H.; Ernst, R. R. Radio-frequency-driven nuclear spin diffusion in solids. *Chem. Phys. Lett.* **1989**, *162*, 417–423.

Appendix for supporting information

Table S1. Dosage and the API loading of the commercial tablets used in the study.

Commercial Tablet	Dosage/(mg)	Mass of a tablet/(mg)	API loading/ (w/w %)
Mecl	25.0	201.3	12.4
Phenaz	97.5	143.2	68.1
Pheny	10.0	141.5	7.1

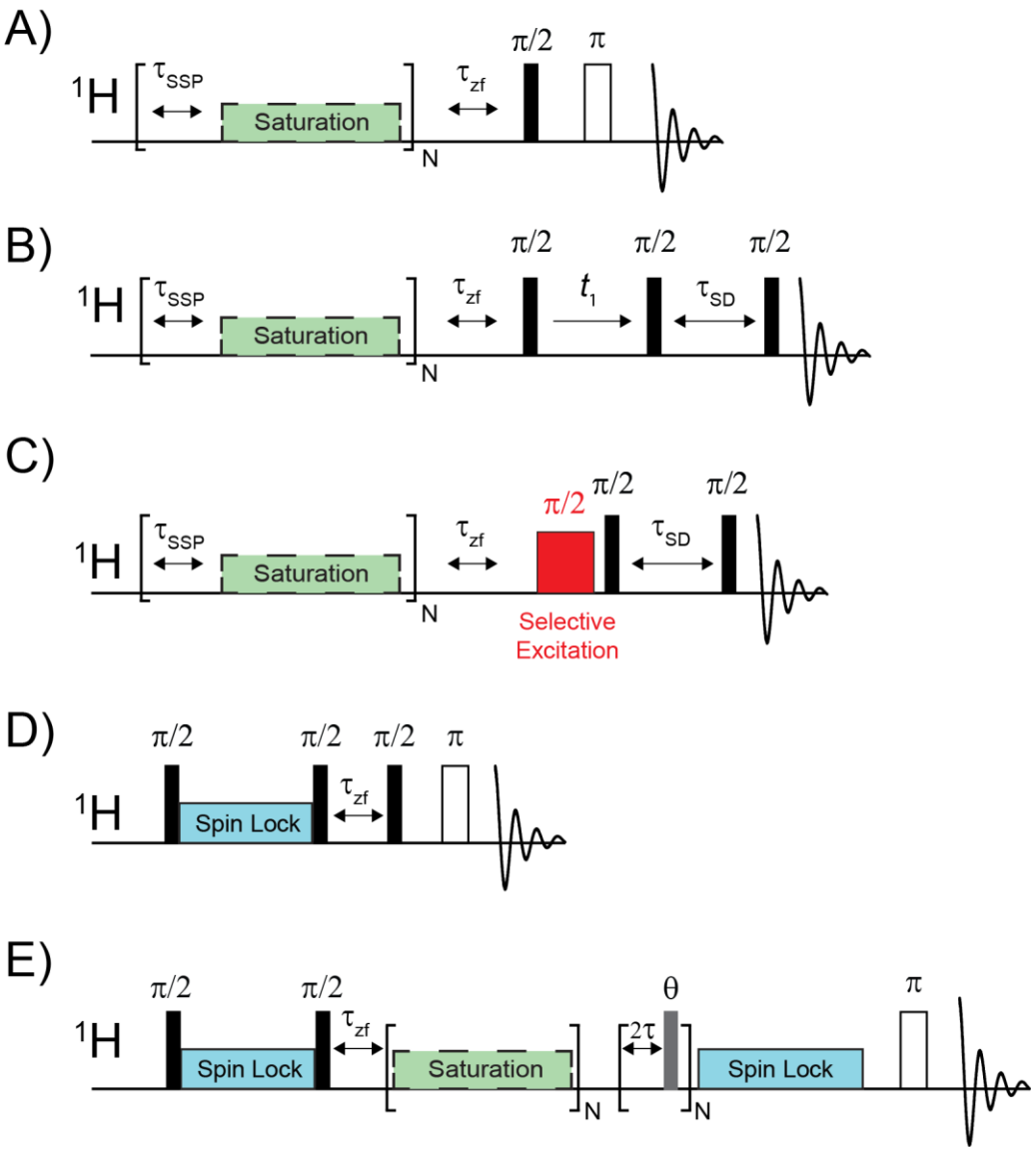

Figure S1. Diagrams of the pulse sequences used in this work. A) SSP optimization pulse sequence, B) 2D ^{1}H spin diffusion with SSP, C) 1D ^{1}H SE-SD, D) 1H spin echo with 1H spin-lock pulse to enhance longitudinal relaxation by ^{1}H spin diffusion and E) 1D SE-SD with spin-lock pulse to enhance ^{1}H longitudinal relaxation and DANTE SE pulse train. In each sequence, dashed

green boxes indicate the optional inclusion of a selective saturation pulse (SSP). τ_{zf} denotes a *z*-filter delay that follows the final SSP. τ_{SSP} denotes a z-filter/spin diffusion delay in between the SSP.

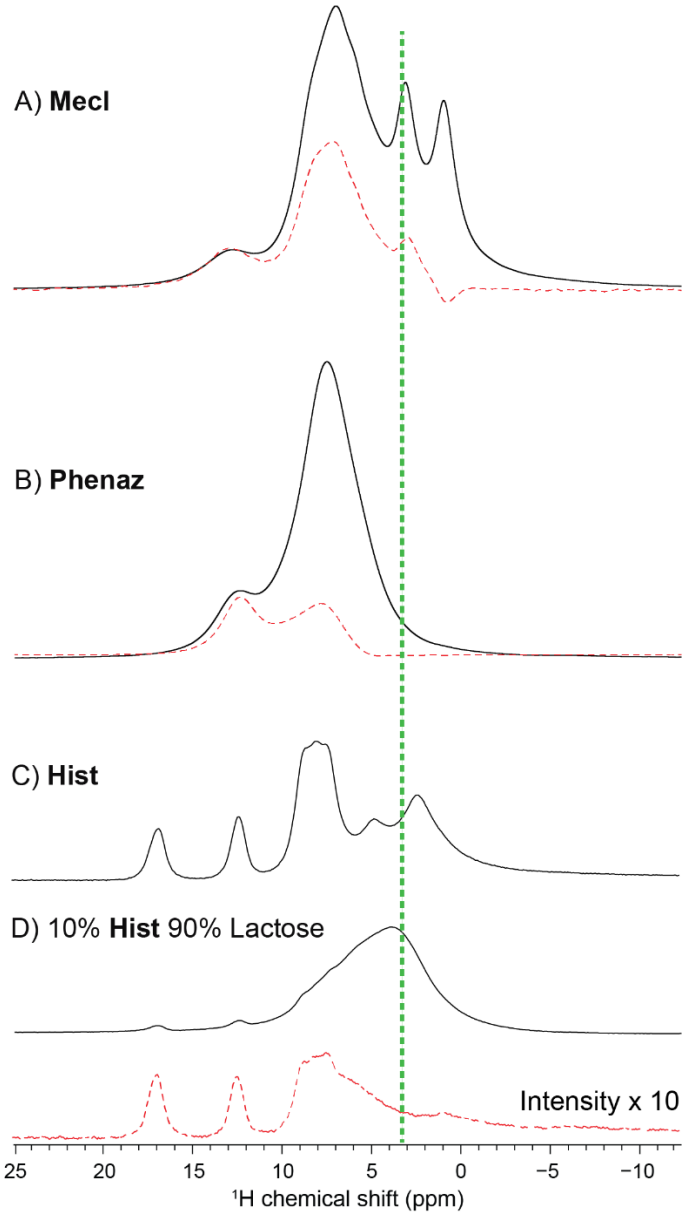

Figure S2. Comparison of ^{1}H spin echo solid-state NMR spectra obtained without (solid trace) or with a single 6 ms SSP (dashed trace) for A) mecl, B) phenaz, C) hist and D) a 10 wt-% hist, 90 wt-% lactose physical mixture. The SSP was applied at an offset of 3.5 ppm in all cases. hist is a convenient sample for the setup and optimization of SSPs, selective excitation pulses and 2D ^{1}H SD NMR experiments incorporating both elements. All spectra acquired at B_0 = 9.4 T with ν_{rot} = 50 kHz the pulse sequence shown in Figure S1A.

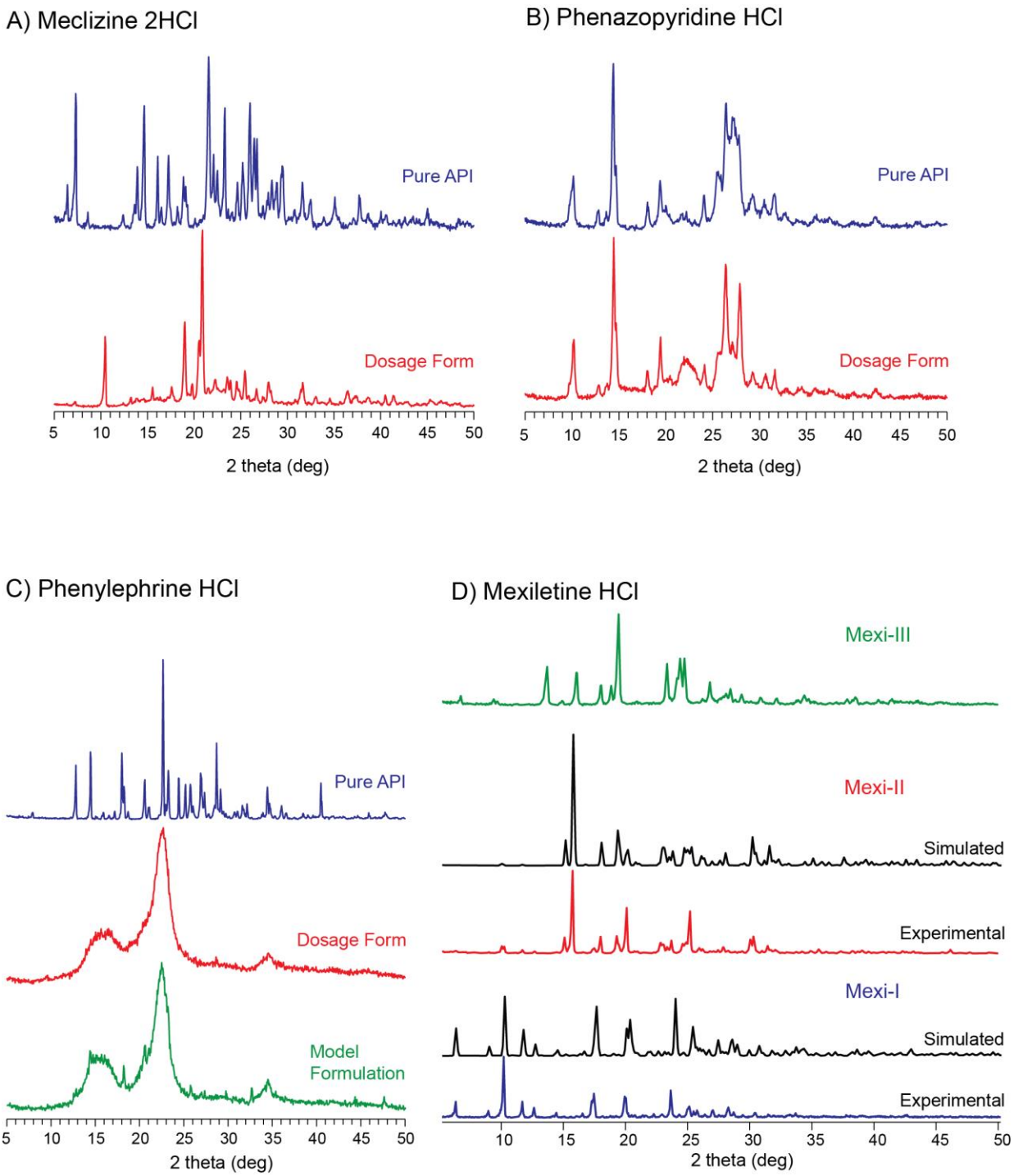

Figure S3. Experimental PXRD patterns for the samples used in this work. The simulated PXRD patterns for mexi-I and mexi-II were calculated from the previously reported single crystal X-ray diffraction structures (CSD codes: JIZJEH and JIZJEH01, respectively).

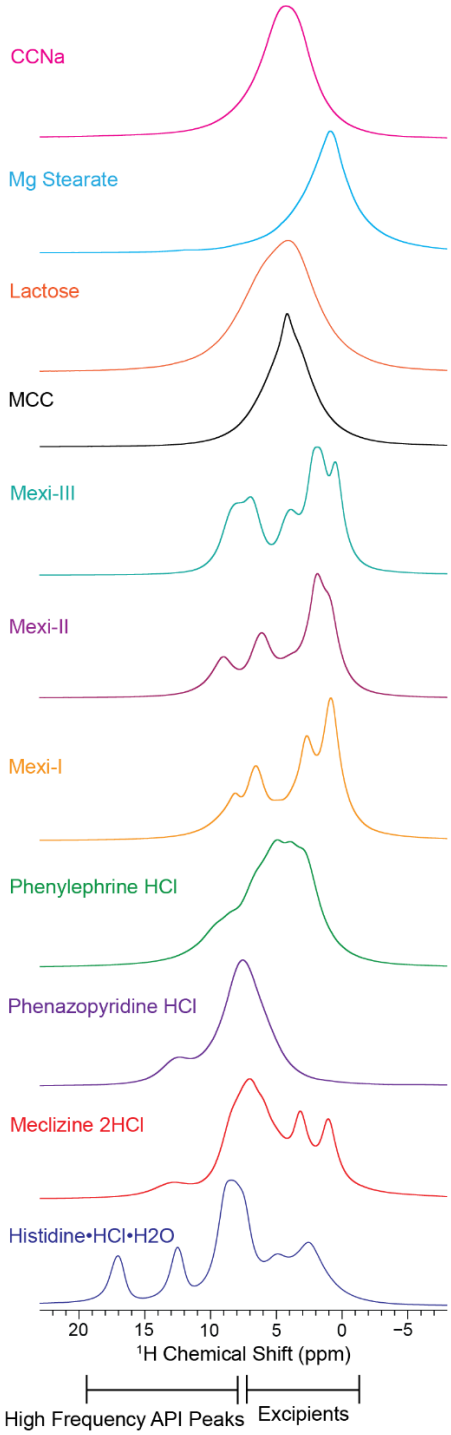

Figure S4. MAS ^{1}H spin-echo NMR spectra of commonly encountered excipients and the APIs studied in this work acquired at $B_0 = 9.4$ T with $\nu_{rot} = 50$ kHz. CCNa is sodium croscarmellose and Mg Stearate is magnesium stearate. All other compounds are defined in Figure 1 of the main text.

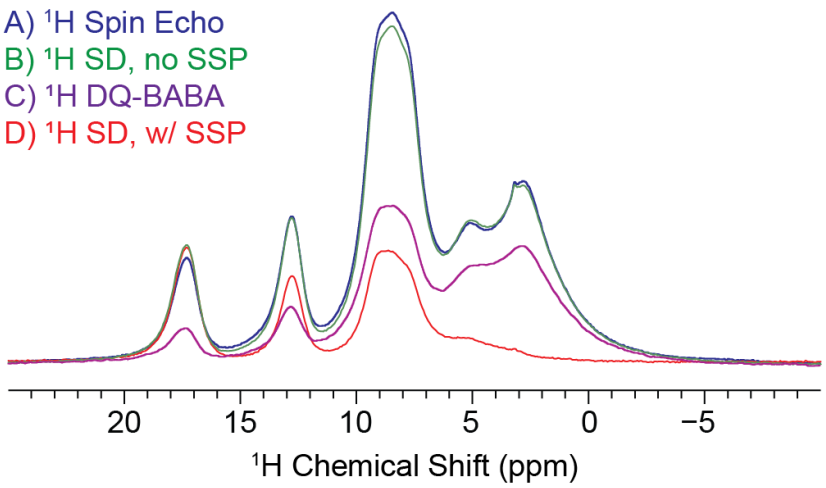

Figure S5. MAS ^{1}H SSNMR spectra of hist acquired with different pulse sequences A) spin echo, B) 2D ^{1}H SD without SSP, C) DQ-filtered spectrum obtained with the BABA pulse sequence and D) 2D ^{1}H SD obtained with a SSP applied at 3.5 ppm. For the 2D NMR experiments, the spectra were obtained from the first t_1 increment of the 2D experiment. The sensitivity of the high frequency feature at *ca.* 17 ppm is similar for all the SQ experiments (A), B), and D)) but substantially decreased in the DQ experiment (C). All experiments were performed at B_0 = 9.4 T with ν_{rot} = 50 kHz.

.

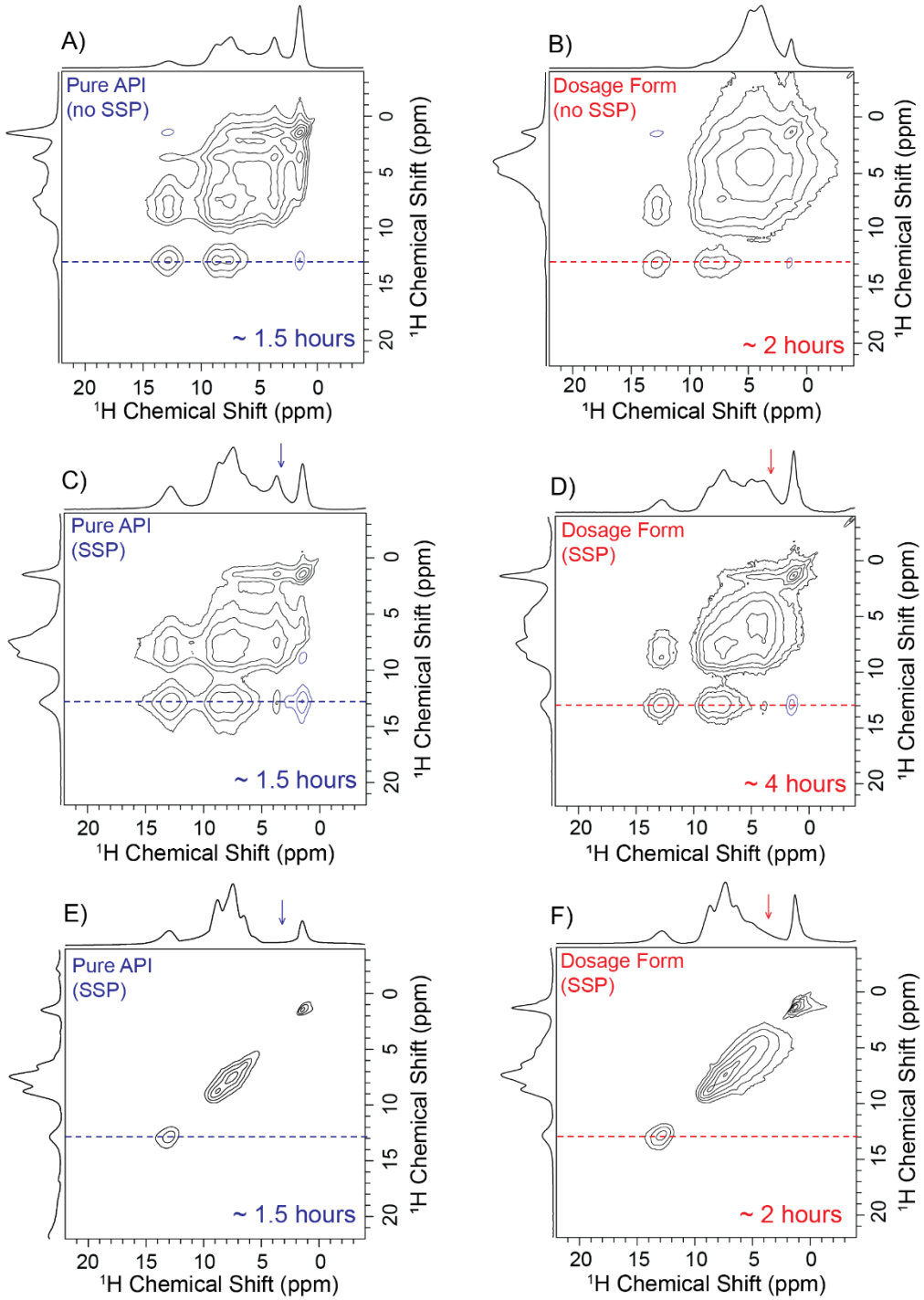

Figure S6. 2D ^{1}H SD NMR spectra of mecl pure (left column) and a commercial mecl tablet with 12.5 wt-% API (right column) acquired at B_0 = 18.8 T with ν_{rot} = 50 kHz. A) and B) acquired without SSP and with a 20 ms spin diffusion period, C) and D) acquired with a 6 ms SSP applied at 3.5 ppm and a 20 ms spin diffusion period. E) and F) were acquired with a 6 ms SSP applied at 3.5 ppm and no spin diffusion period. Rows indicated with the dashed lines are shown in Figure S7. Arrows indicate the frequency of the SSP. Total experiment times are indicated on the 2D NMR spectra.

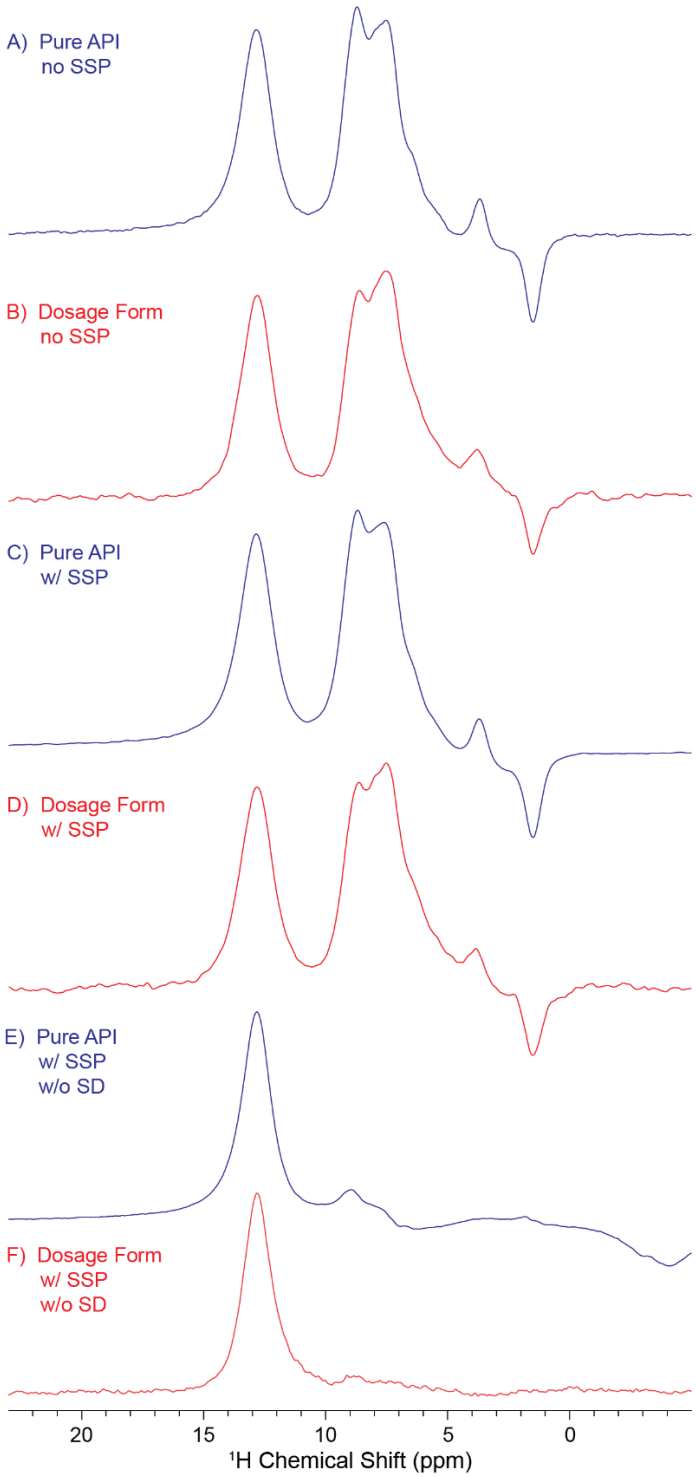

Figure S7. ^{1}H SSNMR spectra of mecl extracted from the indicated rows of the 2D SD ^{1}H NMR spectra shown in Figure S6. NMR spectra shown in (A-D) were acquired with 20 ms spin diffusion delay, while those in E) and F) were obtained without a diffusion delay.

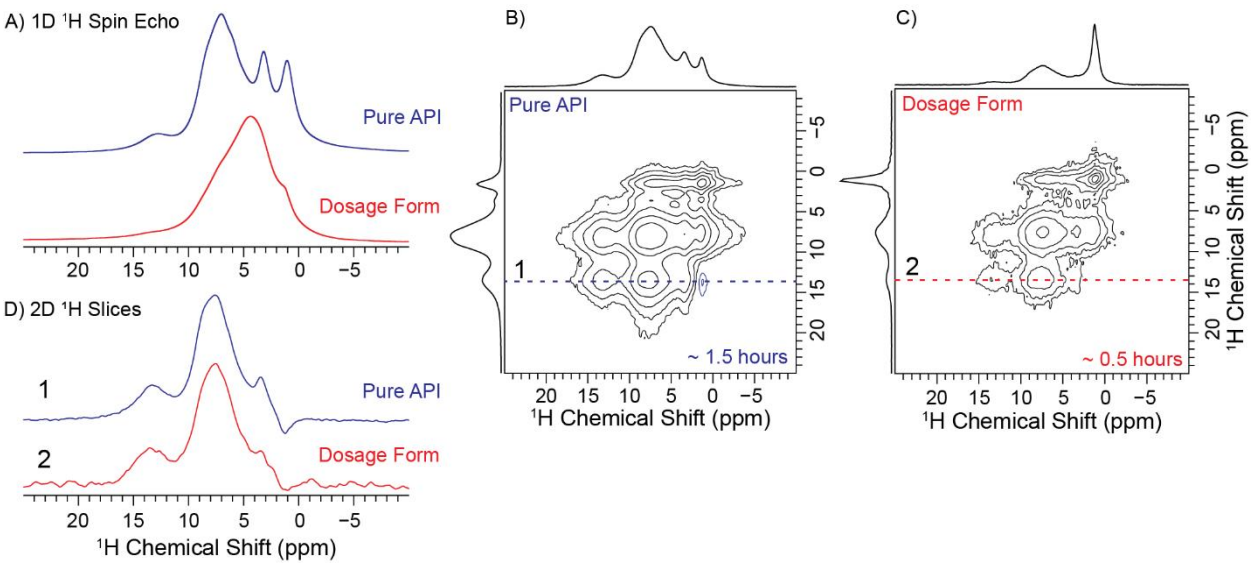

Figure S8. MAS ^{1}H SSNMR spectra of mecl pure and a commercial mecl tablet acquired at B_0 = 9.4 T with ν_{rot} = 50 kHz. A) 1D spin echo NMR spectra. B) and C) 2D ^{1}H SD NMR spectra acquired with a SSP applied at 3.5 ppm and a 20 ms spin diffusion period (see Figure S1 for the corresponding pulse sequence). D) 1D ^{1}H NMR spectra extracted from rows of the 2D NMR spectra, indicated with dashed lines.

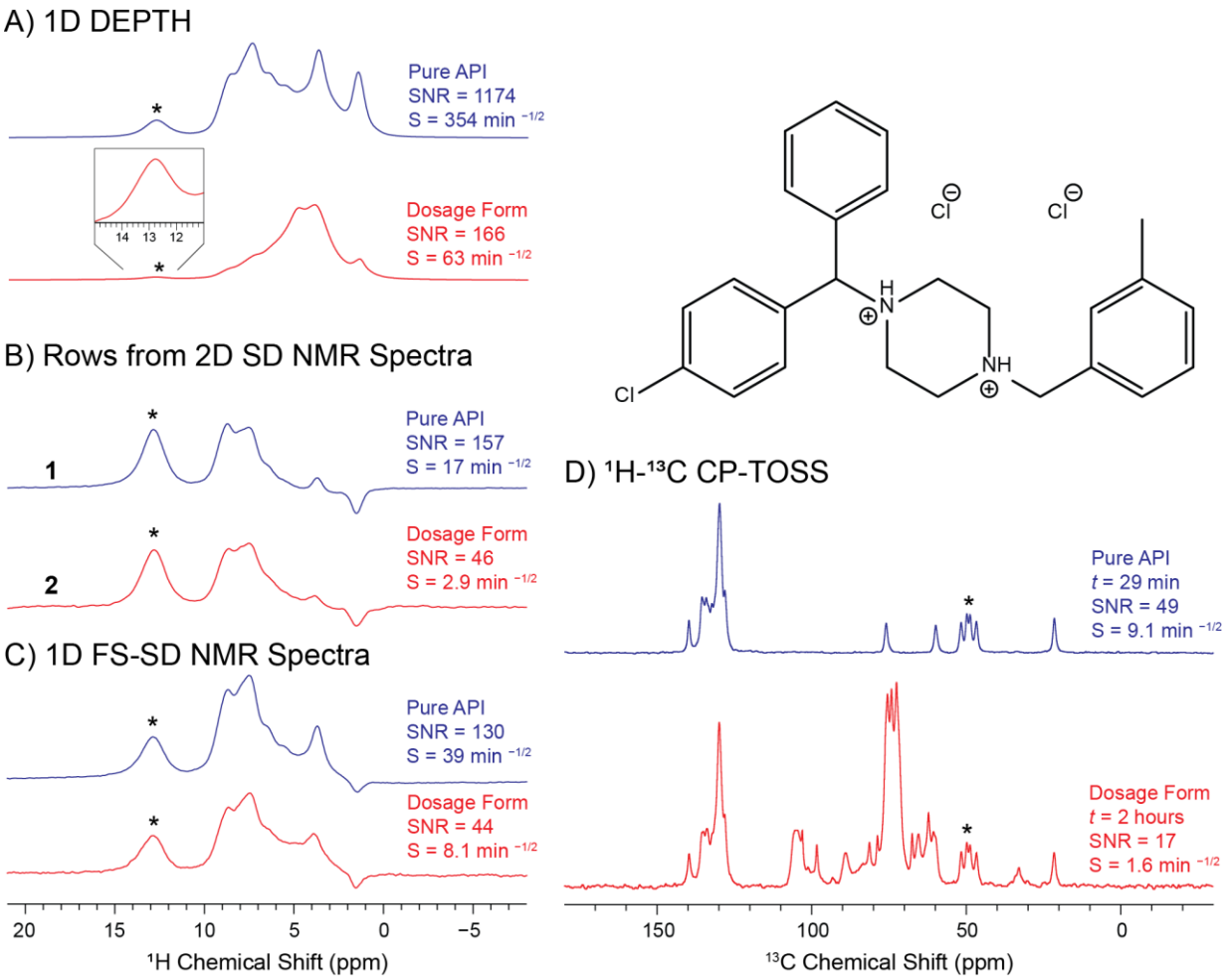

Figure S9. MAS ^{1}H and ^{1}H-^{13}C CP-TOSS SSNMR spectra of pure mecl (blue traces) and a mecl tablet (red traces). A) 1D DEPTH ^{1}H SSNMR spectra, B) ^{1}H SSNMR spectra extracted from rows of the 2D NMR spectra shown in Figure 2 of the main text, C) 1D SE-SD NMR SSNMR spectra, D) ^{1}H-^{13}C CP-TOSS. The sensitivities (*S*) and SNR ratios of the API signals are listed with each spectrum. The asterisks denote the peak used for determination of SNR and calculation of *S*. Note that because of signal overlap from multiple carbon atoms the aromatic ^{13}C NMR signals at *ca*. 130 ppm have much higher intensity, SNR and *S* than the NMR signal at 50 ppm used for determination of ^{13}C sensitivity (S = 5.8 min$^{-1/2}$ for the aromatic signals in the tablet). However, because of the peak overlap, the aromatic carbon NMR signals will likely not be diagnostic for different solid forms of mecl. Consequently, the second most intense and resolved ^{13}C NMR signal at *ca*. 50 ppm was used for the determination of ^{13}C sensitivity. ^{1}H SSNMR experiments were performed with 1.3 mm rotors, B_0 = 18.8 T and ν_{rot} = 50 kHz (left column). ^{1}H-^{13}C CP-TOSS SSNMR experiments were performed with 4.0 mm rotors, B_0 = 9.4 T and ν_{rot} = 8 kHz (right column).

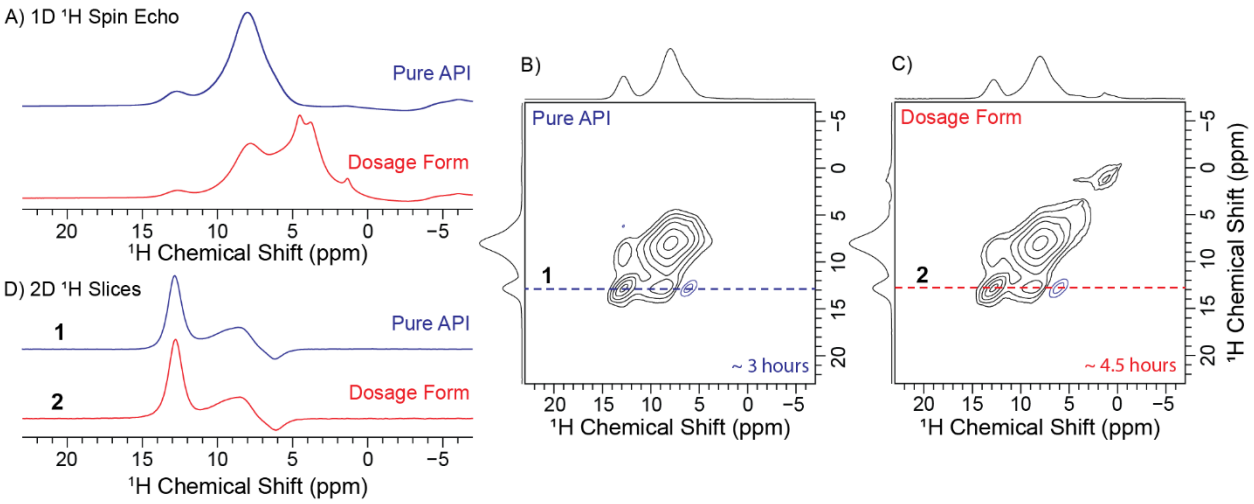

Figure S10. MAS ^{1}H SSNMR spectra of pure phenaz and a commercial phenaz tablet acquired at B_0 = 18.8 T with ν_{rot} = 50 kHz. A) 1D spin echo NMR spectra. B) and C) 2D ^{1}H SD NMR spectra acquired with a SSP applied at 3.5 ppm and a 20 ms spin diffusion time. D) ^{1}H SD NMR spectra extracted from the indicated rows of the 2D NMR spectra. Total experiment times are indicated on the 2D NMR spectra.

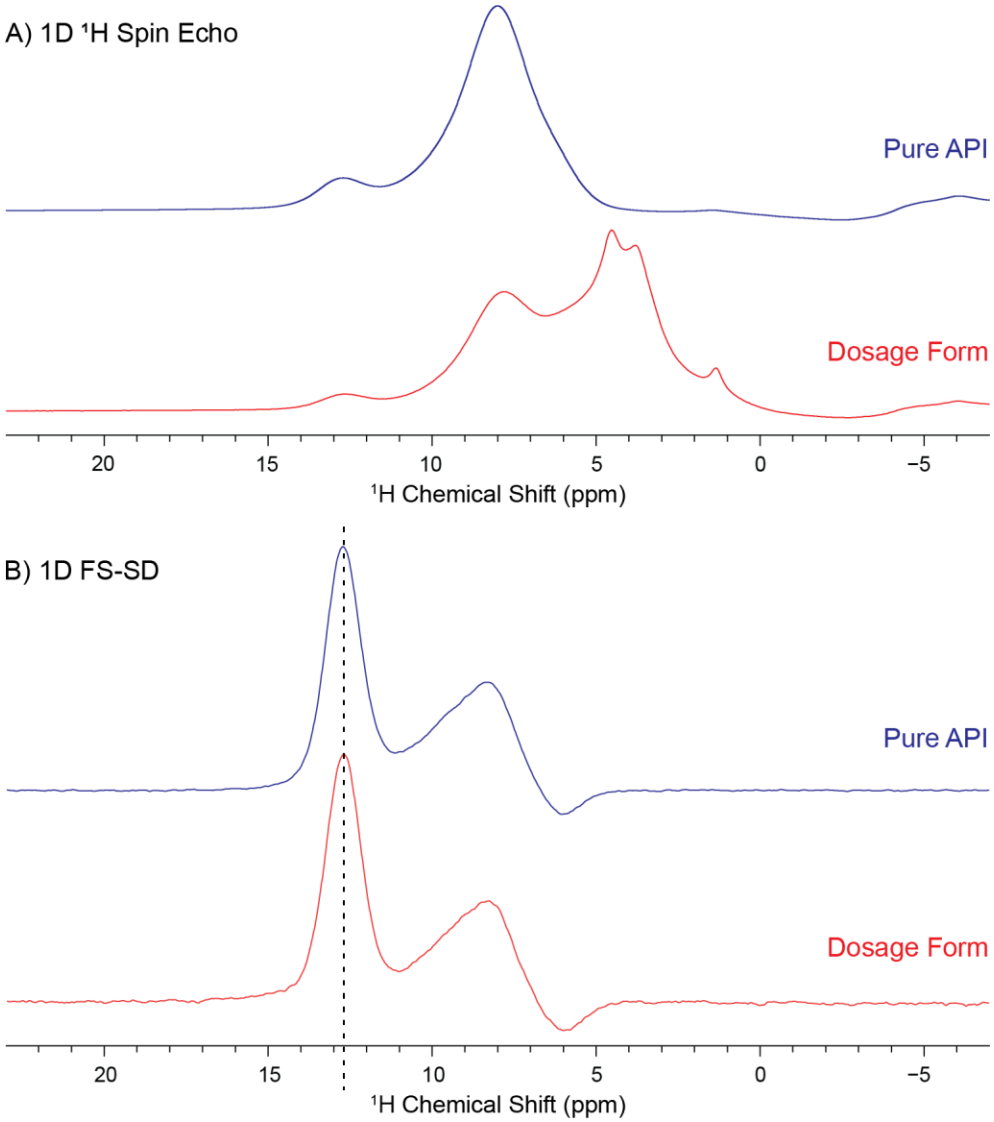

Figure S11. MAS ^{1}H SSNMR spectra acquired at B_0 = 18.8 T with ν_{rot} = 50 kHz of phenaz pure (blue traces) and a commercial phenaz tablet with 68-wt% API loading (red traces). A) ^{1}H spin echo SSNMR spectra. B) 1D SE-SD NMR spectra obtained with a 20 ms spin diffusion time. The dashed line indicates the transmitter position for the selective excitation pulse. The NMR spectrum of the phenaz tablet in B) was obtained in 4 minutes.

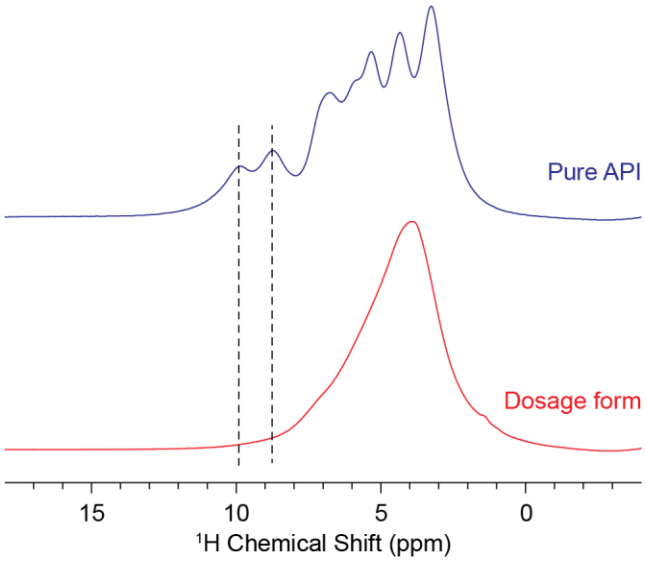

Figure S12. 1D ^{1}H MAS SSNMR spectra of pheny pure and a commercial pheny tablet. Both spectra were acquired at B_0 = 18.8 T with ν_{rot} = 50 kHz. Dashed lines indicate positions of the two features assigned to crystallographically-distinct ammonium protons in the pure material. These features are not visible in the spectrum of the dosage material likely because the API exists in a different solid phase in the tablet.

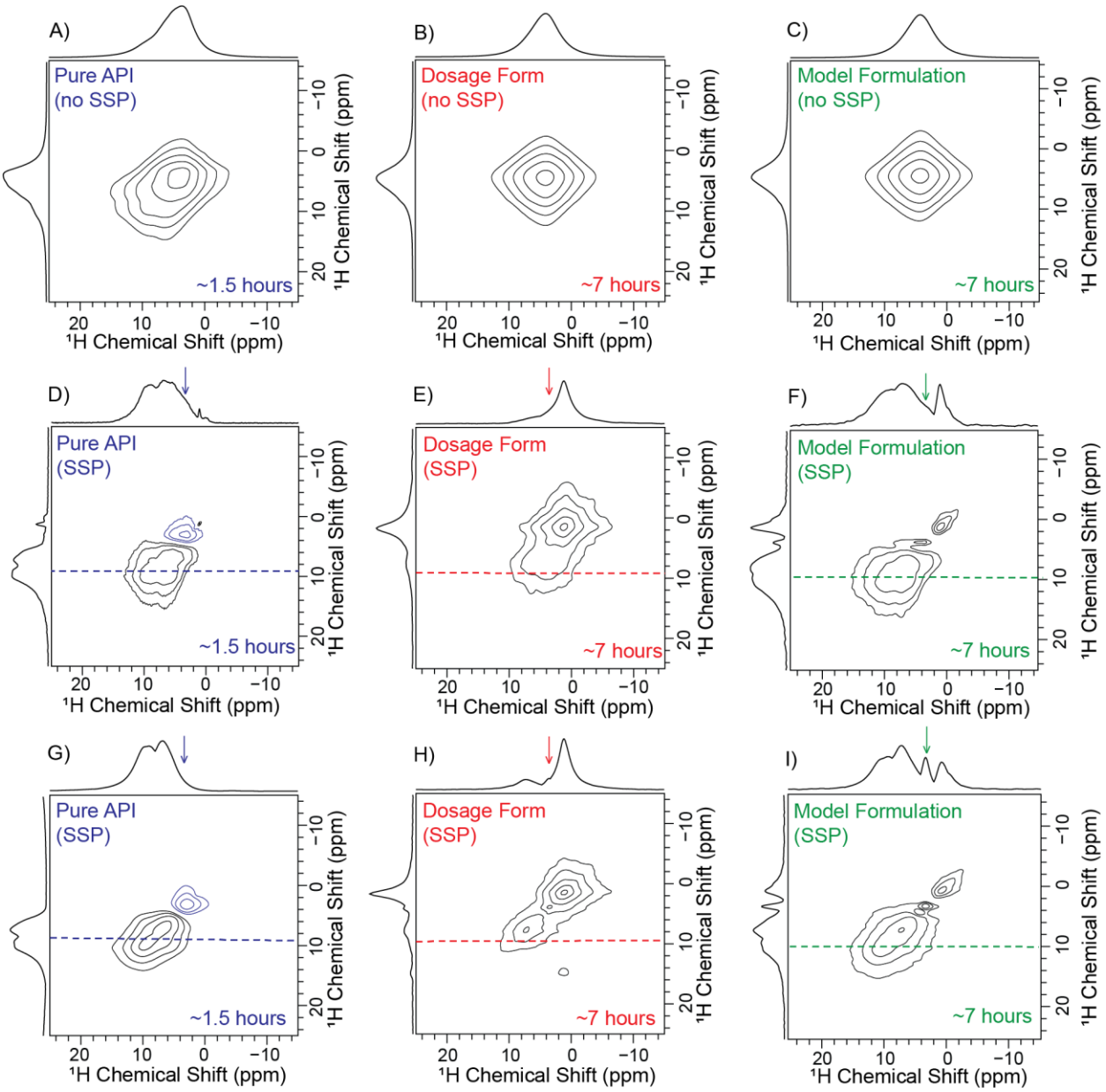

Figure S13. 2D ^{1}H SD NMR spectra of pure pheny (left column), a commercial 7 wt-% pheny tablet (middle column) and a model formulation consisting of a physical mixture of 7 wt-% pheny in MCC (right column). All spectra were acquired at B_0 = 9.4 T with ν_{rot} = 50 kHz. A), B) and C) acquired with 20 ms spin diffusion and no SSP D), E) and F) acquired with 20 ms spin diffusion and a 6 ms SSP applied at 4.5 ppm and G), H) and I) acquired with no spin diffusion period and a 6 ms SSP applied at 4.5 ppm. Rows indicated with the dashed lines are shown in Figure S14. The arrow indicates the transmitter offset of the SSP. Total experiment times are indicated on the 2D NMR spectra.

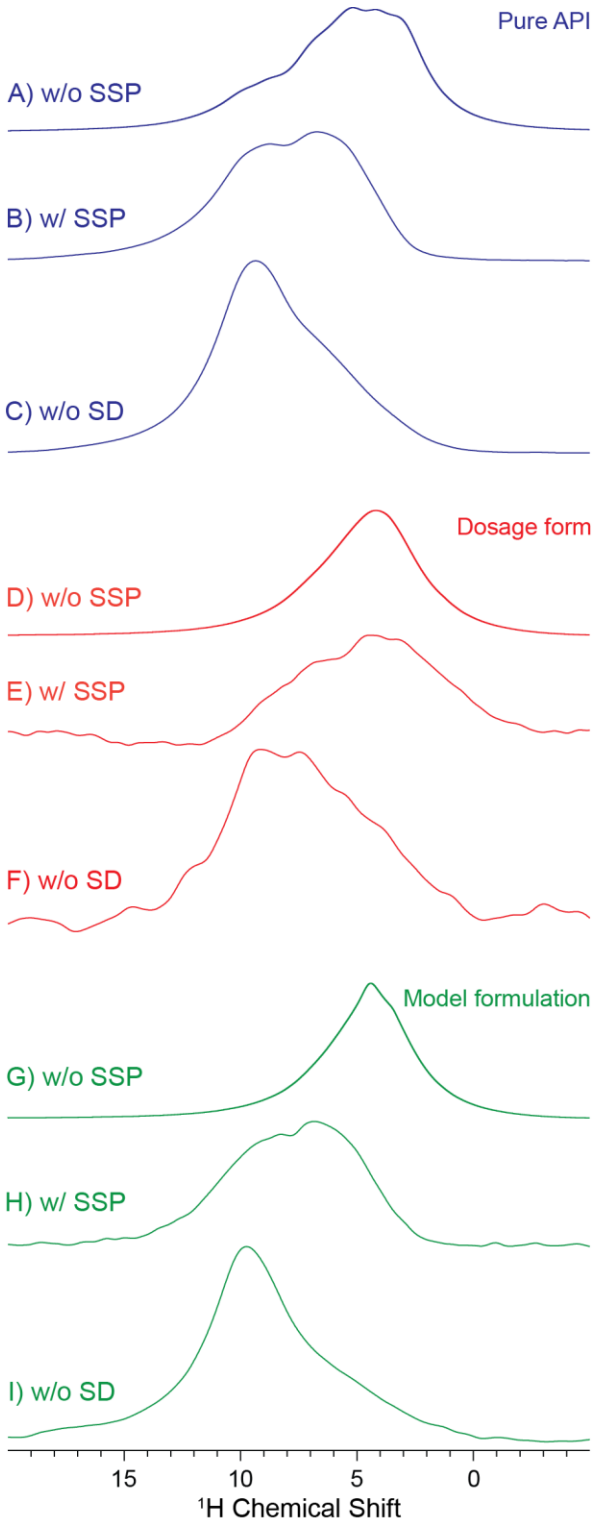

Figure S14. MAS ^{1}H SSNMR spectra of pure pheny (blue), commercial pheny tablet (red), and a model pheny formulation (green). A), D), and G) 1D ^{1}H spin echo NMR spectra. B), C), E), F), H) and I) 1D NMR spectra extracted from rows of the 2D ^{1}H SD NMR spectra were obtained at a 9.9 ppm chemical shift in the indirect dimension (Figure S13). All NMR spectra were acquired at B_0 = 9.4 T with ν_{rot} = 50 kHz.

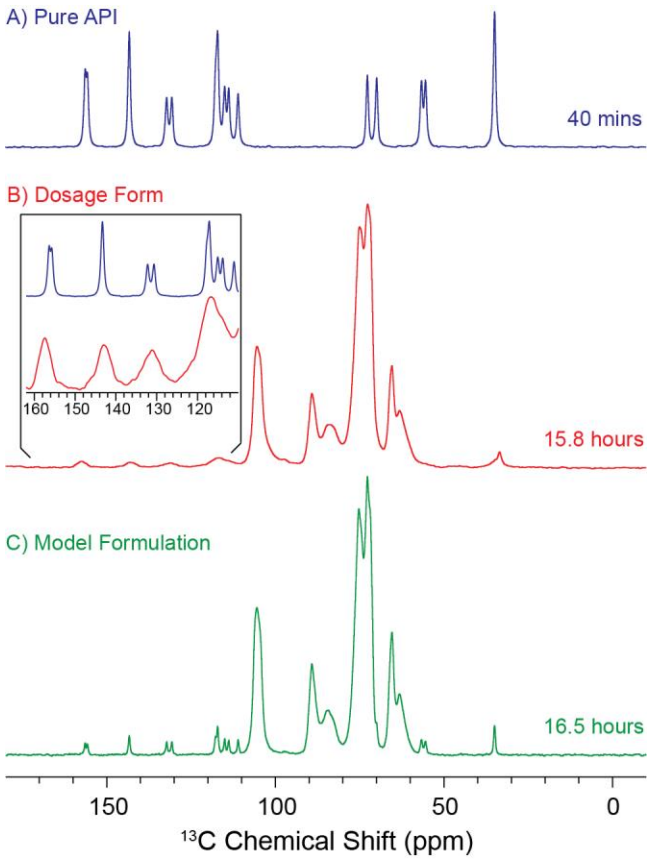

Figure S15. ^{1}H-^{13}C CP-TOSS/MAS spectra of A) pure pheny, B) a commercial pheny tablet with 7 wt-% API and C) a model formulation consisting of a physical mixture of 7 wt-% pure pheny and MCC. The inset in B) compares spectra of pure crystalline pheny and the commercial pheny tablet. All spectra were acquired with B_0 = 9.4 T, a 4.0 mm rotor and ν_{rot} = 8 kHz. Total experiment times are indicated. The ^{13}C SSNMR spectra suggest that the commercial tablet contains a different solid form of pheny that is clearly different from the crystalline pure form. The pheny in the tablet is likely amorphous.

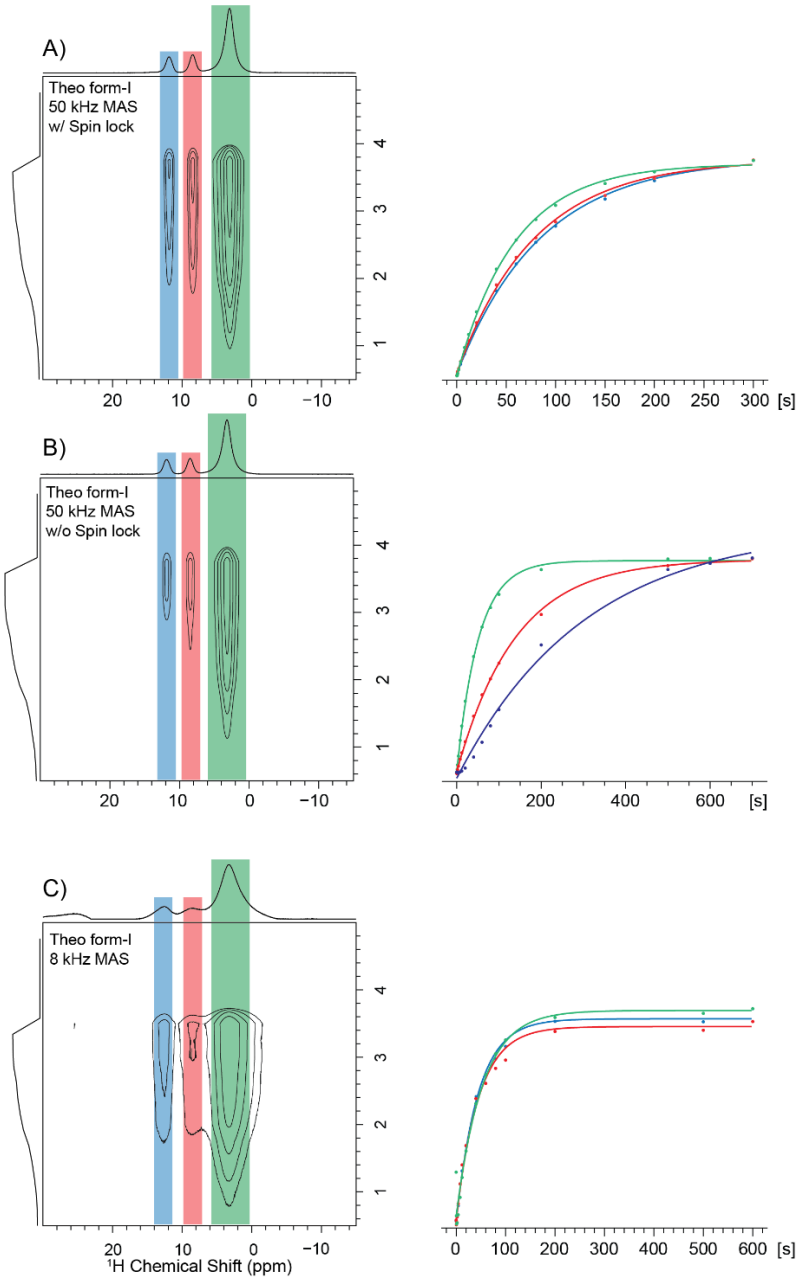

Figure S16. Summary of ^{1}H saturation recovery experiments on theo-I. Signal build-up plots are shown for the amine (NH, blue), methine (CH, red) and methyl (CH_3, green) protons of theo-I. The saturation recovery experiments were performed with A) 50 kHz MAS and a 1.8 ms spin-lock pulse to promote spin diffusion from methyl ^{1}H to the other ^{1}H, B) 50 kHz MAS without a spin-lock pulse and C) 8 kHz MAS. All experiments were performed with B_0 = 9.4 T. T_1 values determined form curve fits are shown in Tables S2 and S3.

Table S2. T_1 (^{1}H) measured for theo-I and theo-II with 8 kHz MAS

Polymorph	T_1 (s)		
	-NH	-CH	-CH_3
theo-I	45	45	53
theo-II	49	56	64

Table S3. T_1 (^{1}H) measured for theo-I and theo-II with 50 kHz MAS

Polymorph	T_1(s)[a]			T_1 w/ ^{1}H spin-lock (s)[b]		
	-NH	-CH	-CH_3	-NH	-CH	-CH_3
theo-I	303	139	52	85	78	59
theo-II	463	109	61	73	72	65

[a]Measured with a standard saturation recovery pulse sequence.
[b]Measured with a 1.8 ms ^{1}H spin-lock pulse inserted prior to the final excitation pulse (pulse sequence similar to that depicted in Figure S1D). The ^{1}H spin-lock pulse promotes spin diffusion between the methyl ^{1}H and high frequency amine and methine ^{1}H spins, resulting in a reduction in the apparent T_1 of the amine and methine.

Table S4. Data used for the calibration plot in Figure 7 of the main text.

theo-II wt. (%)	Integrated Intensity	Predicted theo-II wt.%[a]	Absolute wt.% Error (wt. %)	Percentage Error (%)
2	1.54	1.50	0.50	24.9
4	4.02	3.92	0.08	1.98
6.1	6.89	6.72	0.62	10.1
9.8	9.80	9.55	0.25	2.55
			Average = 0.36 wt.%	Average = 9.9 %

[a] The predicted theo-II wt.% was calculated using the equation from the calibration curve:

Predicted wt.% = (Integrated Intensity)/1.03.

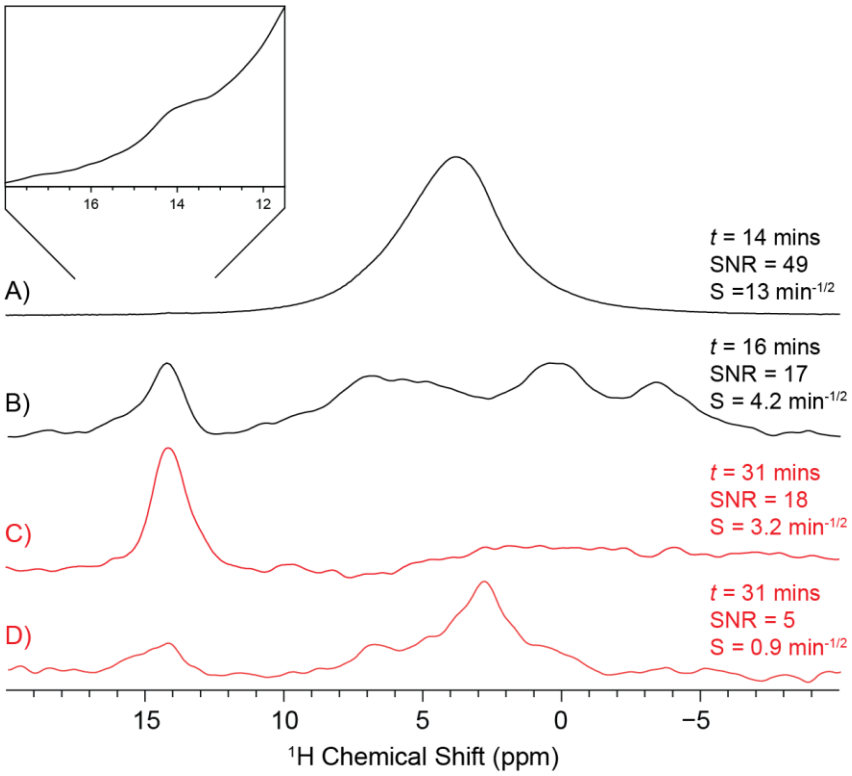

Figure S17. ^{1}H SSNMR spectra of a physical mixture of 98 wt% MCC and 2 wt% theo-II. ^{1}H spin echo spectrum recorded (A) without and (B) with SSP on resonance with MCC. (C, D) 1D SE-SD ^{1}H SSNMR spectra with the DANTE excitation pulse on resonance with the high frequency amine ^{1}H NMR signal of theo-II. The 1D SE-SD spectrum in (C) was recorded with a 20 μs spin-lock pulse to minimize ^{1}H spin diffusion. The 1D SE-SD spectrum in (D) was obtained with a 1.8 ms spin-lock pulse following the SE DANTE pulse to promote ^{1}H spin diffusion. ^{1}H SSNMR spectra were obtained with a 50 kHz MAS frequency at B_0 = 9.4 T.

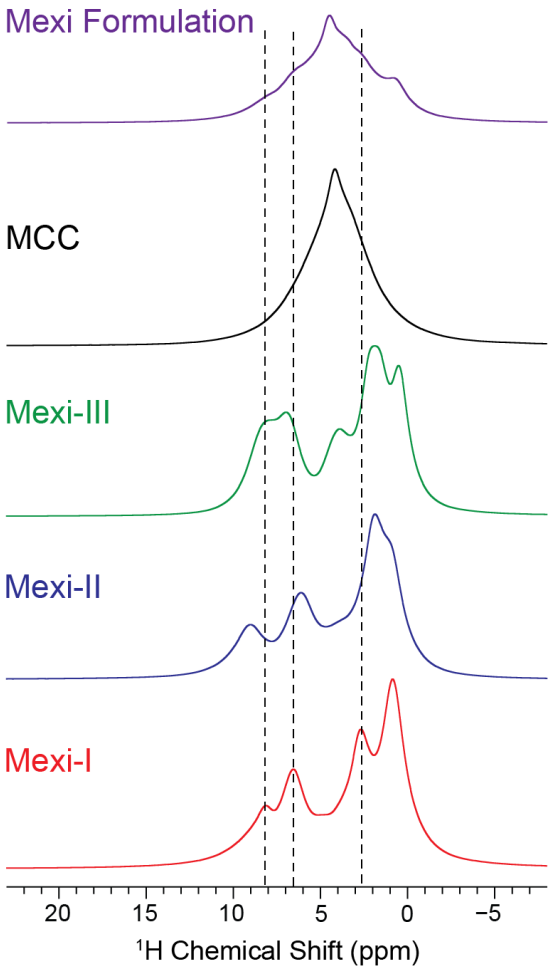

Figure S18. MAS ^{1}H spin-echo NMR spectra of the three mexi polymorphs, MCC and the model mexi formulation acquired at B_0 = 9.4 T with ν_{rot} = 50 kHz. Vertical lines are guides for the eye to illustrate differences in isotropic ^{1}H chemical shifts.

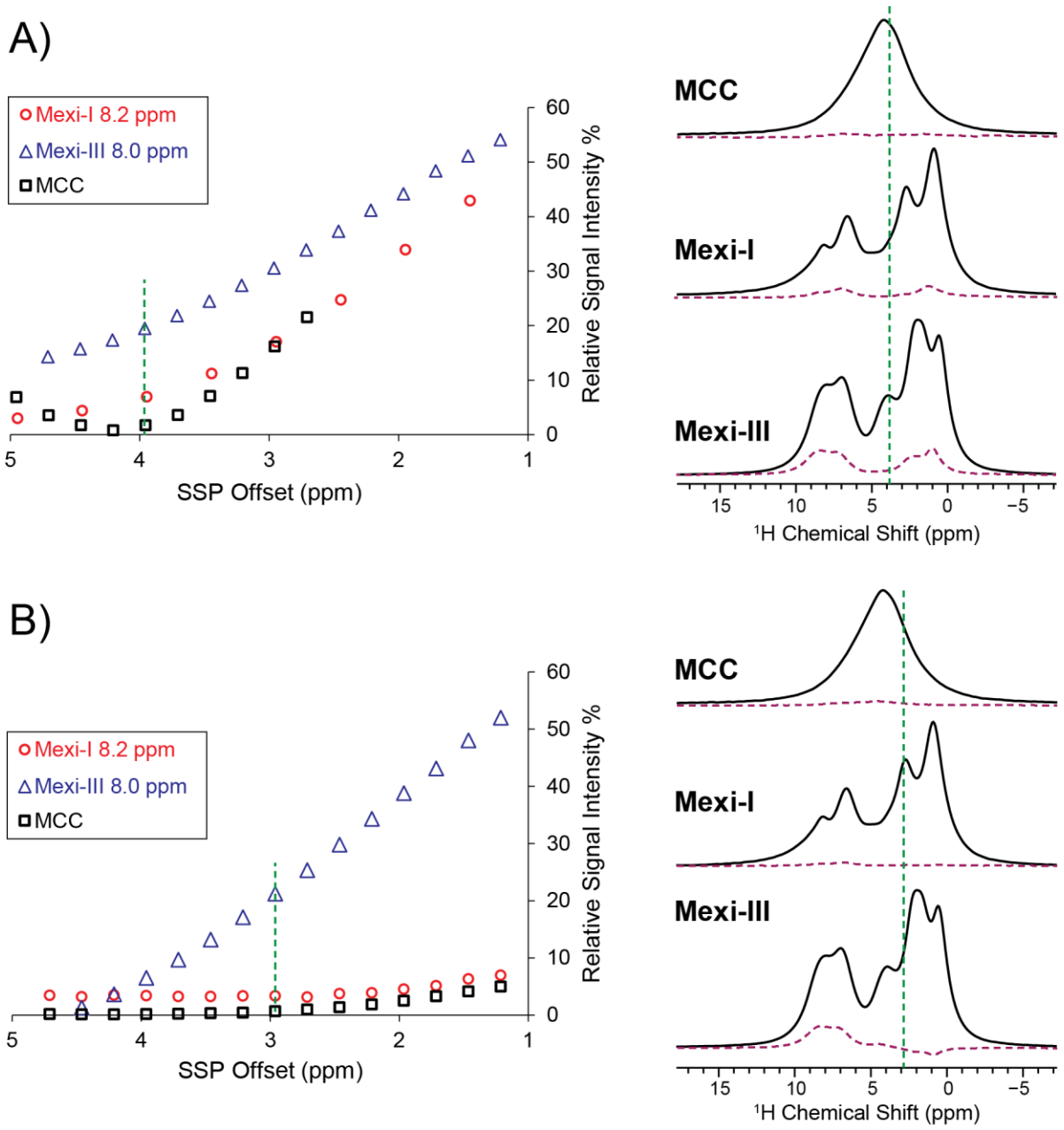

Figure S19. Optimization of SSP conditions on mexi-I, mexi-III and MCC. The plots show the relative signal intensities as a function of the SSP offset. For mexi-I and mexi-III only the relative signal intensity of the ammonium ^{1}H signal with the highest chemical shift is plotted. A) A single 6 ms SSP was applied with a 20 μs z-filter delay preceding the spin echo. ^{1}H NMR spectra are shown without any SSP (solid trace) and with an SSP offset of 3.95 ppm (dashed trace). B) Three 6 ms SSP were applied, with a 20 ms delay (τ_{SSP}) in between each SSP and a 20 μs z-filter delay preceding the spin echo. ^{1}H NMR spectra are shown without any SSP (solid trace) and with three SSP applied at an offset of 2.9 ppm (dashed trace). The vertical dashed lines indicate the SSP offset. All data acquired at B_0 = 9.4 T with ν_{rot} = 50 kHz with the pulse sequence shown in Figure S1A.

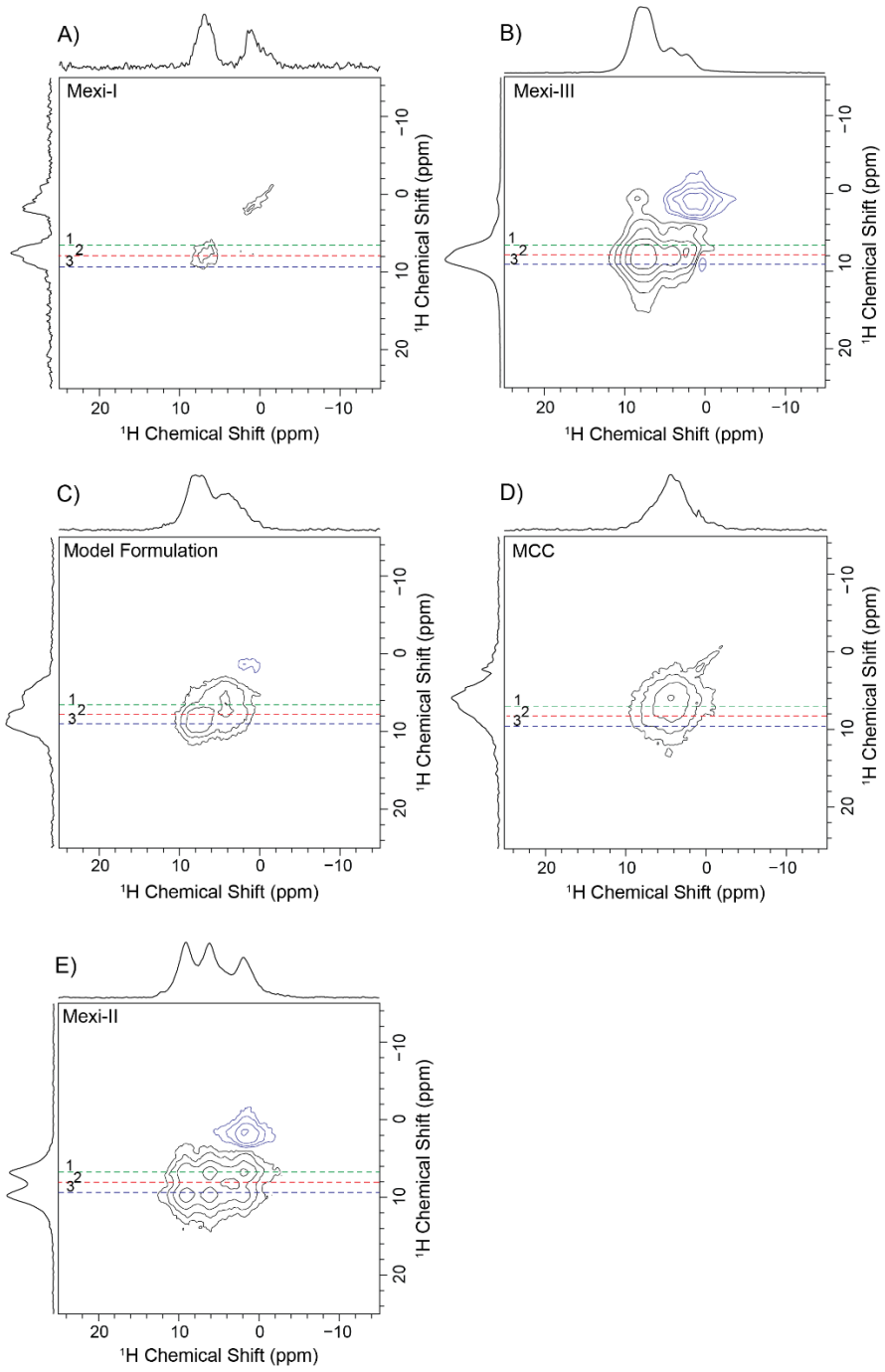

Figure S20. 2D ^{1}H SD NMR spectra acquired at B_0 = 9.4 T with ν_{rot} = 50 kHz. A) mexi-I, B) mexi-III, and C) a model formulation, D) MCC and E) mexi-II. The model formulation is a physical mixture of 5.2 wt-% mexi-III, 26.7 wt-% mexi-I, and 68.0 wt-% MCC (total API load of 32 wt-%). Three SSPs were applied at an offset of 2.9 ppm with a spin diffusion period of 20 ms separating each SSP. This SSP condition saturates mexi-I and the MCC, allowing the ^{1}H SSNMR signals from mexi-III to be selectively detected in the model formulation (see Figure S19). Different rows extracted from the 2D SD ^{1}H NMR spectra are compared in Figure S21 and Figure 6 of the main text.

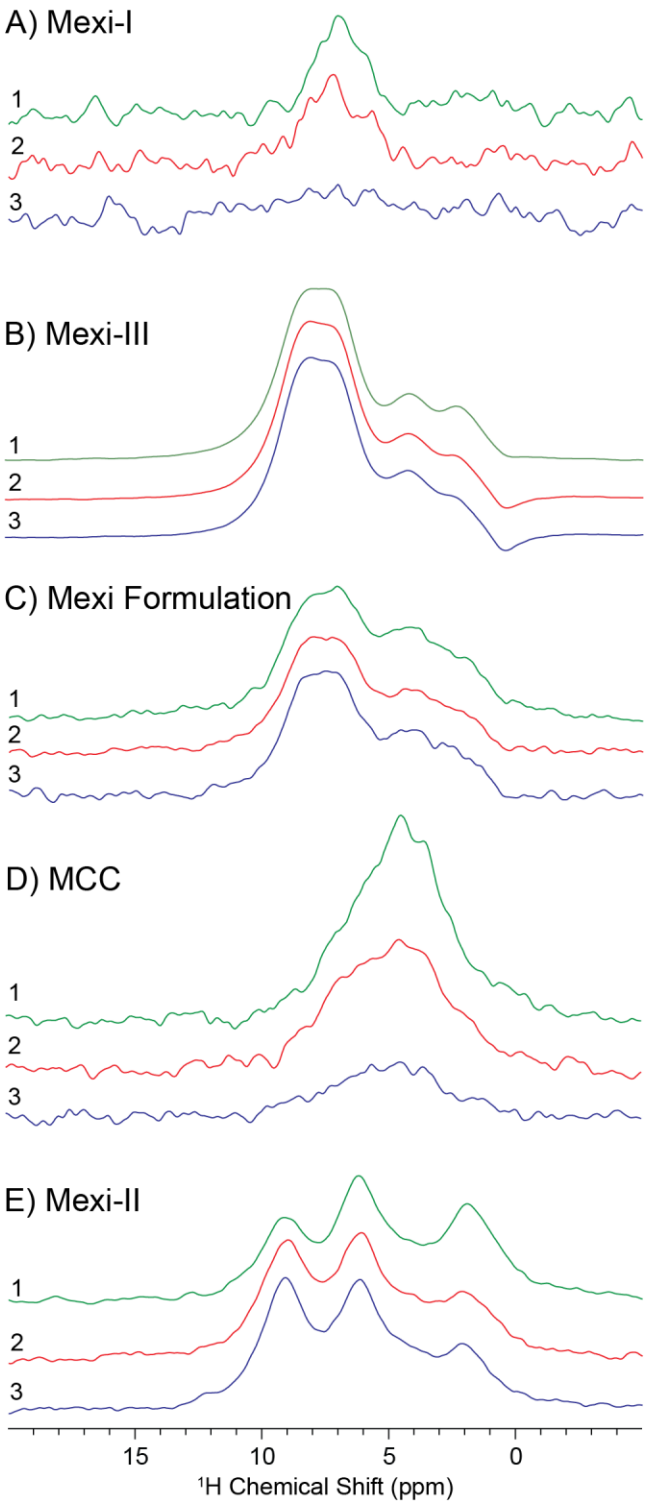

Figure S21. Comparison of rows extracted from the 2D SD ^{1}H NMR spectra of the different mexi forms. The corresponding 2D NMR spectra are shown in Figure S20. Rows 1, 2 and 3 were extracted from indirect dimension chemical shifts of 6.8 ppm, 8.0 ppm and 9.7 ppm. Figure 6 of the main text compares the 9.7 ppm rows for the different samples.

Table S5. ^{1}H Longitudinal Relaxation Time Constants (T_1) * for Different Samples

Sample	T_1 (s)	Magnetic Field (T)
pure mecl	7.6	18.8
pure mecl	5.3	9.4
mecl tablet	5.3	18.8
pure phenaz	7.0	18.8
phenaz tablet	12	18.8
pure phenaz	10.4	9.4
phenaz tablet	22	9.4
pure pheny	18	9.4
pheny model formulation	15	9.4
pure mexi-I	6.3	9.4
pure mexi-II	4.6	9.4
pure mexi-III	1.5	9.4

*The T_1 is reported for the ^{1}H signal with the highest chemical shift.

References

(1) Hildebrand, M.; Hamaed, H.; Namespetra, A. M.; Donohue, J. M.; Fu, R.; Hung, I.; Gan, Z.; Schurko, R. W. *CrystEngComm* **2014**, *16*, 7334.

(2) Namespetra, A. M.; Hirsh, D. A.; Hildebrand, M. P.; Sandre, A. R.; Hamaed, H.; Rawson, J. M.; Schurko, R. W. *CrystEngComm* **2016**, *18*, 6213–6232.

(3) Pinon, A. C.; Rossini, A. J.; Widdifield, C. M.; Gajan, D.; Emsley, L. Polymorphs of Theophylline Characterized by DNP Enhanced Solid-State Nmr. *Mol. Pharm.* **2015**, *12*, 4146-4153

(4) Harris, R. K.; Becker, E. D.; Cabral de Menezes, S. M.; Granger, P.; Hoffman, R. E.; Zilm, K. W. *Pure Appl. Chem.* **2008**, *80*, 59–84.

(5) Cory, D. .; Ritchey, W. . *J. Magn. Reson.* **1988**, *80*, 128–132.

(6) Song, Z.; Antzutkin, O. N.; Feng, X.; Levitt, M. H. *Solid State Nucl. Magn. Reson.* **1993**, *2*, 143–146.

(7) Antzutkin, O. N. *Prog. Nucl. Magn. Reson. Spectrosc.* **1999**, *35*, 203–266.

(8) Fung, B. M.; Khitrin, A. K.; Ermolaev, K. *J. Magn. Reson.* **2000**, *142*, 97–101.

CHAPTER 3. FAST ACQUISITION OF PROTON DETECTED HETCOR SOLID-STATE NMR SPECTRA OF QUADRUPOLAR NUCLEI AND RAPID MEASUREMENT OF NH BOND LENGTHS BY FREQUENCY SELECTIVE HMQC AND RESPDOR PULSE SEQUENCES

Modified from a manuscript published in Chem. Eur. J.

Anuradha V. Wijesekara,[a,b]† Amrit Venkatesh,[a,b]† Bryan J. Lampkin,[a] Brett VanVeller,[a] Joseph W. Lubach,[c] Karthik Nagapudi,[c] Ivan Hung,[d] Peter L. Gor'kov,[d] Zhehong Gan,[d] Aaron J. Rossini[a,b]*

[a] Department of Chemistry Iowa State University Ames, IA, USA, 50011

[b] US DOE Ames Laboratory, Ames, IA, USA, 50011

[c] Genentech Inc. South San Francisco, CA, USA, 94080

[d] Center of Interdisciplinary Magnetic Resonance (CIMAR) National High Magnetic Field Laboratory (NHMFL) Tallahassee, FL, USA, 32310

Abstract

Fast magic angle spinning (MAS), frequency selective (FS) heteronuclear multiple quantum coherence (HMQC) experiments which function in an analogous manner to solution SOFAST HMQC NMR experiments are demonstrated. Fast MAS enables efficient FS excitation of ^{1}H solid-state NMR signals. Selective excitation and observation preserve ^{1}H magnetization, leading to a significant shortening of the optimal inter-scan delay. Dipolar and scalar ^{1}H{^{14}N} FS HMQC solid-state NMR experiments routinely provide 4- to 9-fold reductions in experiment times as compared to conventional ^{1}H{^{14}N} HMQC solid-state NMR experiments. ^{1}H{^{14}N} FS resonance-echo saturation-pulse double-resonance (RESPDOR) allowed dipolar dephasing curves to be obtained in minutes, enabling the rapid determination of NH dipolar coupling

constants and inter-nuclear distances. $^{1}H\{^{14}N\}$ FS RESPDOR was used to assign multicomponent active pharmaceutical ingredients (APIs) as salts or cocrystals. FS HMQC also provided enhanced sensitivity for $^{1}H\{^{17}O\}$ and $^{1}H\{^{35}Cl\}$ HMQC experiments on ^{17}O labeled Fmoc-alanine and histidine hydrochloride monohydrate, respectively. FS HMQC and FS RESPDOR experiments will provide access to valuable structural constraints from materials that are challenging to study due to unfavorable relaxation times or dilution of the nuclei of interest.

Introduction

^{14}N is an attractive nucleus for solid-state NMR spectroscopy because it has a 99.6% natural isotopic abundance. Unfortunately, ^{14}N is a spin-1 quadrupolar nucleus with a low gyromagnetic ratio (γ) and low Larmor frequency (ν_0 = 28.9 MHz at 9.4 T). Static and MAS ^{14}N solid-state NMR spectra typically cover spectral widths of several MHz because of broadening by the quadrupolar interaction.[1] Schurko and co-workers have demonstrated a number of wideline techniques for broadband signal excitation that enable routine acquisition of ^{14}N solid-state NMR spectra of stationary powders.[2] But, these experiments require ca. 50–100 mg of material and samples containing multiple ^{14}N environments may be difficult to study because overlap of ^{14}N powder patterns will complicate analysis.

Gan and Bodenhausen demonstrated that 2D heteronuclear multiple quantum coherence (HMQC) experiments can be used to indirectly detect ^{14}N signals via high-resolution magic angle spinning (MAS) ^{13}C or ^{1}H NMR signals.[3] Efficient excitation of the ^{14}N spins can be achieved with low power ^{14}N pulses or DANTE pulse trains.[3a, 4] Detection of the "spy-nucleus" simultaneously enhances sensitivity and spectral resolution.[3] Solid-state $^{1}H\{^{14}N\}$ HMQC experiments are normally performed with fast MAS frequencies above 30 kHz to enhance ^{1}H resolution and sensitivity.[4a, 5] In dipolar-HMQC (D-HMQC) experiments dipolar recoupling is

applied to the spin-1/2 spy-nucleus to accelerate coherence transfer and allow observation of through-space proximities.[4a, 6] Alternative indirect detection schemes utilizing ^{1}H-^{14}N cross-polarization[7] or TRAPDOR HMQC pulse sequences using long-duration ^{14}N pulses for simultaneous recoupling and excitation have also been demonstrated.[8] Nishiyama showed that 80 kHz MAS 2D $^{1}H\{^{14}N\}$ J- or D-HMQC NMR spectra of simple organic molecules such as glycine or alanine could be obtained in several minutes from less than 1 mg of material.[9] Brown and co-workers have used 60 kHz MAS $^{1}H\{^{14}N\}$ D-HMQC experiments to determine the protonation states of multi-component active pharmaceutical ingredients (APIs).[10] They have also studied hydrogen bonding in amorphous dispersions of APIs[11] and other organic solids.[12] HMQC pulse sequences have also been applied for proton detection of half-integer quadrupolar nuclei such as ^{27}Al, ^{35}Cl, and ^{71}Ga,[13] spin-1/2 nuclei such as ^{195}Pt that exhibit large chemical shift anisotropy (CSA),[13c, 14] and low-γ spin-1/2 nuclei such as ^{89}Y.[15]

However, the intrinsically poor sensitivity of NMR spectroscopy often leads to long experiment times or prevents NMR experiments altogether. One way to improve NMR sensitivity is to use refocusing pulses, spin-locking and/or frequency-selective (FS) excitation to conserve magnetization and reduce recycle delays.[16] For example, solution $^{1}H\{^{15}N\}$ SOFAST HMQC NMR experiments on biomolecules use FS ^{1}H pulses to selectively excite and refocus high frequency amide ^{1}H NMR signals correlated to amide ^{15}N spins.[16d, 16e] The magnetization of ^{1}H spins in the amino acid side chains are unaffected by the FS pulses, consequently, amide ^{1}H spins are rapidly re-polarized by ^{1}H spin diffusion driven by the Overhauser effect, resulting in dramatically faster signal build-up.[16c-e] Typically, SOFAST HMQC provides 2-3 fold improved sensitivity for solution NMR experiments and order of magnitude reductions in experiment times.[16d, 16e]

Here, we demonstrate that DANTE pulse trains[17] provide efficient FS ^{1}H excitation pulses for fast MAS ^{1}H solid-state NMR experiments on organic solids, enabling FS scalar or dipolar ^{1}H{^{14}N} HMQC experiments (FS J-HMQC and FS D-HMQC, respectively). The solid-state FS HMQC sequences operate in a similar manner to solution SOFAST HMQC sequences by preserving longitudinal ^{1}H magnetization that is not correlated to the heteronuclear spins of interest. FS HMQC signal build-up rates may be accelerated by a factor 4-9 compared to conventional solid-state ^{1}H{^{14}N} J- and D-HMQC, enabling application of these NMR experiments to challenging samples and previously inaccessible systems. Additionally, ^{1}H{^{14}N} FS RESPDOR experiments[18] allow rapid measurements of ^{1}H-^{14}N dipolar couplings and NH bond lengths. Accelerated acquisition of 2D ^{1}H{^{17}O} and ^{1}H{^{35}Cl} solid-state NMR spectra with FS HMQC pulse sequences is also demonstrated.

Results and Discussion

DANTE pulse trains, Gaussian pulses or low-power rectangular pulses have previously been used for frequency selective excitation and inversion in fast MAS ^{1}H solid-state NMR experiments.[19] Here, ^{1}H{^{14}N} FS HMQC was implemented by using DANTE pulse trains[17] for efficient and selective excitation of high-frequency ^{1}H spins associated with amine and ammonium groups. The DANTE blocks consist of a periodic train of small tip angle excitation pulses.[17] The pulses were 0.1 or 0.2 μs in duration (2° or 5.0° tip angle) and separated by two rotor cycles. The total duration of DANTE pulse trains was between 347 μs and 640 μs (see SI for details). The ^{1}H solid-state NMR spectrum of histidine•HCl•H_2O (hist) obtained with 50 kHz MAS shows that the amine and ammonium ^{1}H spins resonate at 17.2 ppm (H_a), 12.7 ppm (H_b), and 8 ppm (H_c) (Figure 1A). Figure 1B demonstrates that a DANTE train can selectively excite the H_a ^{1}H NMR signal with 86% efficiency of the rectangular high-power pulse. Figure 1C

shows a ^{1}H spin echo spectrum obtained with a DANTE train applied to the H_a ^{1}H NMR signal prior to the broadband read pulses. This experiment demonstrates that the DANTE train minimally perturbs lower-frequency ^{1}H magnetization. I_a is 0.45 in Figure 1C, but is expected to be 0.14 because the peak intensities in Figure 1B and 1C should add up to 1.00. The intensity of I_a is likely higher than expected in Figure 1C because ^{1}H spin diffusion occurs during the course of the 640 μs DANTE block. In summary Figures 1A-1C show that after selective excitation of the H_a ^{1}H NMR signal with a DANTE train, there is a large amount of ^{1}H magnetization that remains on the low-frequency ^{1}H spins. The high-frequency H_a ^{1}H spins can then be rapidly re-polarized via ^{1}H spin diffusion.

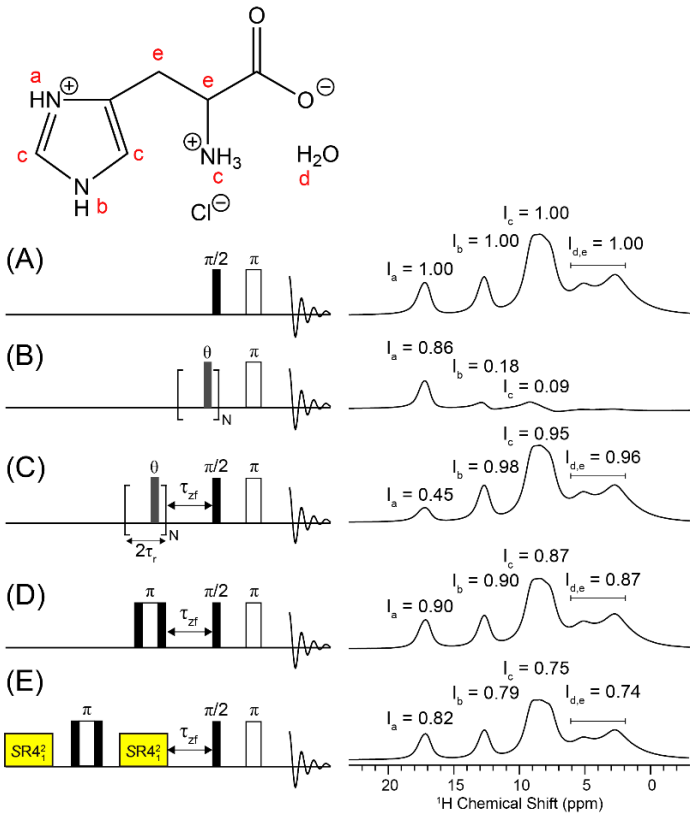

Figure 1. Quantification of DANTE excitation efficiency and magnetization losses on hist for pulse sequence elements required to implement solid-state FS HMQC. The molecular structure of hist is shown with assignment of the ^{1}H peaks. Pulse sequences are shown on the left and the resulting NMR spectra on the right. Relative ^{1}H NMR signal intensities are indicated. (A) Reference spectrum obtained with a broadband spin echo. (B) Selective spin echo with DANTE

train for excitation. (C) Selective saturation of the high-frequency ^{1}H NMR signal with a DANTE train. (D) A broadband spin echo with a composite π-inversion pulse. (E) Broadband spin echo with 480 μs of $SR4_1^2$ dipolar recoupling and inversion pulse prior to excitation. All spectra were obtained with 8 scans, τ_{zf} = 40 μs, ν_{rot} = 50 kHz, B_0 = 9.4 T and recycle delays of 16 s (> 5 ×T_1).

Figure 1D and 1E shows how to implement the remaining pulse sequence elements required for a solid-state FS HMQC pulse sequences. In the solution SOFAST HMQC pulse sequence the central π-pulse must also be frequency-selective, otherwise magnetization of ^{1}H spins that were not excited by the initial π /2-pulse will be inverted, then undergo inversion recovery. However, given the short homogeneous transverse relaxation times (T_2') of ^{1}H in the solid-state it is difficult to incorporate an efficient FS-refocusing pulse into the HMQC block. Fortunately, there is a simpler solution. The magnetization of all ^{1}H spins can be inverted at the start of the sequence by a composite π-pulse (90_Y-180_X-90_Y, Figure 1D and Figure 2B). The composite pulse is more tolerant to rf inhomogeneity, slightly improving inversion efficiency.[20] The inversion pulse results in the loss of ca. 10-13% of the ^{1}H magnetization (Figure 1D). In the FS HMQC pulse sequence (Figure 2B), the inversion pulse is followed by a DANTE train, then scalar or dipolar couplings evolve to generate multiple quantum coherence. The broadband π-pulse that follows will simultaneously refocus transverse ^{1}H magnetization and invert the longitudinal ^{1}H magnetization back to the +z-axis. After signal detection, the high-frequency ^{1}H spins are then repolarized by ^{1}H spin diffusion from lower-frequency ^{1}H spins, leading to shortened optimal recycle delays. Therefore, it is straightforward to implement pulse sequences analogous to SOFAST HMQC for solid-state ^{1}H{^{14}N} J-HMQC experiments where no dipolar recoupling is applied.

What about D-HMQC pulse sequences where recoupling pulse sequences are applied on the ^{1}H channel? The most widely applied recoupling sequence for proton detected D-HMQC is

currently $SR4_1^2$,[19a] which consists of an even number of π-pulses and each π-pulse has 180° phase alternation.[19a] Therefore, there will be no net rotation of longitudinal ^{1}H magnetization by $SR4_1^2$ recoupling, even in the presence of an inhomogeneous RF-field. Fortunately, longitudinal ^{1}H magnetization also decays slowly under $SR4_1^2$ symmetry-based recoupling so that there are minimal losses in longitudinal ^{1}H magnetization, even after several milliseconds of dipolar recoupling (Figure 1E and Figure S1). Overall, Figure 1 clearly illustrates that ca. 75-80% of the longitudinal ^{1}H magnetization can be preserved in the presence of all pulse sequence elements required for FS D-HMQC/FS RESPDOR sequences.

Scalar and dipolar FS HMQC solid-state NMR experiments were performed on hist and compared to standard HMQC experiments (Figure 2A and 2B). Figure 2C shows measurements of the relative sensitivity (S_{rel} = signal intensity × $\tau_{rd}^{-1/2}$) as function of the inter-scan delay (τ_{rd}). FS and broadband dipole recoupled spin echo and standard spin echo pulse sequences were used for all of the relaxation experiments presented here (Figure S2). The spin echo sequences are identical to the corresponding D-HMQC/J-HMQC pulse sequences, except the ^{14}N pulses are excluded. The spin echo experiments have the same signal build-up characteristics as HMQC experiments but offer better sensitivity for the relaxation measurements since the direct ^{1}H magnetization is monitored without any ^{14}N filtering/dephasing. The sensitivity curves in Figures 2C and 2D were fit with a slightly modified version of the function describing the relative sensitivity of flip-back CPMAS experiments proposed by Emsley and co-workers:[16j]

$$S_{rel}(f_e, f_0, \tau_{rd}) = f_e \frac{A}{\sqrt{\tau_{rd}}} \frac{1 - \exp\left(-\frac{\tau_{rd}}{T_B}\right)}{1 - f_0 \exp\left(-\frac{\tau_{rd}}{T_B}\right)} \qquad (1)$$

S_{rel} is the relative sensitivity, f_e accounts for the efficiency of the excitation pulse, f_0 is the fraction of magnetization left after a single scan, T_B is the build-up time constant (usually equal

to T_1), and A is a scaling factor adjusted so that S_{rel} = 1.00 for conventional HMQC experiments performed with $\tau_{rd} = 1.26 \times T_B$. For a broadband $\pi/2$ pulse f_e = 1.0, while for DANTE f_e may be less than 1.0 due to relaxation losses. DANTE excitation on the H_a signal of hist gives $f_e \approx 0.86$ (Figure 1B).

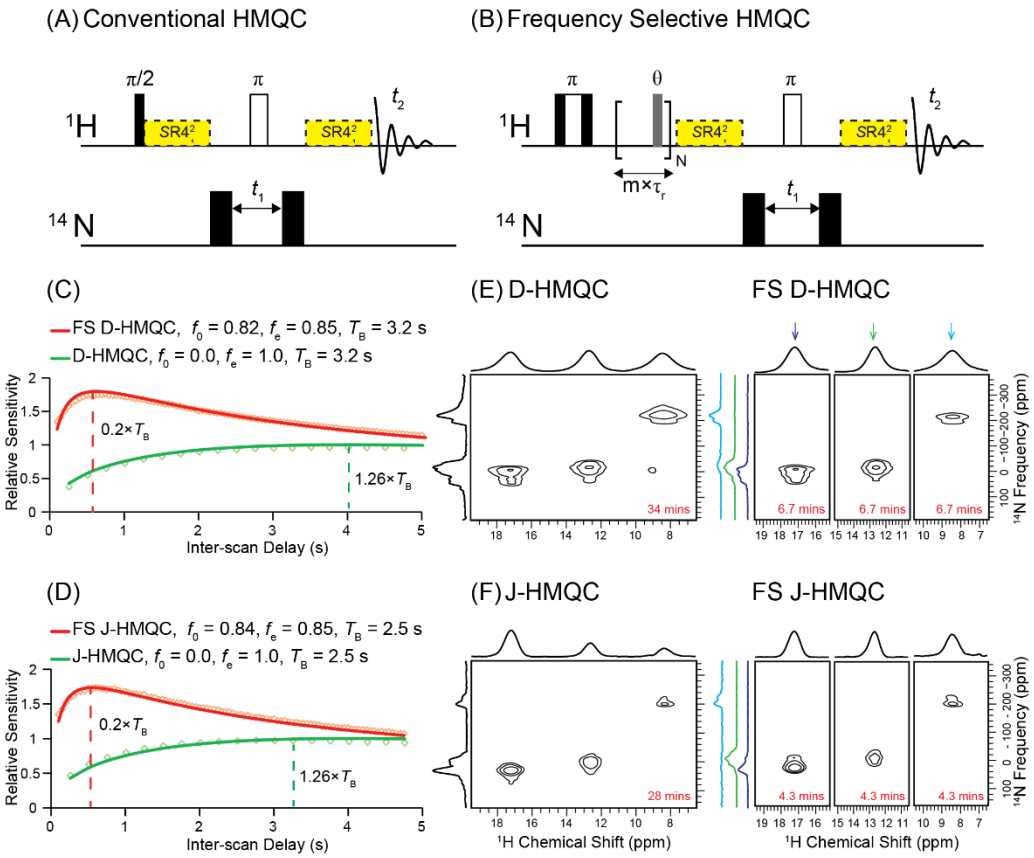

Figure 2. (A, B) Pulse sequences for (A) conventional HMQC and (B) FS HMQC. $SR4_1^2$ dipolar recoupling is not applied in the J-HMQC experiments. (C, D) Measurement of relative sensitivity for conventional and FS (C) D-HMQC and (D) J-HMQC for the H_A NMR signal of hist. In (C) and (D) spin echo pulse sequences were used as described in the main text. Experimental sensitivity curves (open diamonds) and fits to equation 1 (solid lines) are shown for the 17.2 ppm ^{1}H NMR signal. Fit parameters are indicated. (E, F) Comparison of 2D ^{1}H{^{14}N} NMR spectra of hist obtained with conventional and FS (E) D-HMQC and (F) J-HMQC. The FS HMQC spectra were obtained with the DANTE pulses on resonance with the different ^{1}H NMR signals. Total experiment times are indicated. D-HMQC experiments were performed with ν_{rot} = 50 kHz and J-HMQC with ν_{rot} = 60 kHz. All experiments performed with B_0 = 9.4 T.

The sensitivity curve for conventional D-HMQC can be fit with f_0 = 0.0 and the build-up time constant (TB) of 3.2 s matches the ^{1}H T_1 measured in a normal ^{1}H saturation recovery

experiment. As expected, the recycle delay that provides optimal sensitivity is approximately 3.9 s (1.26×TB) for conventional D-HMQC. The shape of the sensitivity curve for FS HMQC matches those previously reported for NMR experiments such as solution SOFAST HMQC or solid-state flip-back CP where residual longitudinal ^{1}H magnetization is preserved after each scan.[16b, 16d, 16e, 16g, 16j] The fit of the FS D-HMQC sensitivity curve yields T_B = 3.2 s and f_0 = 0.82, suggesting that 82% of the ^{1}H polarization is retained after each scan. The conservation of ^{1}H magnetization leads to a reduced optimal recycle delay of 0.7 s (0.2×TB). The faster recycling provides a factor 1.8 improvement in relative sensitivity and reduces experiment times by a factor 3.2 for FS D-HMQC as compared to standard D-HMQC. A sensitivity gain and reduction in the optimal recycle delay was also observed for FS spin echo experiments that are analogous to FS J-HMQC (Figure 2D). For 60 kHz J-HMQC experiments T_B was reduced to 2.5 s because of sample heating caused by the increase in MAS frequency. While conventional HMQC also performs well for hist, the sensitivity gains provided by FS HMQC enables high-quality 2D ^{1}H{^{14}N} dipolar- or scalar-HMQC NMR spectra of hist to be recorded in only a few minutes for each ^{1}H peak (Figures 2E and 2F). The sensitivity of the NMR spectra extracted from the ^{1}H HMQC signal at 17.2 ppm are compared in Figure S3 and the sensitivity gains with the FS HMQC experiments are consistent with the relaxation experiments.

^{1}H{^{14}N} FS D- and J-HMQC experiments on hist were also repeated at an ultra-fast MAS frequency of 95 kHz on an 18.8 T (800 MHz) NMR spectrometer. With these conditions, the DANTE pulses have a high excitation efficiency of 96% for the H_a ^{1}H NMR signal (Figure S4). As expected, the efficiency and selectivity of the DANTE pulses improves with increased MAS frequency and magnetic field. One challenge with higher fields and faster MAS frequencies is that ^{1}H spin diffusion is slowed, which can result in a distinct ^{1}H T_1 for the different peaks in the

spectrum,[19d, 21] hindering recovery of ^{1}H magnetization by spin diffusion. To address this problem the conventional and the FS HMQC sequences were slightly modified for the 18.8 T experiments. The initial inversion pulse is replaced with a 90°Y – spin-lockX – 90°Y block that inverts all magnetization. The spin-lock pulse accelerates ^{1}H spin diffusion and makes the ^{1}H magnetization more homogeneous across the entire ^{1}H spectrum.[19d, 21b] Figure S5 shows the sensitivity curves for FS and conventional D- and J-HMQC experiments at 18.8 T. For D-HMQC the gain in sensitivity was about a factor 1.8, similar to that observed at 9.4 T. However, for J-HMQC, a factor 3 gain in sensitivity was observed at 18.8 T, corresponding to factor of 9 gain in acceleration of the acquisition (Figure S6). Comparing FS J-HMQC and FS D-HMQC at 18.8 T the large gain in sensitivity for the J-HMQC experiments likely occurs because of the better efficiency of the DANTE pulse and the absence of ^{1}H dipolar recoupling pulses that cause some loss of magnetization. $^{1}H\{^{14}N\}$ FS J-HMQC spectra of hist were acquired in only 30 seconds each (Figure 3). The MAS spectrum of the I = 1 nuclei ^{14}N and ^{2}H are very sensitive to the precision of the magic angle setting.[1a, 22] Therefore, $^{1}H\{^{14}N\}$ FS HMQC experiments can also be used to rapidly calibrate the magic angle (Figure 3A). This approach is useful because when probes are configured for ^{14}N experiments there are few standards available to accurately calibrate the magic angle.

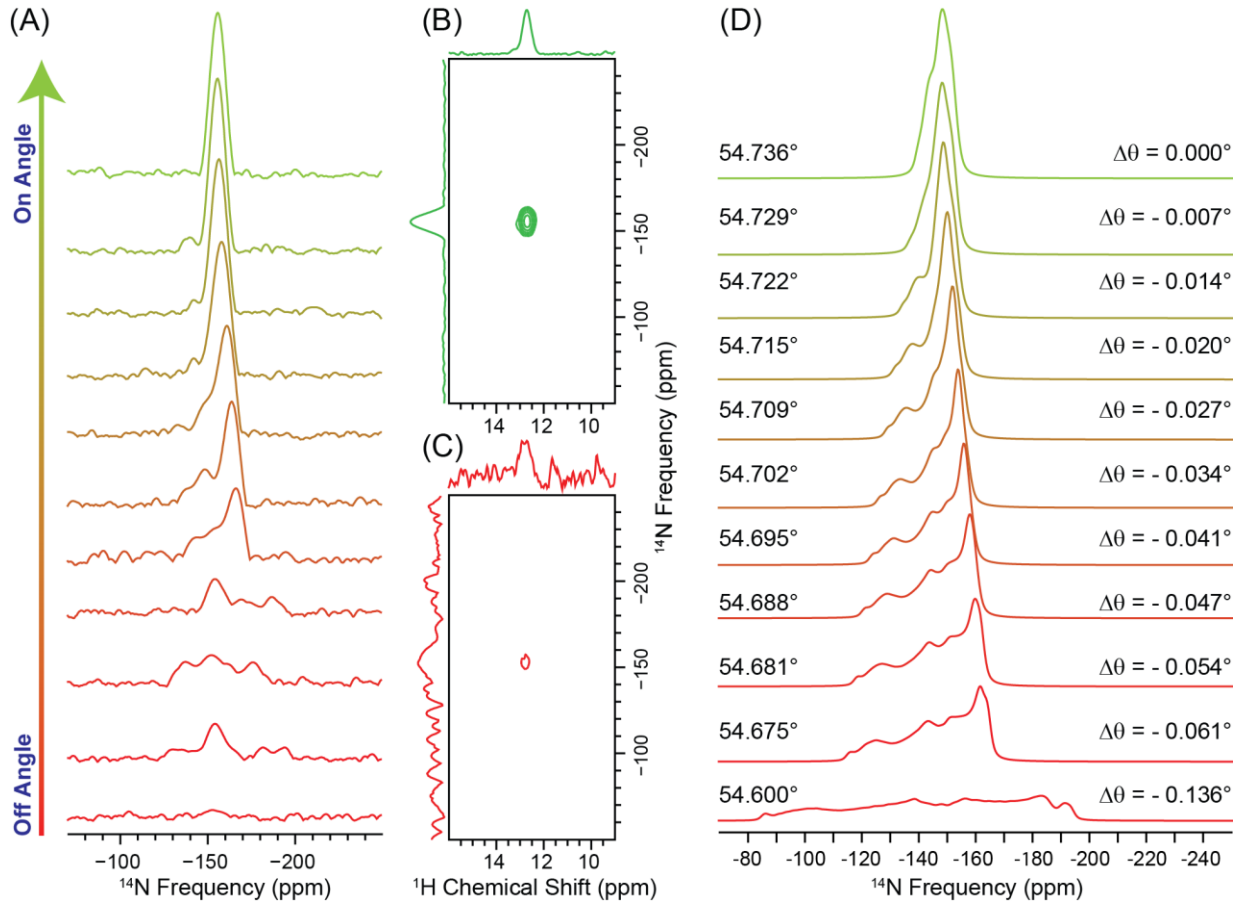

Figure 3. Setting the magic angle using FS J-HMQC and hist. (A) Stack of ^{14}N SSNMR spectra of hist extracted from 2D ^{1}H{^{14}N} FS J-HMQC. The upper row shows the spectrum when the magic angle is accurately adjusted and the bottom most row shows the spectrum when the magic angle is mis-set. Comparison of the 2D ^{1}H{^{14}N} FS J-HMQC spectra when (B) magic angle is accurately adjusted and (C) magic angle is mis-set. Each spectrum was obtained in 30 seconds. All experiments were performed ν_{rot} = 95 kHz and B_0 = 18.8 T. (D) Analytical simulations of ^{14}N solid-state NMR spectra as a function of the MAS rotation angle.

The added sensitivity and significantly reduced experiment times provided by FS HMQC are very beneficial for ^{1}H{^{14}N} HMQC experiments on larger molecules where NH functional groups will be more dilute. For example, multi-component active pharmaceutical ingredients are typically formed by reacting a basic API with an acid coformer.[10-11, 23] It is important to determine whether the reaction of the API and coformer results in a salt, formed when a basic group of the API is protonated, or a cocrystal, formed when the proton from the acid is not fully transferred, but forms a hydrogen bond with the API.[10-11, 23] Brown and co-workers have used

$^{1}H\{^{14}N\}$ D-HMQC[10-11] and $^{15}N\{^{1}H\}$ J-resolved solid-state NMR experiments[10] to qualitatively probe NH bond lengths and differentiate salts and cocrystals. Recently we have used DNP-enhanced ^{15}N solid-state NMR to measure NH bond lengths and determine protonation states of the API GDC-0022 when it is reacted with different acid co-formers.[23]

Figure 4A shows the single-crystal X-ray diffraction structures of the tosylic acid salt of GDC-0022 (denoted as 1) and a cocrystal formed by reacting two equivalents of GDC-0022 with fumaric acid (2, see Scheme 1 in the SI for full molecular structures).[23] All H-atom positions were optimized by plane-wave DFT.[23] 1 is a salt since the hydrogen atom from tosylic acid is transferred to the API ($r_{NH\ calc}$ = 1.07 Å), while 2 is a cocrystal since the hydrogen remains bound to fumaric acid and forms a hydrogen bond to the API ($r_{NH\ calc}$ = 1.53 Å and 1.55 Å, the second hydrogen bond is not shown).[23] The ^{1}H spin echo spectra of 1 and 2 shows that the hydrogen atoms involved in bonds to the API/acid co-formers resonate at high-frequency and are well resolved from the other ^{1}H NMR signals (Figure 4B), consistent with previously published DNP-enhanced 2D ^{1}H-^{15}N and ^{1}H-^{13}C HETCOR NMR spectra.[23] Note that the ^{1}H NMR signals of ammonium, amine and carboxylic groups often resonate at a high ^{1}H chemical shifts and are usually resolved from other ^{1}H NMR signals when fast MAS is used.[19d] Conventional $^{1}H\{^{14}N\}$ D-HMQC spectra of 1 and 2 recorded with short dipolar recoupling times (τ_{rec} < 0.75 ms) only show the high-frequency acid ^{1}H NMR signals because only these ^{1}H spins reside within 2 Å of a nitrogen atom. Consequently, FS and conventional $^{1}H\{^{14}N\}$ D-HMQC spectra of 1 and 2 will provide the exact same information, but, FS D-HMQC provides 2.2- and 1.9-fold higher sensitivity for 1 and 2, respectively (Figures S7 and S8). The 2D $^{1}H\{^{14}N\}$ D-HMQC spectra of 1 and 2 clearly shows correlations between the ^{1}H and ^{14}N of the nitrogen and hydrogen atoms that are bonded, and hydrogen bonded, respectively (Figure 4B).

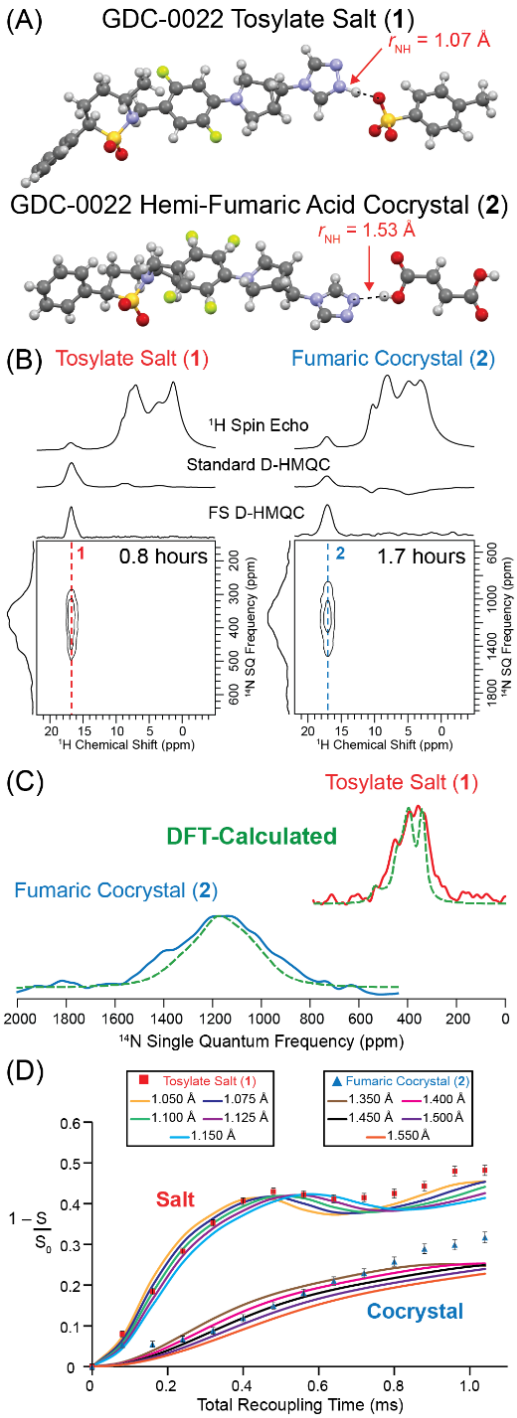

Figure 4. (A) Crystal structures of the tosylate salt (1) and hemi-fumaric acid cocrystal (**2**) of GDC-0022 with DFT-optimized NH bond lengths indicated. (B) ^{1}H and ^{1}H{^{14}N} D-HMQC SSNMR spectra of 1 and 2. (C) Comparison of ^{14}N SSNMR spectra of 1 and 2. Analytically simulated ^{14}N SSNMR spectra using ^{14}N NMR parameters obtained from plane-wave DFT calculations are shown as dashed lines. (D) Comparison of experimental and SIMPSON simulated (solid lines) ^{1}H{^{14}N} RESPDOR dipolar dephasing curves for 1 and 2 with ^{1}H-^{14}N dipolar coupling constants corresponding to the indicated inter-nuclear distances. All experiments performed with B_0 = 9.4 T at ν_{rot} = 50 kHz.

$^{1}H\{^{14}N\}$ HMQC and RESPDOR experiments[18] can be used to probe NH bond length and differentiate salts and cocrystals. First, the $C_Q(^{14}N)$ is larger for 2 than 1 as indicated by the more positive frequency of the ^{14}N SSNMR signal in 2; the peak position is determined by the combined effects of the chemical shift and quadrupole induced shift (QIS),[3b, 8b] with the latter dominating at 9.4 T. Analytically simulated ^{14}N solid-state NMR spectra are shown as dashed lines and allow $C_Q(^{14}N)$ and $\delta_{iso}(^{14}N)$ to be estimated (Figure 4C). The values of $C_Q(^{14}N)$ and $\delta_{iso}(^{14}N)$ determined from simulations in good agreement with those predicted by plane-wave DFT for 1 and 2 (Tables S1 and S2). The observed and DFT predicted differences in $C_Q(^{14}N)$ for 1 and 2 suggest that $C_Q(^{14}N)$ increases as the NH bond length increases. Second, NH bond lengths can be directly measured with $^{1}H\{^{14}N\}$ RESPDOR experiments as was recently demonstrated by Nishiyama and Goldbourt.[24] However, experiment times of 6-10 hours have been reported to record $^{1}H\{^{14}N\}$ RESPDOR dipolar dephasing curves of amino acids[24] and multicomponent APIs.[25] Here, $^{1}H\{^{14}N\}$ FS RESPDOR experiments allowed complete dipolar dephasing curves to be obtained in only 20 minutes each for 1 and 2 (Figure 4D, Figures S9 and S10). $^{1}H\{^{14}N\}$ RESPDOR curves for 1 and 2 were calculated with the SIMPSON simulation program for a ^{1}H-^{14}N-^{14}N spin system. This 3-spin system was used to mimic the interactions present in 1 and 2. C_Q values and nitrogen chemical shifts obtained from plane-wave DFT were used in the simulations. Dipolar dephasing curves were then calculated for different dipolar coupling constants (NH bond lengths) and r_{NH} = 1.10 Å and r_{NH} = 1.40 Å were found to give the best fits for 1 and 2, respectively (Figure S9 and Figure S10). These bond lengths are in good agreement with the NH bond lengths predicted by plane-wave DFT calculations and previously measured by DNP-enhanced ^{1}H-^{15}N DIPSHIFT experiments on 1 and 2.[23] Note that the DNP-enhanced DIPSHIFT experiments required ca. 4 hours each, therefore, the $^{1}H\{^{14}N\}$ FS

RESPDOR is likely the fastest and most sensitive method to measure NH bond lengths for natural abundance materials. For 2 there is substantial uncertainty in r_{NH} because the saturation factor (f) was also included as an adjustable parameter in the fits of experiment RESPDOR curves (see SI). The accuracy of the NH bond length measurements can be improved by using a phase modulated saturation pulse to more reliably saturate the ^{14}N spins.[24-25]

^{1}H{^{14}N} FS RESPDOR was also performed on the ammonium ^{1}H signal at 17.2 ppm of hist to confirm the accuracy of the NH distance measurements (Figures S11). Using ^{1}H{^{14}N} FS RESPDOR r_{NH} = 1.10 Å was determined, in good agreement with the value of r_{NH} = 1.09 Å measured by Levitt and co-workers with ^{15}N{^{1}H} symmetry-based recoupling, separated local field (SLF) experiments on ^{15}N-enriched hist.[26]

FS HMQC experiments were also performed on other samples and with different NMR-active nuclei. Sulfathiazole is a well-studied pharmaceutical compound with many different known polymorphs.[27] Solid-state NMR experiments on sulfathiazole are challenging because T_1(^{1}H) is very long, approximately 900 s for the sample examined here (Figure S12). Therefore, performing conventional ^{1}H{^{14}N} HMQC is extremely time consuming because inter-scan delays of ca. 1200 s would be required for optimal sensitivity and total experiment times on the order of days would result. With FS D-HMQC the inter-scan delay could be significantly reduced to ca. 0.1×T_1. The ^{1}H{^{14}N} FS D-HMQC spectrum was obtained in 8.5 hours (Figure S12). This example demonstrates FS HMQC may provide large absolute time savings for experiments on solids with long proton T_1.

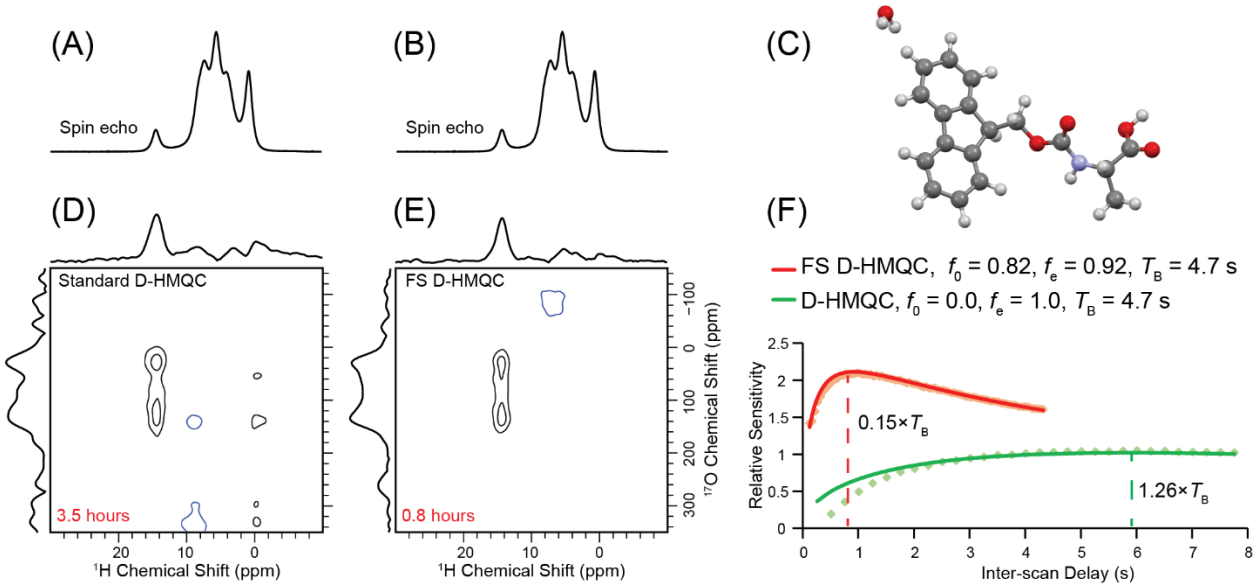

Figure 5. Comparison of (A, B) ^{1}H spin echo, (C) Geometry optimized crystal structure of FMOC-alanine (D) conventional ^{1}H{^{17}O} D-HMQC and (E) ^{1}H{^{17}O} FS D-HMQC. The experiment times for the 2D spectra are indicated. (F) Measurement of the relative sensitivities for conventional and FS D-HMQC for different inter-scan delays. The fit parameters are indicated along with the curves. The experiments were performed with B_0 = 9.4 T at ν_{rot} = 50 kHz.

Proton detected X→^{1}H D-RINEPT experiments have previously been used to obtain 2D ^{1}H-X correlation NMR spectra with X = ^{17}O and ^{35}Cl.[13b, 28] D-HMQC can theoretically provide better sensitivity than D-RINEPT because the initial polarization is derived from ^{1}H spins in the HMQC experiment, while in a D-RINEPT experiment it is derived from the lower-γ quadrupolar spin.[13b] Carboxylic acid groups often give rise to high-frequency ^{1}H NMR signals.[19d, 28a] The acid ^{1}H NMR signals can be used for ^{1}H{^{17}O} FS HMQC experiments on ^{17}O-labelled carboxylic acids. Figures 5D and E compare the conventional and FS ^{1}H{^{17}O} D-HMQC spectra of Fmoc-alanine with each oxygen atom in the carboxylic acid enriched to ca. 20% ^{17}O.[28a] Similar to the ^{1}H{^{14}N} HMQC experiments, a factor of 2 gain in sensitivity can be obtained for ^{1}H{^{17}O} FS HMQC experiments (Figure 5F), allowing a complete 2D spectrum to be obtained in only 0.8 hours. The 2D D-HMQC spectra were obtained with 80 μs of total recoupling, hence, only the ^{17}O central-transition NMR signal from the protonated oxygen atom of the carboxylic

acid was observed. We previously showed that the ^{1}H-^{17}O J-coupling in Fmoc-alanine was 58 Hz.[28a] This J-coupling is large enough to allow $^{1}H\{^{17}O\}$ J-HMQC experiments (Figure S13). FS J-HMQC was two times more sensitive and four times faster than conventional J-HMQC.

^{35}Cl solid-state NMR has been shown to be a sensitive probe of molecular structure for hydrochloride salts of pharmaceuticals.[29] A $^{1}H\{^{35}Cl\}$ FS D-HMQC spectrum of hist was acquired in only 8.5 minutes (Figure S14). However, for the ^{35}Cl NMR experiments on hist, FS D-HMQC shows only ca. 1.3 times better sensitivity than conventional D-HMQC. The sensitivity gains are limited in the $^{1}H\{^{35}Cl\}$ FS HMQC experiments because the NH_3^+ groups found in the middle of the ^{1}H NMR spectrum show the strongest correlation to ^{35}Cl. The imperfect selectivity of the ^{1}H DANTE pulse trains leads to partial saturation of other ^{1}H spins, reducing the amount of preserved ^{1}H polarization and the FS HMQC sensitivity gains.

Conclusions

In summary, scalar and dipolar $^{1}H\{^{14}N\}$ FS HMQC solid-state NMR experiments, analogous to solution SOFAST HMQC NMR experiments, are straightforward to implement with fast MAS and can routinely provide factor 2 to 9 reductions in experiment times as compared to conventional HMQC solid-state NMR experiments. $^{1}H\{^{14}N\}$ FS RESPDOR experiments allowed NH internuclear distances to be rapidly determined, enabling multicomponent APIs to be assigned as salts and cocrystals. FS pulse sequences also accelerated $^{1}H\{^{17}O\}$ and $^{1}H\{^{35}Cl\}$ HMQC solid-state NMR experiments. The only criteria for FS HMQC and FS RESPDOR experiments to succeed is that the ^{1}H spins correlated to hetero-nucleus are resolved from the other ^{1}H NMR signals. Therefore, FS HMQC and RESPDOR should be applicable to many other nuclei and these experiments should provide access to valuable structural constraints in a variety of organic, inorganic and biological systems. We also anticipate that significant time savings could also be realized with FS versions of TRAPDOR-HMQC[8a, 8c]

and ^{14}N overtone HMQC.[30] The reduced recycle delays provided by FS experiments also allows more scans to be obtained in a given unit time which should also help to reduce t_1-noise in 2D experiments.[31] Finally, fast MAS is crucial to enhance ^{1}H resolution and sensitivity and allow efficient FS excitation. Therefore, the continued development of MAS probes capable of faster MAS frequencies will likely further improve the sensitivity gains provided by the FS pulse sequences.

Acknowledgements

This material is based upon work supported by the National Science Foundation under Grant No. 1709972 to AJR. We thank Genentech, Inc. and its Innovation Fund, for providing additional financial support for this work. AJR also thanks Iowa State University for additional support. A portion of this work was performed at the National High Magnetic Field Laboratory, which is supported by the National Science Foundation Cooperative Agreement No. DMR-1644779 and the State of Florida.

References

[1] a) H. J. Jakobsen, H. Bildsøe, J. Skibsted, T. Giavani, *J. Am. Chem. Soc.*, **2001**, *123*, 5098-5099; b) L. A. O'Dell, R. W. Schurko, K. J. Harris, J. Autschbach, C. I. Ratcliffe, *J. Am. Chem. Soc.*, **2011**, *133*, 527-546.

[2] a) K. J. Harris, S. L. Veinberg, C. R. Mireault, A. Lupulescu, L. Frydman, R. W. Schurko, *Chem. Eur. J.*, **2013**, *19*, 16469-16475; b) L. A. O'Dell, R. W. Schurko, *J. Am. Chem. Soc.*, **2009**, *131*, 6658-6659; c) R. W. Schurko, *Acc. Chem. Res.*, **2013**, *46*, 1985-1995.

[3] a) S. Cavadini, A. Lupulescu, S. Antonijevic, G. Bodenhausen, *J. Am. Chem. Soc.*, **2006**, *128*, 7706-7707; b) Z. H. Gan, *J. Am. Chem. Soc.*, **2006**, *128*, 6040-6041.

[4] a) S. Cavadini, A. Abraham, G. Bodenhausen, *Chem. Phys. Lett.*, **2007**, *445*, 1-5; b) A. G. M. Rankin, J. Trébosc, P. Paluch, O. Lafon, J.-P. Amoureux, *J. Magn. Reson.*, **2019**, *303*, 28-41.

[5] a) Y. Ishii, R. Tycko, *J. Magn. Reson.*, **2000**, *142*, 199-204; b) Y. Nishiyama, *Solid State Nucl. Magn. Reson.*, **2016**, *78*, 24-36; c) R. Zhang, K. H. Mroue, A. Ramamoorthy, *Acc. Chem. Res.*, **2017**, *50*, 1105-1113.

[6] Z. H. Gan, *J. Magn. Reson.*, **2007**, *184*, 39-43.

[7] D. Carnevale, X. Ji, G. Bodenhausen, *J. Chem. Phys.*, **2017**, *147*, 184201.

[8] a) J. A. Jarvis, I. M. Haies, P. T. F. Williamson, M. Carravetta, *Phys. Chem. Chem. Phys.*, **2013**, *15*, 7613-7620; b) J. A. Jarvis, M. Concistre, I. M. Haies, R. W. Bounds, I. Kuprov, M. Carravetta, P. T. F. Williamson, *Phys. Chem. Chem. Phys.*, **2019**, *21*, 5941-5949; c) I. Hung, P. Gor'kov, Z. Gan, *J. Chem. Phys.*, **2019**, *151*, 154202.

[9] Y. Nishiyama, Y. Endo, T. Nemoto, H. Utsumi, K. Yamauchi, K. Hioka, T. Asakura, *J. Magn. Reson.*, **2011**, *208*, 44-48.

[10] A. S. Tatton, T. N. Pham, F. G. Vogt, D. Iuga, A. J. Edwards, S. P. Brown, *CrystEngComm*, **2012**, *14*, 2654-2659.

[11] A. S. Tatton, T. N. Pham, F. G. Vogt, D. Iuga, A. J. Edwards, S. P. Brown, *Mol. Pharm.*, **2013**, *10*, 999-1007.

[12] G. N. M. Reddy, M. Malon, A. Marsh, Y. Nishiyama, S. P. Brown, *Anal. Chem.*, **2016**, *88*, 11412-11419.

[13] a) M. K. Pandey, H. Kato, Y. Ishii, Y. Nishiyama, *Phys. Chem. Chem. Phys.*, **2016**, *18*, 6209-6216; b) A. Venkatesh, M. P. Hanrahan, A. J. Rossini, *Solid State Nucl. Magn. Reson.*, **2017**, *84*, 171-181; c) A. J. Rossini, M. P. Hanrahan, M. Thuo, *Phys. Chem. Chem. Phys.*, **2016**, *18*, 25284-25295.

[14] F. A. Perras, A. Venkatesh, M. P. Hanrahan, T. W. Goh, W. Huang, A. J. Rossini, M. Pruski, *J. Magn. Reson.*, **2017**, *276*, 95-102.

[15] F. A. Perras, T. W. Goh, L.-L. Wang, W. Huang, M. Pruski, *Solid State Nucl. Magn. Reson.*, **2019**, *98*, 12-18.

[16] a) E. D. Becker, J. A. Feretti, T. C. Farrar, *J. Am. Chem. Soc.*, **1969**, *91*, 7784-7785; b) J. Tegenfeldt, U. Haeberlen, *Journal of Magnetic Resonance (1969)*, **1979**, *36*, 453-457; c) K. Pervushin, B. Vögeli, A. Eletsky, *J. Am. Chem. Soc.*, **2002**, *124*, 12898-12902; d) P. Schanda, B. Brutscher, *J. Am. Chem. Soc.*, **2005**, *127*, 8014-8015; e) P. Schanda, Ē. Kupče, B. Brutscher, *J. Biomol. NMR*, **2005**, *33*, 199-211; f) J. J. Lopez, C. Kaiser, S. Asami, C. Glaubitz, *J. Am. Chem. Soc.*, **2009**, *131*, 15970-15971; g) A. Lupulescu, L. Frydman, *J. Chem. Phys.*, **2011**, *135*, 134202; h) T. Gopinath, G. Veglia, *Angew. Chem. Int. Ed.*, **2012**, *51*, 2731-2735; i) J. R. Banigan, N. J. Traaseth, *J. Phys. Chem. B*, **2012**, *116*, 7138-7144; j) S. Björgvinsdóttir, B. J. Walder, A. C. Pinon, J. R. Yarava, L. Emsley, *J. Magn. Reson.*, **2018**, *288*, 69-75; k) N. T. Duong, J. Trébosc, O. Lafon, J.-P. Amoureux, *Solid State Nucl. Magn. Reson.*, **2019**, *100*, 52-62; l) S. Jayanthi, A. Lupulescu, *Solid State Nucl. Magn. Reson.*, **2020**, 101652.

[17] a) G. Bodenhausen, R. Freeman, G. A. Morris, *Journal of Magnetic Resonance (1969)*, **1976**, *23*, 171-175; b) G. A. Morris, R. Freeman, *Journal of Magnetic Resonance (1969)*, **1978**, *29*, 433-462.

[18] a) L. Chen, Q. Wang, B. Hu, O. Lafon, J. Trébosc, F. Deng, J.-P. Amoureux, *Phys. Chem. Chem. Phys.*, **2010**, *12*, 9395-9405; b) Z. H. Gan, *Chem. Commun.*, **2006**, 4712-4714.

[19] a) A. Brinkmann, A. P. M. Kentgens, *J. Am. Chem. Soc.*, **2006**, *128*, 14758-14759; b) V. S. Mithu, K. O. Tan, P. K. Madhu, *J. Magn. Reson.*, **2013**, *237*, 11-16; c) A. J. Robertson, M. K. Pandey, A. Marsh, Y. Nishiyama, S. P. Brown, *J. Magn. Reson.*, **2015**, *260*, 89-97; d) D. A. Hirsh, V. A. Wijesekara, S. L. Carnahan, I. Hung, J. W. Lubach, K. Nagapudi, A. J. Rossini, *Mol. Pharm.*, **2019**, *16*, 3121-3132.

[20] M. H. Levitt, *eMagRes*, **2007**.

[21] a) Y. Q. Ye, M. Malon, C. Martineau, F. Taulelle, Y. Nishiyama, *J. Magn. Reson.*, **2014**, *239*, 75-80; b) A. Venkatesh, I. Hung, K. C. Boteju, A. D. Sadow, P. L. Gor'kov, Z. Gan, A. J. Rossini, *Solid State Nucl. Magn. Reson.*, **2020**, *105*, 101636.

[22] a) A. K. Khitrin, B. M. Fung, *J. Chem. Phys.*, **1999**, *111*, 8963-8969; b) T. Giavani, H. Bildsøe, J. Skibsted, H. J. Jakobsen, *Chem. Phys. Lett.*, **2003**, *377*, 426-432; c) S. Antonijevic, G. Bodenhausen, *Angew. Chem. Int. Ed.*, **2005**, *44*, 2935-2938.

[23] L. Zhao, M. P. Hanrahan, P. Chakravarty, A. G. DiPasquale, L. E. Sirois, K. Nagapudi, J. W. Lubach, A. J. Rossini, *Cryst. Growth Des.*, **2018**, *18*, 2588-2601.

[24] N. T. Duong, F. Rossi, M. Makrinich, A. Goldbourt, M. R. Chierotti, R. Gobetto, Y. Nishiyama, *J. Magn. Reson.*, **2019**, *308*, 106559.

[25] D. Bernasconi, S. Bordignon, F. Rossi, E. Priola, C. Nervi, R. Gobetto, D. Voinovich, D. Hasa, N. T. Duong, Y. Nishiyama, M. R. Chierotti, *Cryst. Growth Des.*, **2020**, DOI:10.1021/acs.cgd.1029b01299.

[26] X. Zhao, J. L. Sudmeier, W. W. Bachovchin, M. H. Levitt, *J. Am. Chem. Soc.*, **2001**, *123*, 11097-11098.

[27] D. C. Apperley, R. A. Fletton, R. K. Harris, R. W. Lancaster, S. Tavener, T. L. Threlfall, *J. Pharm. Sci.*, **1999**, *88*, 1275-1280.

[28] a) S. L. Carnahan, B. J. Lampkin, P. Naik, M. P. Hanrahan, I. I. Slowing, B. VanVeller, G. Wu, A. J. Rossini, *J. Am. Chem. Soc.*, **2019**, *141*, 441-450; b) E. G. Keeler, V. K. Michaelis, M. T. Colvin, I. Hung, P. L. Gor'kov, T. A. Cross, Z. Gan, R. G. Griffin, *J. Am. Chem. Soc.*, **2017**, *139*, 17953-17963.

[29] a) H. Hamaed, J. M. Pawlowski, B. F. T. Cooper, R. Fu, S. H. Eichhorn, R. W. Schurko, *J. Am. Chem. Soc.*, **2008**, *130*, 11056-11065; b) M. Hildebrand, H. Hamaed, A. M. Namespetra, J. M. Donohue, R. Q. Fu, I. Hung, Z. H. Gan, R. W. Schurko, *Crystengcomm*, **2014**, *16*, 7334-7356; c) D. A. Hirsh, A. J. Rossini, L. Emsley, R. W. Schurko, *Phys. Chem. Chem. Phys.*, **2016**, *18*, 25893-25904.

[30] L. A. O'Dell, R. He, J. Pandohee, *CrystEngComm*, **2013**, *15*, 8657-8667.

[31] F. A. Perras, M. Pruski, *J. Magn. Reson.*, **2019**, *298*, 31-34.

Appendix for supporting information

Experimental

Sample preparation

L-histidine hydrochloride monohydrate (hist) and Sulfathiazole were purchased from Sigma-Aldrich and used without further purification. GDC-0022 tosylate salt (1) and GDC-0022 fumaric cocrystal (2) were provided by Genentech Inc. ^{17}O-labeled FMOC-alanine monohydrate was synthesized by a previously reported method.[1] The percentage enrichment of ^{17}O-labeled FMOC-alanine monohydrate was determined by solution ^{17}O NMR experiments to be ca. 20% for each carboxylic acid oxygen atom.

Solid-State NMR Spectroscopy

All samples were gently ground into a powder using a mortar and pestle before packing into 1.3 mm or 0.75 mm zirconia rotors for solid-state NMR (SSNMR) experiments. ^{1}H, ^{14}N, ^{17}O and ^{35}Cl SSNMR experiments were performed on a 400 MHz (B_0 = 9.4 T) Bruker Avance III HD spectrometer with a 1.3 mm double resonance HX probe. Additional ^{1}H and ^{14}N SSNMR experiments were performed on an 800 MHz (B_0 = 18.8 T) Bruker Avance III HD spectrometer at the National High Field Magnetic Laboratory (NHFML) in Tallahassee, Florida with a home-built triple resonance 0.75 mm ultra-fast MAS probe containing a 0.75 mm JEOL stator. All 9.4 T D-HMQC experiments were performed with a 50 kHz MAS frequency and the 9.4 T J-HMQC experiments were performed with a 60 kHz MAS frequency. For 50-60 kHz MAS experiments the magic angle was carefully set using the ^{2}H signal of a deuterated oxalic acid sample.[1, 2] For 18.8 T experiments with a 95 kHz MAS frequency the magic angle was directly set using FS J-HMQC experiments as shown in the main text (Figure 3). ^{1}H rf pulses were directly calibrated on each sample and ^{1}H chemical shifts were referenced to neat tetramethylsilane (δ_{iso} = 0 ppm) using adamantane (δ_{iso} = 1.82 ppm) as a secondary standard. ^{14}N, ^{17}O and ^{35}Cl chemical shifts

were indirectly referenced using IUPAC frequency ratios.[3] All ^{14}N spectra were referenced to the nitromethane scale.

In all D-HMQC experiments the symmetry-based recoupling sequence $SR4_1^2$ [4] was applied on the ^{1}H channel at the 2nd order rotary resonance recoupling condition.[5-7] For ^{1}H{^{14}N} D-HMQC experiments the optimum total dipolar recoupling times used for hist and compounds 1 and 2 were 480 μs, 400 μs and 720 μs, respectively. A shorter recoupling time of 80 μs was used for the ^{1}H{^{17}O} D-HMQC of FMOC-alanine to selectively observe the protonated oxygen site whereas the longer ^{1}H-^{35}Cl distances and weaker dipolar coupling constants in hist necessitated a recoupling duration of 1.6 ms. For all ^{1}H{^{14}N} HMQC experiments, the ^{14}N excitation and reconversion pulse lengths had a duration of one rotor period. The RF field was 37 kHz for 9.4 T experiments and 53 kHz for 18.8 T experiments. ^{1}H{^{17}O} and ^{1}H{^{35}Cl} HMQC experiments were performed with central transition-selective pulse lengths of 4.75 μs and 4.5 μs for ^{35}Cl and ^{17}O, respectively. In the FS HMQC and FS RESPDOR experiments DANTE pulses were used for selective excitation of ^{1}H NMR signals. For the 9.4 T FS D-/J-HMQC experiments, the DANTE pulse trains consisted of 0.2 μs DANTE pulses with an RF field of 65 kHz (ca. 5° tip angle) and each pulse separated by 2 rotor cycles. For the 18.8 T experiments with 95 kHz MAS frequency, the DANTE pulse trains consisted of 0.1 μs DANTE pulses with an RF field of 65 kHz and each pulse separated by 2 rotor cycles. The number of pulses in the DANTE train were optimized on each sample to maximize signal and between 14-16 pulses and 33 pulses were applied at 9.4 T and 18.8 T, respectively. The total duration of the DANTE pulse trains was between 347 μs and 640 μs and varied because of the differences in MAS frequency (50 kHz, 60 kHz or 95 kHz) and the number of pulses. For 9.4 T experiments a 90_Y-180_X-90_Y composite π-inversion pulse was used to invert all ^{1}H

magnetization at the start of the FS HMQC pulse sequences. For the 18.8 T experiments with 95 kHz MAS frequency, a 90^{o}_{Y} – spin $lock_{X}$ – 90^{o}_{Y} pulse block was used to simultaneously invert all initial ^{1}H magnetization and homogenize ^{1}H polarization across the spectrum by accelerating ^{1}H spin diffusion (see reference 21b of the main text for more details). The duration of the spin-lock pulse was 2 ms and the RF field of the spin-lock pulse was 240 kHz. These parameters were optimized to maximize ^{1}H spin diffusion and minimize magnetization losses due to rotating-frame relaxation during the spin-lock pulse.

The NH bond distances were determined using the FS RESPDOR sequence (Figure S9). A saturation pulse (τ_{sat}) with a duration of 1.5 rotor cycles (30 μs with a 50 kHz MAS frequency) was used on the ^{14}N channel. The RF field of the ^{14}N saturation pulse was 64 kHz. Experimental RESPDOR dipolar dephasing curves ($1\text{-}S/S_0$) were obtained by measuring the ^{1}H NMR signal for each recoupling time without the ^{14}N dephasing pulse (S_0) and with the ^{14}N dephasing pulse (S). $^{1}H\{^{14}N\}$ RESPDOR curves for 1 and 2 were calculated using SIMPSON *v*4.1.1 simulation program.[8-10] A ^{1}H-^{14}N-^{14}N spin system was used for simulations to reflect the molecular structure of 1 and 2. Simulated dipolar dephasing curves were calculated for several different dipolar coupling constants (NH bond lengths) between the ^{1}H spin and the first ^{14}N spin. When the NH bond length was varied, the distance and dipolar coupling constant between ^{1}H and the 2^{nd} nitrogen spin was also varied accordingly. The simulated SIMPSON curves were scaled by a saturation factor (f) to match the experimentally observed dipolar dephasing curve intensities (Simulated RESPDOR Intensity = $1\text{-}f*S/S_0$). The root mean square deviation (RMSD) was calculated for each simulated RESPDOR dephasing curve and different values of the saturation factor (Figure S9, S10 and S11B). The simulated dipolar dephasing curve and saturation factor that gave the lowest RMSD were then used to determine the NH bond length. For 2, there is

large uncertainty in the NH bond length because many combinations of the NH bond length and saturation factor give a reasonable fit of the RESPDOR curve.

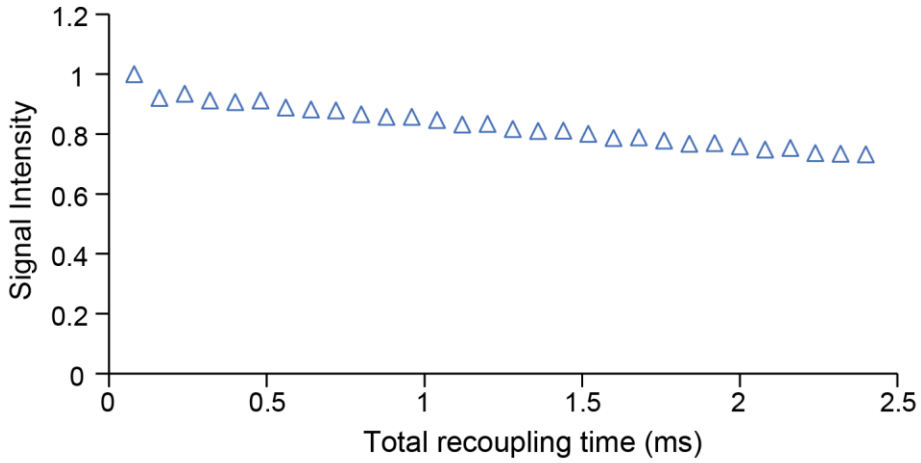

Figure S1. The decay of the longitudinal ^{1}H magnetiation under $SR4_1^2$ symmetry based recoupling sequence measured using the pulse sequence shown in Figure 1E of the main text. Approximately 80% of the longitudinal ^{1}H magnetization still remains after 2.0 ms total of $SR4_1^2$ recoupling. Data was obtained with ν_{rot} = 50 kHz and B_0 = 9.4 T.

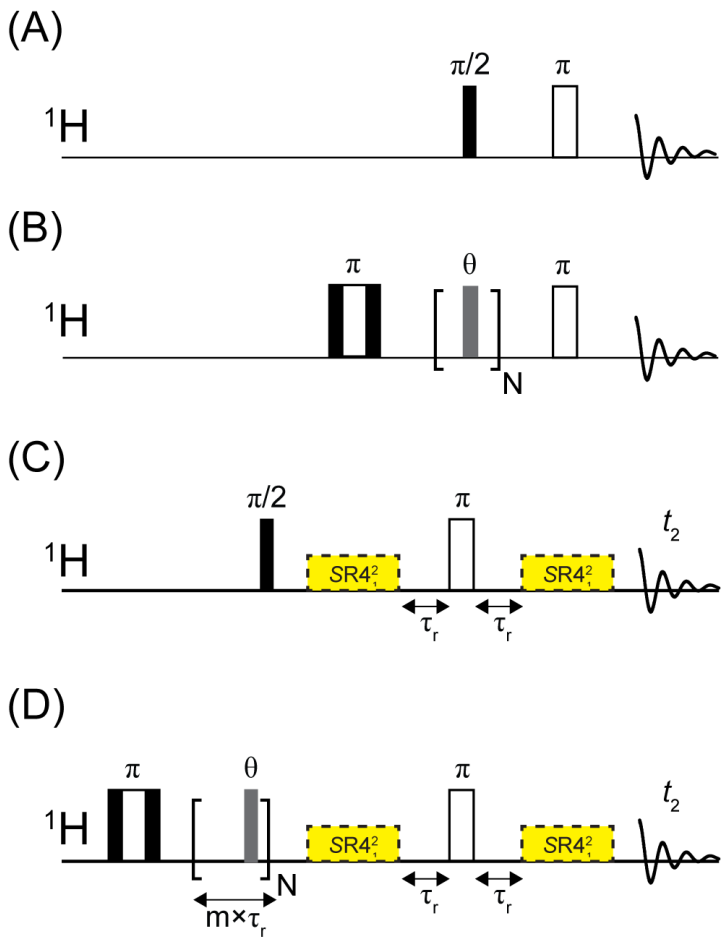

Figure S2. Spin echo pulse sequences used for relaxation measurements shown in Figures 2C, 2D, and 5F in the main text. (A) Conventional spin echo, (B) FS spin echo used to measure sensitivity curves for conventional and FS J-HMQC experiments, respectively. (C) Recoupled spin echo and (D) FS recoupled spin echo used to measure sensitivity curves for conventional and FS D-HMQC/RESPDOR experiments, respectively.

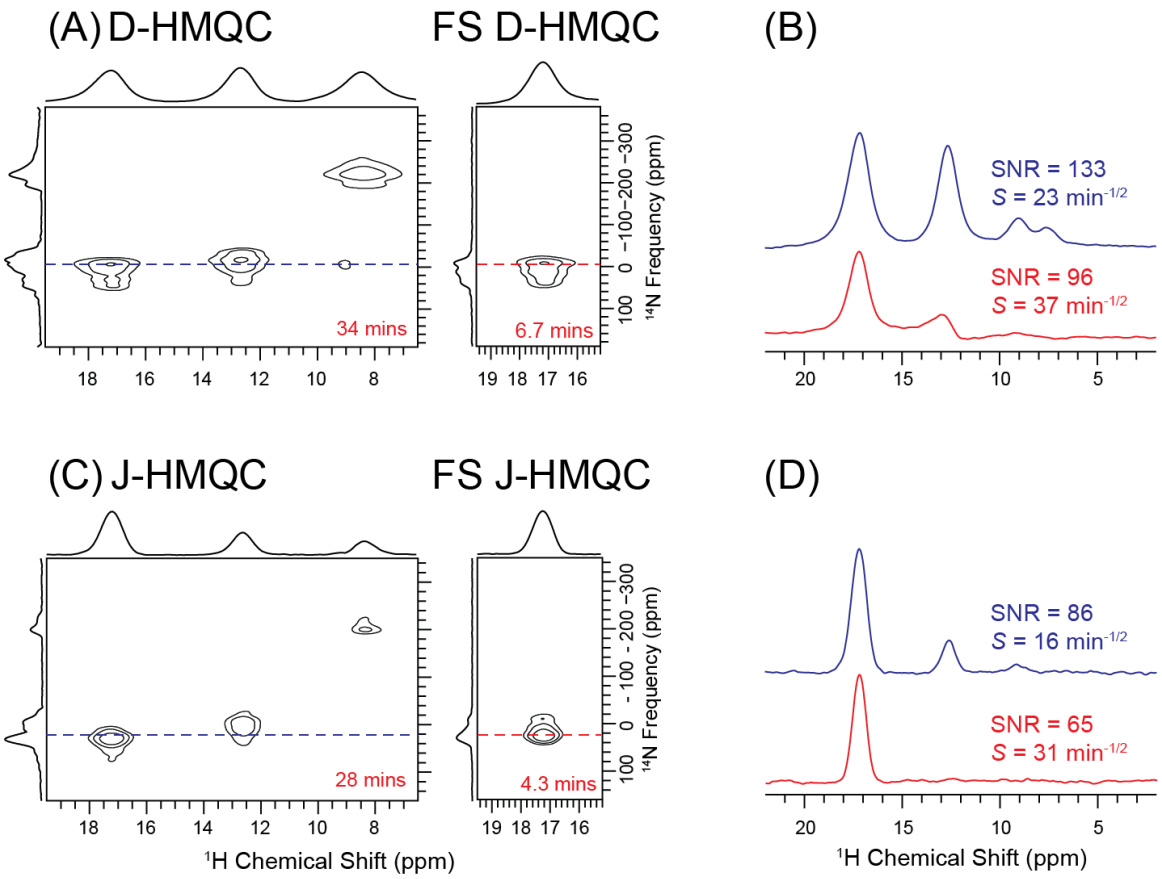

Figure S3. Comparison of 2D $^{1}H\{^{14}N\}$ NMR spectra of hist obtained with conventional and FS (A) D-HMQC or (C) J-HMQC. The FS HMQC spectra were obtained with the DANTE pulses on resonance with the acid ^{1}H NMR signal at 17.2 ppm. Total experiment times are indicated on the 2D NMR spectra. Comparison of the ^{1}H spectra extracted from the row indicated by dashed lines for conventional (blue trace) or FS (red trace) (B) D-HMQC and (D) J-HMQC. The signal-to-noise-ratio (SNR) and sensitivity (S = SNR × time$^{-1/2}$) are indicated. The D-HMQC experiments were performed with ν_{rot} = 50 kHz and J-HMQC with ν_{rot} = 60 kHz. All experiments performed with B_0 = 9.4 T.

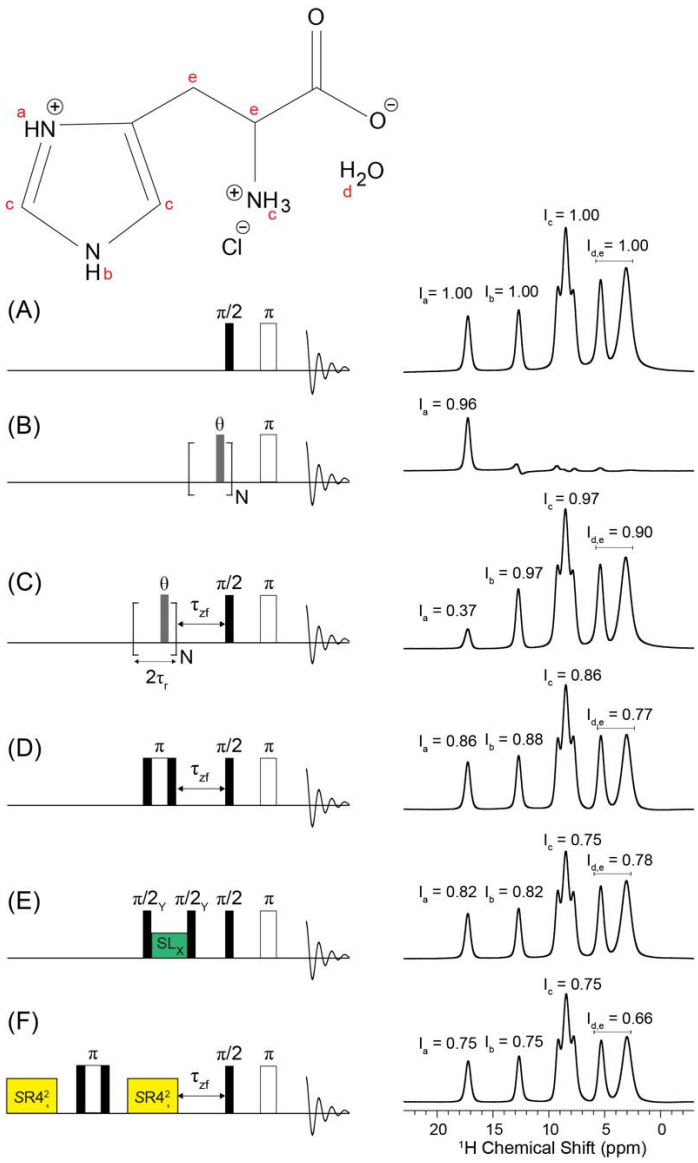

Figure S4. Quantification of DANTE excitation efficiency and magnetization losses on hist caused by pulse sequence elements required to implement solid-state FS HMQC at 18.8 T. Pulse sequences are shown on the left and the resulting NMR spectra on the right. Relative ^{1}H NMR signal intensities are indicated. (A) Reference spectrum obtained with a broadband spin echo. (B) Selective spin echo with DANTE train for excitation. (C) Selective saturation of the high-frequency ^{1}H NMR signal with a DANTE train. (D) A broadband spin echo with a composite π-inversion pulse prior to excitation. (E) A $90°_{Y}$ – spin-lock$_{X}$ – $90°_{Y}$ inversion block prior to a broadband spin echo. (F) 253 μs of total $SR4_1^2$ dipolar recoupling and a composite inversion pulse prior to a broadband spin echo. All spectra were obtained with 8 scans, τ_{zf} = 40 μs, ν_{rot} = 95 kHz, B_0 = 18.8 T and recycle delays of 50 s (> 5 ×T_1).

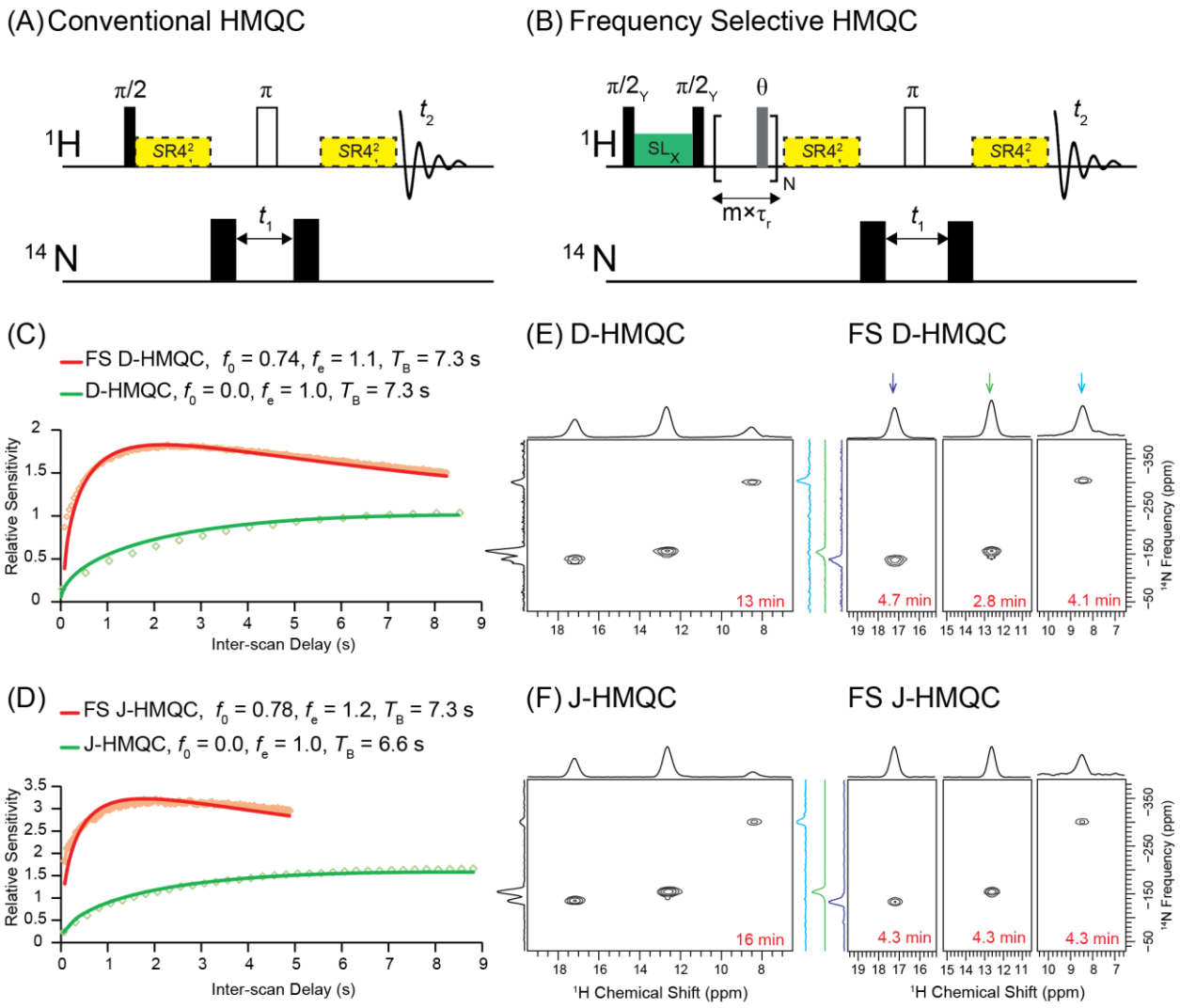

Figure S5. (A, B) Pulse sequences for (A) conventional HMQC and (B) FS HMQC. $SR4_1^2$ dipolar recoupling was not applied in the J-HMQC experiments. (C, D) Measurement of relative sensitivity for conventional and FS (C) D-HMQC and (D) J-HMQC for the H_a NMR signal of hist. Experimental sensitivity curves (open diamonds) and fits to equation 1 in the main text (solid lines) are shown. Fit parameters are indicated. (E, F) Comparison of 2D ^{1}H{^{14}N} NMR spectra of hist obtained with conventional and FS (E) D-HMQC or (F) J-HMQC. The FS HMQC spectra were obtained with the DANTE pulses on resonance with the different ^{1}H NMR signals. For the FS HMQC experiments an inversion pulse block with a 2 ms spin-lock was applied prior to the frequency selective DANTE block. Total experiment times are indicated. All the experiments performed with ν_{rot} = 95 kHz and B_0 = 18.8 T.

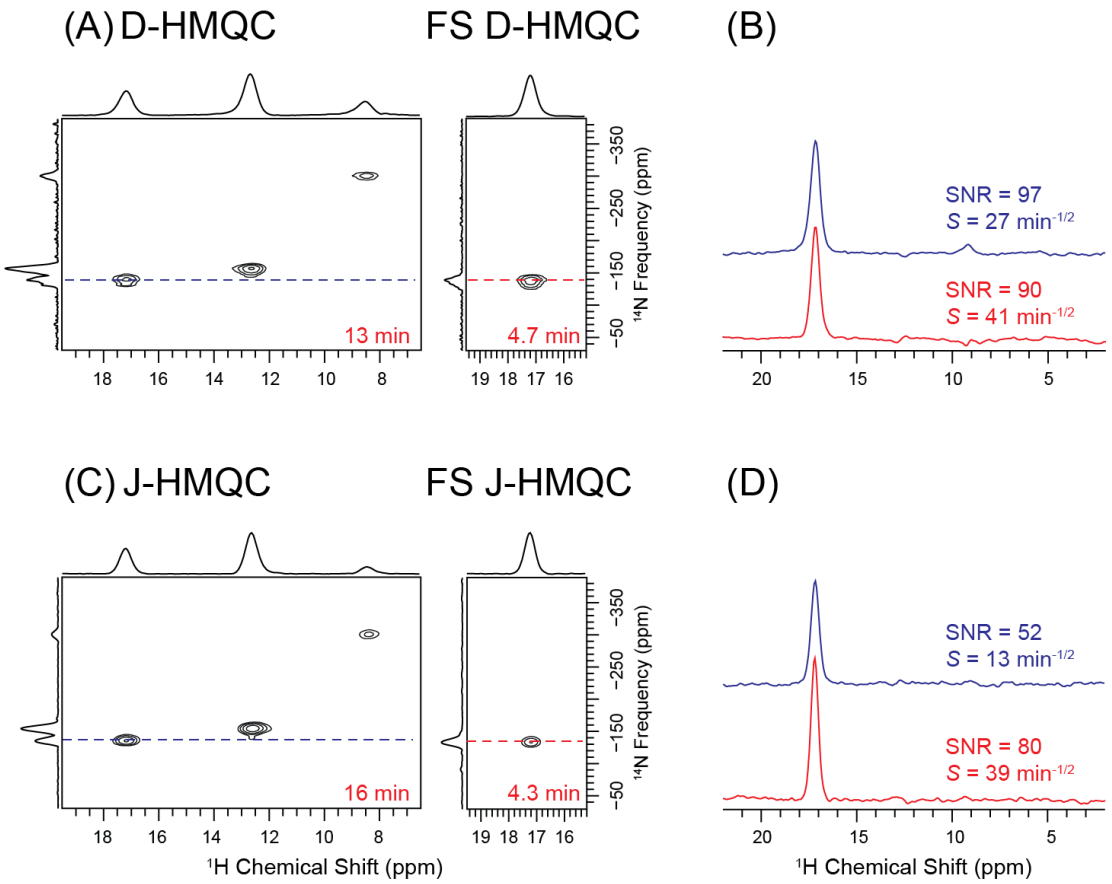

Figure S6. Comparison of conventional and FS 2D $^{1}H\{^{14}N\}$ (A) D-HMQC or (C) J-HMQC spectra of hist. The FS HMQC spectra were obtained with the DANTE pulses on resonance with the acid ^{1}H NMR signal at 17.2 ppm. (B) and (D) show the rows extracted from the conventional D or J-HMQC (blue dash lines) and the FS HMQC (red dash lines) and the corresponding SNR and sensitivities. Total experiment times are indicated. All experiments were performed with ν_{rot} = 95 kHz and B_0 = 18.8 T.

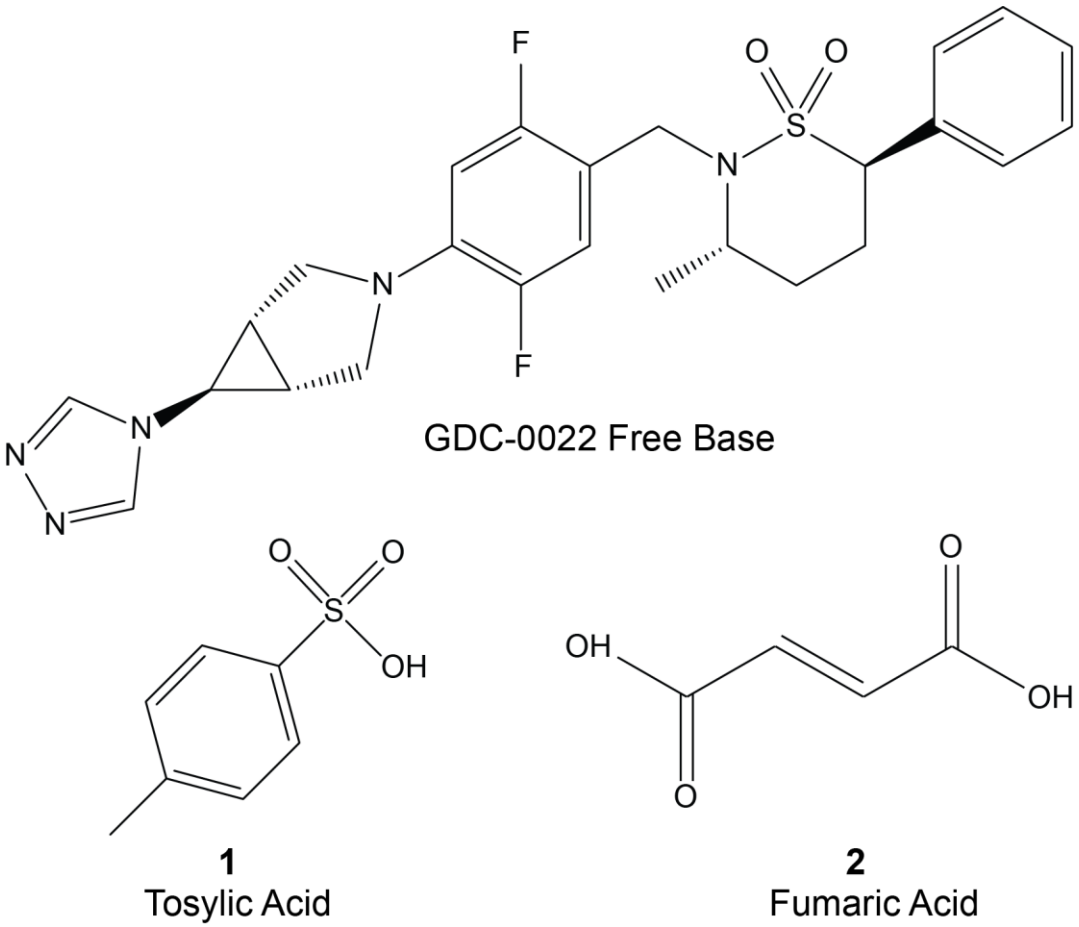

Scheme 1. Molecular structures of GDC-0022 free base and the coformers tosylic acid and fumaric acid.

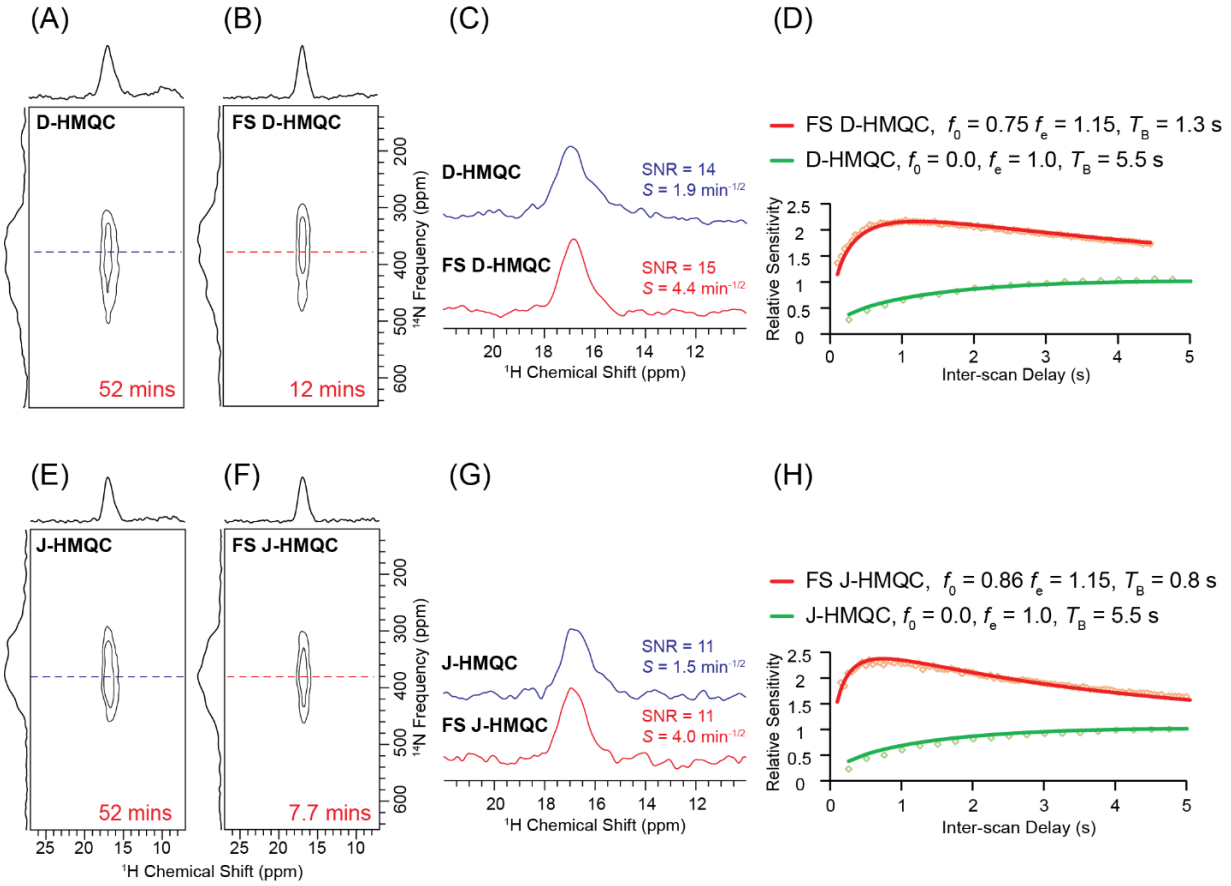

Figure S7. Comparison of conventional and FS ^{1}H{^{14}N} HMQC experiments on compound 1. (A) Conventional D-HMQC, (B) FS D-HMQC, and (C) SNR and the sensitivity comparison for the row indicated by the dashed line. (D) Measurement of the relative sensitivity of D-HMQC and FS D-HMQC for the high-frequency ammonium peak. (E) Conventional J-HMQC, (F) FS J-HMQC, and (G) SNR and the sensitivity comparison of the row indicated by the dashed lines. (H) Measurement of the relative sensitivity of the conventional and FS J-HMQC for the high-frequency ammonium peak. The total experimental times are noted on the 2D spectra. The values of f_o, f_e and T_B used for the curve fitting are indicated on each plot. D-HMQC experiments were performed with ν_{rot} = 50 kHz and J-HMQC with ν_{rot} = 60 kHz. All experiments were performed with B_0 = 9.4 T.

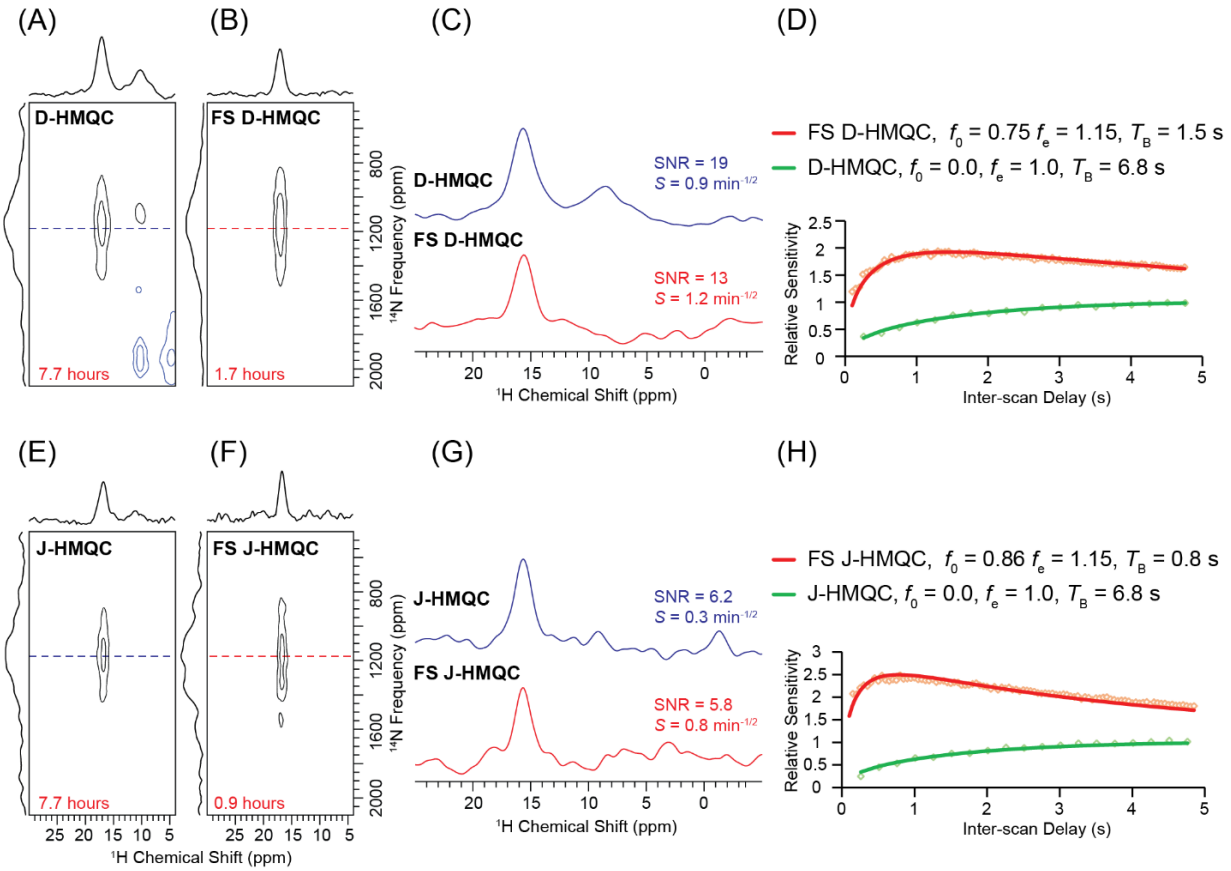

Figure S8. Comparison of conventional and FS ^{1}H{^{14}N} HMQC experiments on compound 2. (A) Conventional D-HMQC, (B) FS D-HMQC, and (C) SNR and the sensitivity comparison for the row indicated by the dashed line. (D) Measurement of the relative sensitivity of D-HMQC and FS D-HMQC for the high-frequency ammonium. (E) Conventional J-HMQC, (F) FS J-HMQC, and (G) SNR and the sensitivity comparison of the row indicated by the dashed lines. (H) Measurement of the relative sensitivity of the conventional and FS J-HMQC for the high-frequency ammonium peak. The total experimental times are noted on the 2D spectra. The values of f_o, f_e and T_B used for the curve fitting are indicated on each plot. D-HMQC experiments were performed with ν_{rot} = 50 kHz and J-HMQC with ν_{rot} = 60 kHz. All experiments were performed with B_0 = 9.4 T.

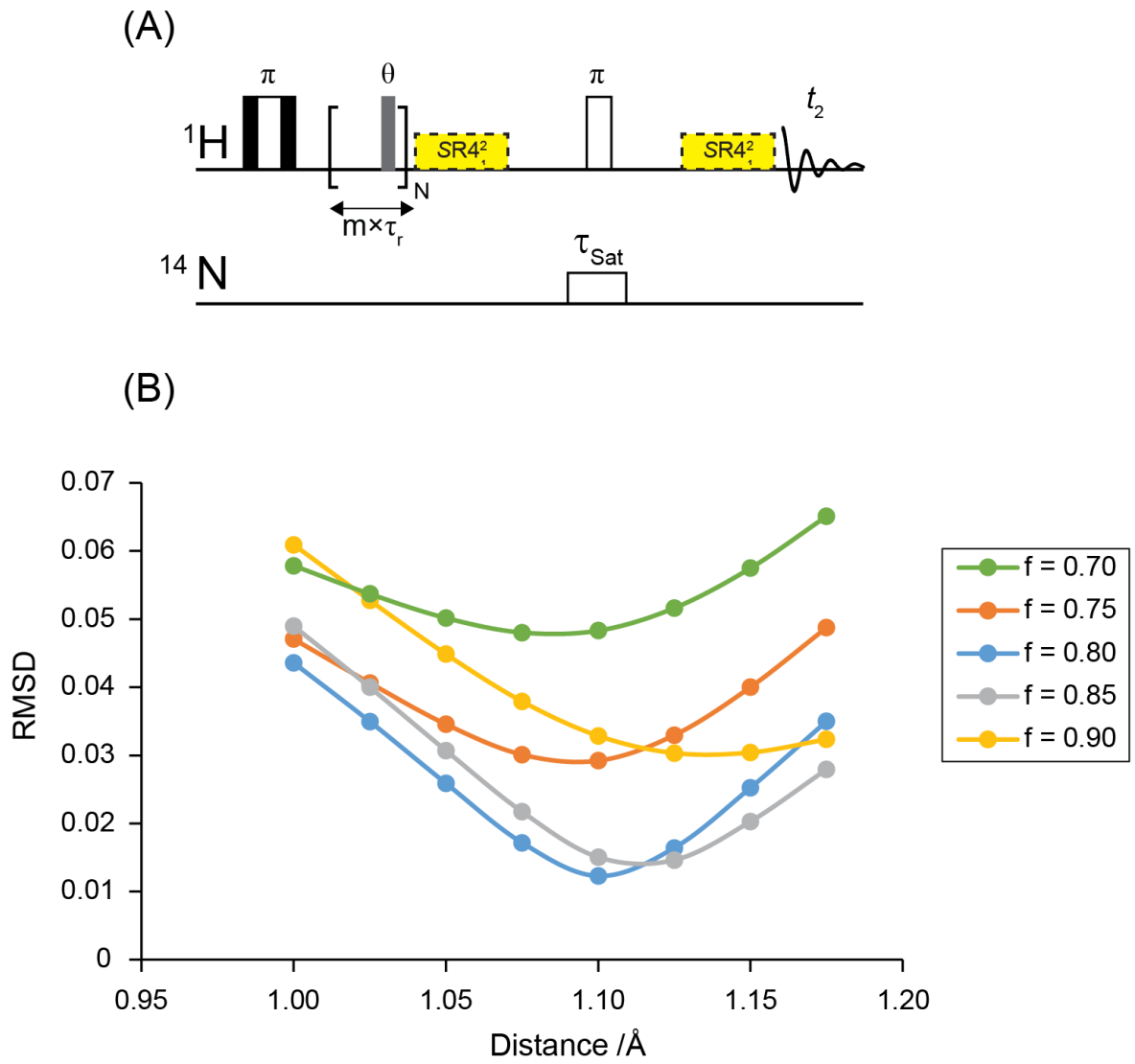

Figure S9. (A) FS RESPDOR pulse sequence used for measurements of NH dipolar couplings and inter-atomic distances. (B) The RMSD of calculated RESPDOR curves compared to the experimental RESPDOR curves for different N-H dipolar couplings (distances) for compound 1. The saturation factor (*f*) was also varied for each distance. A scaling factor of 0.80 gives the minimum RMSD. Calculated curves for different distances are compared to the experimental curve in Figure 4D of the main text. Only the initial part of the experimental curve was used to determine the RMSD values.

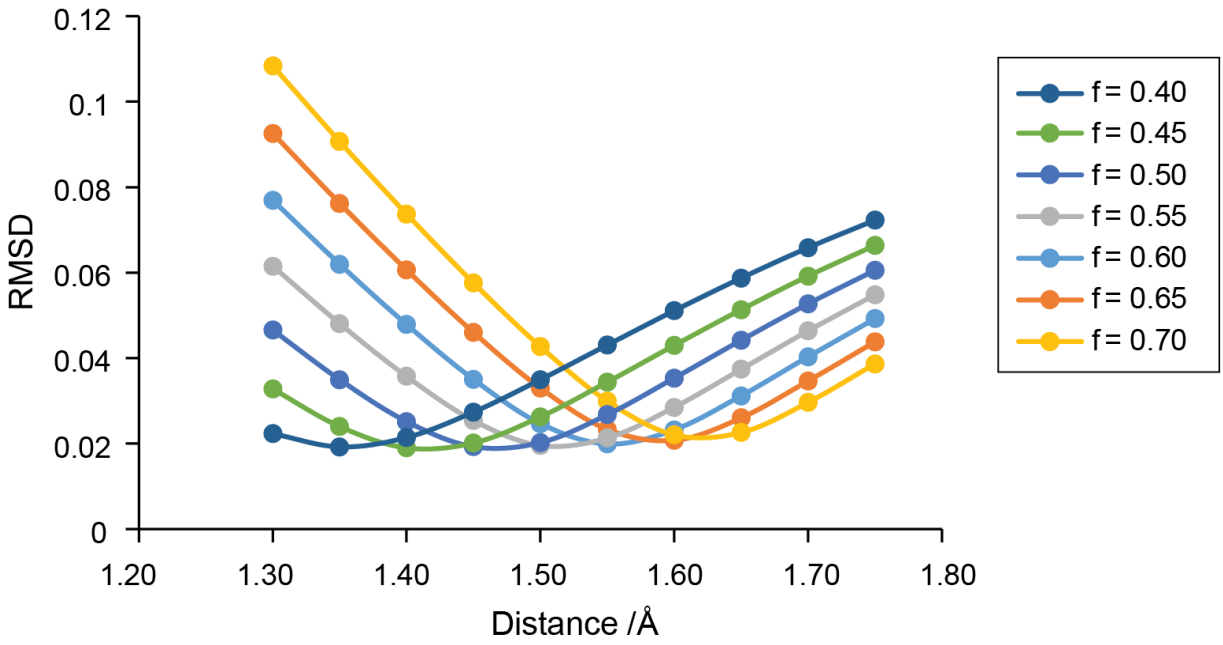

Figure S10. The RMSD of calculated RESPDOR curves compared to the experimental RESPDOR curves for different N-H dipolar couplings (distances) for compound 2. The saturation factor (*f*) was also varied for each distance. A scaling factor of 0.45 gives the minimum RMSD. Calculated curves for different distances are compared to the experimental curve in Figure 4D of the main text.

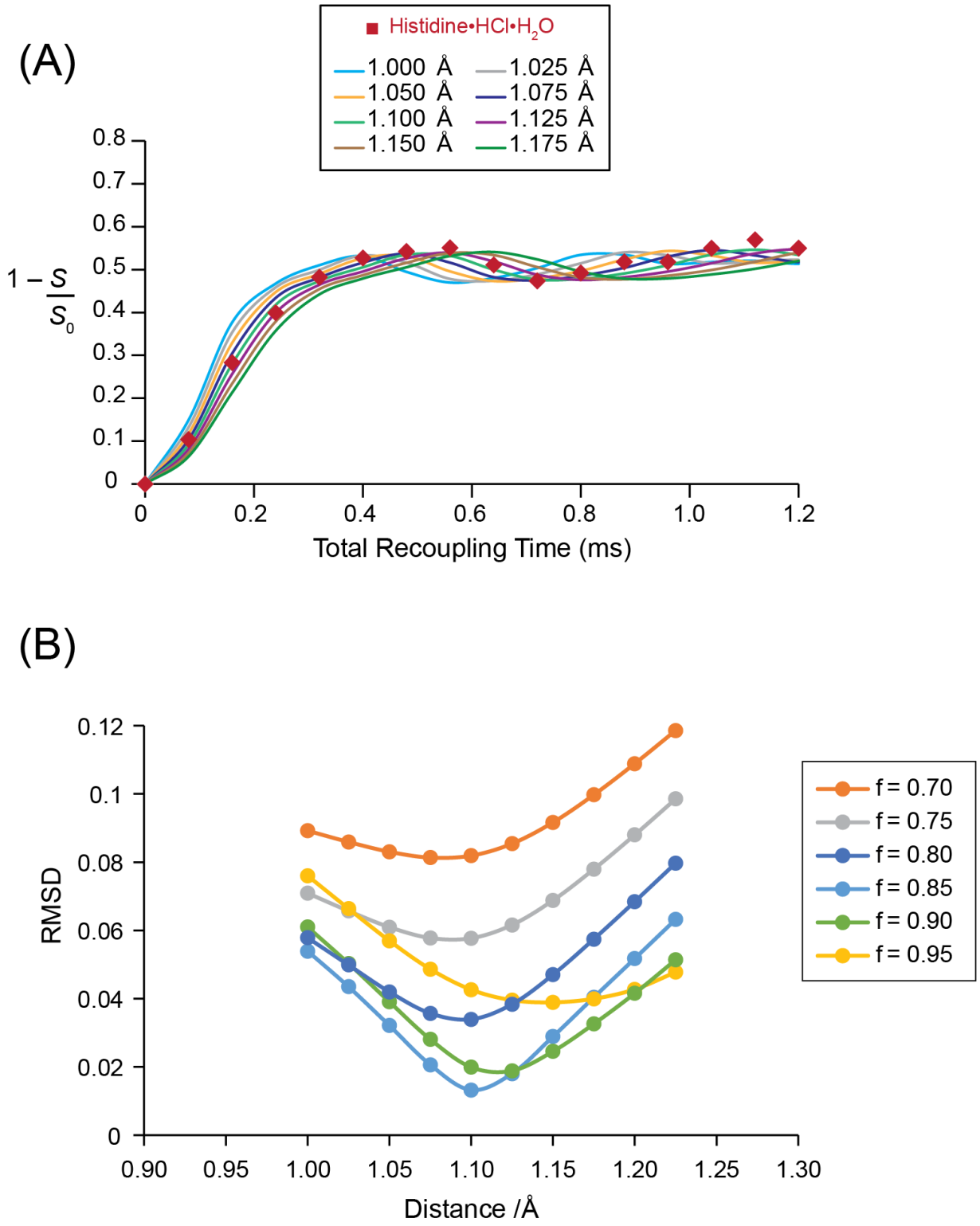

Figure S11. (A) FS-RESPDOR curves for the high frequency ^{1}H signal at 17.2 ppm of hist. The plot shows the experimental curve (red squares) and numerical simulations for different distances. The saturation factor (*f*) was set to 0.85. (B) The RMSD plots for hist with varying the scaling factor used for the distance estimation in (A). A scaling factor of 0.85 gives the minimum standard deviation for hist.

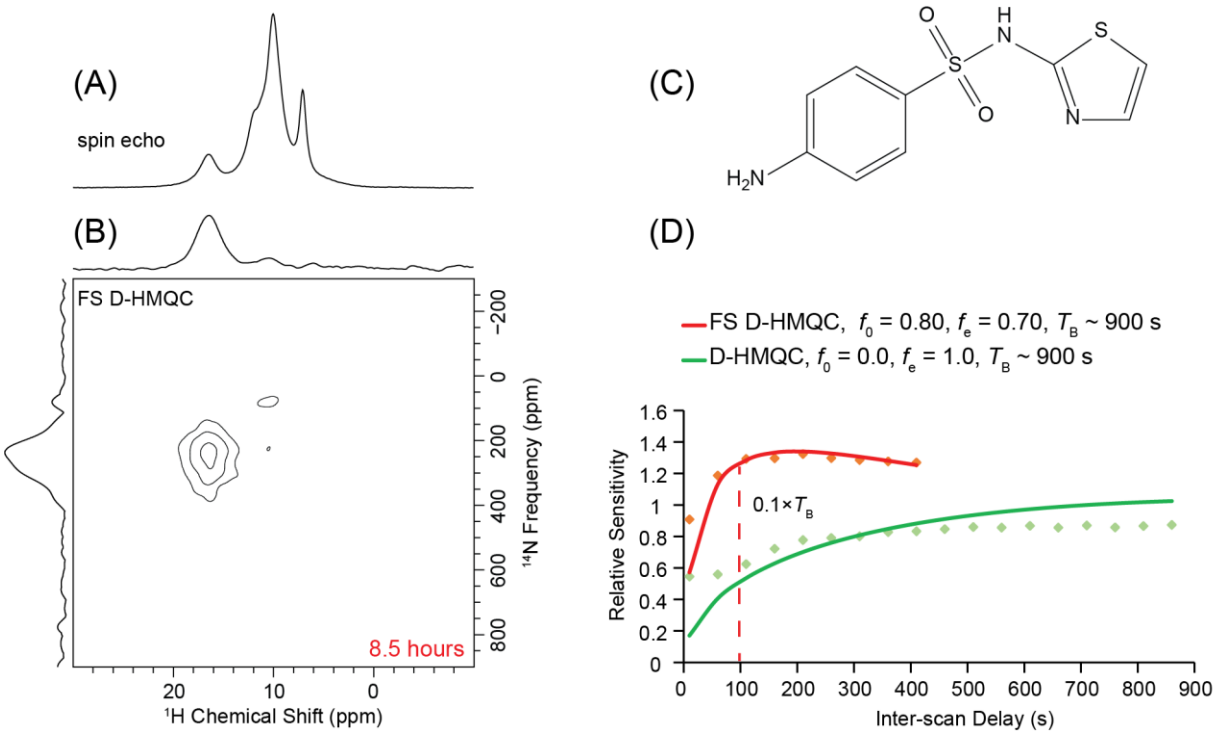

Figure S12. (A) 1D ^{1}H spin echo and (B) 2D ^{1}H{^{14}N} FS D-HMQC spectrum of sulfathiazole. A recycle delay of 60 s was used. The experiment time is indicated. (C) The molecular structure of sulfathiazole. (D) Comparison of the relative sensitivity of conventional and FS D-HMQC as a function of inter-scan delay. The fitting parameters are indicated on the plots.

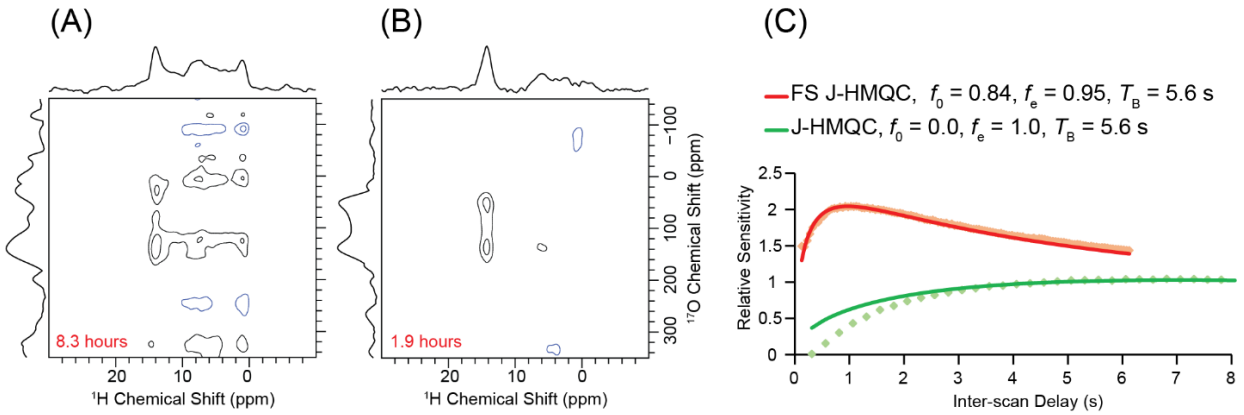

Figure S13. Comparison of (A) $^{1}H\{^{17}O\}$ J-HMQC and (B) $^{1}H\{^{17}O\}$ FS J-HMQC spectra of ^{17}O-labelled Fmoc-alanine. The experiment times for the 2D spectra are indicated. (C) Comparison of relative sensitivities for conventional and FS J-HMQC for different inter-scan delays. The fit parameters are indicated along with the curves. The experiments were performed with B_0 = 9.4 T and ν_{rot} = 60 kHz.

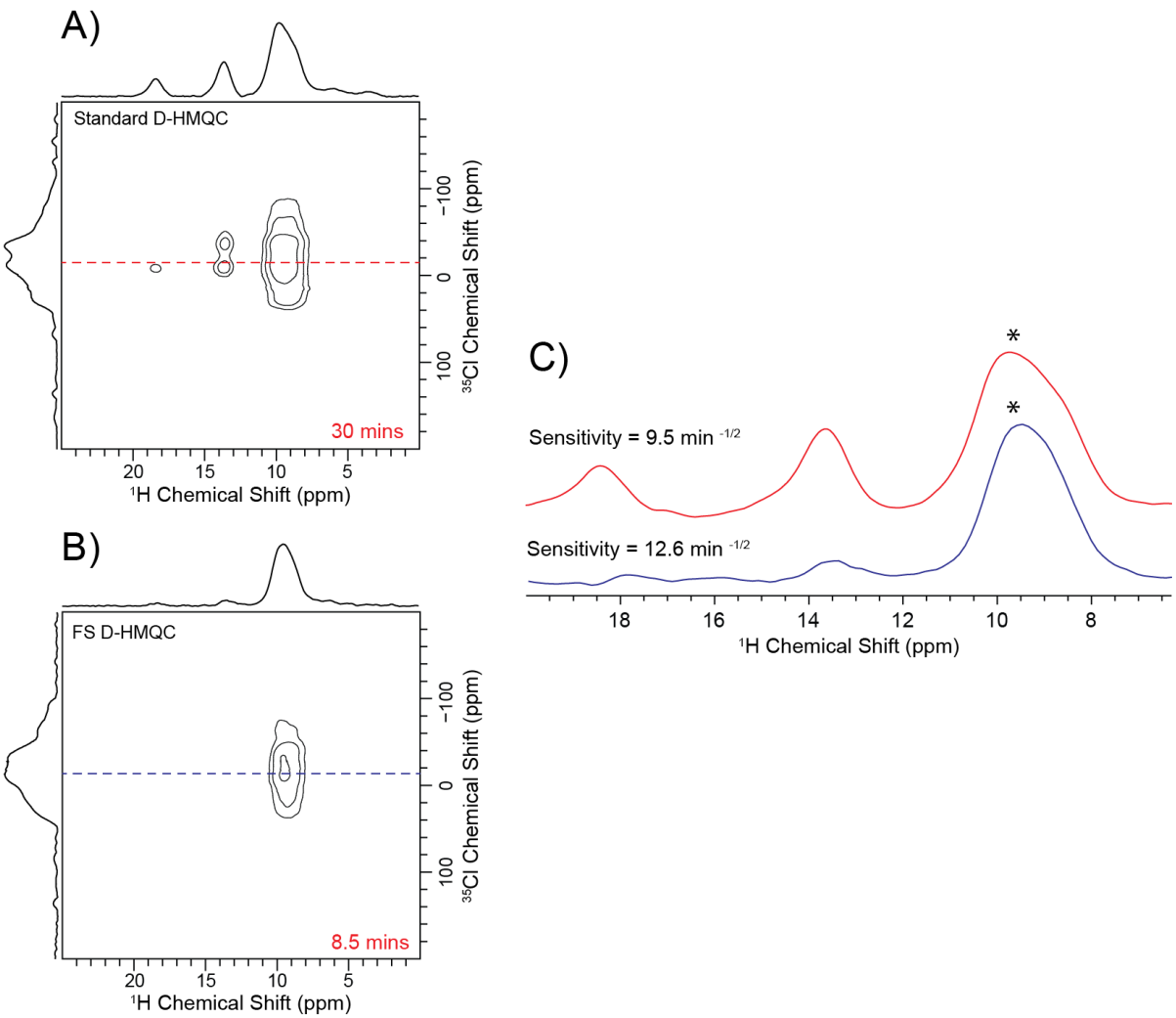

Figure S14. Comparison of (A) $^{1}H\{^{35}Cl\}$ D-HMQC and (B) $^{1}H\{^{35}Cl\}$ FS D-HMQC spectra of hist. The experiment times for the 2D spectra are indicated. (C) SNR and the sensitivity comparison for the row indicated by the dashed line. The experiments were performed with B_0 = 9.4 T at ν_{rot} = 50 kHz.

Table S1. Simulated and calculated ^{14}N NMR parameters for 1 and 2.

Compound	δ_{iso} (ppm)[a]	C_Q (MHz)	η_Q
(1) – Simulated[a]	–160	2.5	0.10
(1) – Calculated[b]	–159.7	2.7	0.10
(2) – Simulated[a]	–90	3.4	0.90
(2) – Calculated[b]	–88.2/89.3[c]	3.6/3.5	0.90/0.70

[a] Simulated parameters were determined from the analytical simulations of the ^{14}N solid-state NMR spectra extracted from the 2D ^{1}H{^{14}N} D-HMQC spectra. The ^{14}N isotropic shift was fixed to the value previously measured with DNP-enhanced ^{15}N solid-state NMR spectroscopy for the analytical simulations. The C_Q and η_Q were then varied to give the best agreement between the simulated and experimental spectrum. There is large uncertainty associated with the experimental values of η_Q. [b] Calculated parameters were obtained from plane-wave DFT calculations. [c] Compound 2 is a hemi-fumaric acid compound where two inequivalent molecules of GDC-0022 form hydrogen bonds to a single fumaric acid molecule. The calculated ^{14}N parameters are given for the two distinct GDC-0022 molecules in the unit cell.

Table S2. Input parameters for SIMPSON simulations of ^{1}H{^{14}N} RESPDOR dephasing curves. (Figures 4D and S11A)

Compound	Dipole-Quadrupole Euler Angles (deg)		^{14}N Frequency Offset[a] (ppm)	δ_{iso} (ppm)	δ_{aniso} (ppm)	η_{CS}	C_Q (MHz)	η_Q
	α	β						
Hist	108	131	+208	-190.7	204	0.4	1.55	0.13
(1) ^{1}H-^{14}N$_A$ [b]	117	135	+661	–159.7	200	0.5	2.7	0.10
(1) ^{1}H-^{14}N$_B$ [b]	28	20		-95.5	342	0.9	4.6	0.60
(2) ^{1}H-^{14}N$_A$ [b]	7	81	+1160	–88.2	320	0.5	3.6	0.70
(2) ^{1}H-^{14}N$_B$ [b]	170	133		-66.3	360	0.7	4.5	0.50

[a] The ^{14}N transmitter frequency was increased by this amount so that the ^{14}N RESPDOR saturation pulse was applied at the approximate center of gravity of the site A MAS powder pattern. This mimics the experimental optimization of the ^{14}N transmitter offset to maximize dephasing. [b] ^{14}N$_A$ corresponds to the protonated nitrogen/nitrogen with shorter ^{1}H-^{14}N distance and ^{14}N$_B$ corresponds to the non-protonated nitrogen atom.

References

1. Carnahan, S.L., et al., *Probing O-H Bonding through Proton Detected ^{1}H-^{17}O Double Resonance Solid-State NMR Spectroscopy.* Journal of the American Chemical Society, **2019**. 141(1): p. 441-450.

2. Antonijevic, S. and G. Bodenhausen, *High-resolution NMR spectroscopy in solids by truly magic-angle spinning.* Angewandte Chemie-International Edition, **2005**. 44(19): p. 2935-2938.

3. Harris, R.K., et al., *NMR Nomenclature. Nuclear Spin Properties and Conventions for Chemical Shifts - (IUPAC Recommendations 2001).* Pure and Applied Chemistry, **2001**. 73(11): p. 1795-1818.

4. Brinkmann, A. and A.P.M. Kentgens, *Proton-selective ^{17}O-^{1}H distance measurements in fast magic-angle-spinning solid-state NMR spectroscopy for the determination of hydrogen bond lengths.* Journal of the American Chemical Society, **2006**. **128**(46): p. 14758-14759.

5. Oas, T.G., R.G. Griffin, and M.H. Levitt, *Rotary Resonance Recoupling of Dipolar Interactions in Solid-State Nuclear Magnetic-Resonance Spectroscopy.* Journal of Chemical Physics, **1988**. **89**(2): p. 692-695.

6. Hu, B., J. Trebosc, and J.P. Amoureux, *Comparison of several hetero-nuclear dipolar recoupling NMR methods to be used in MAS HMQC/HSQC.* J. Magn. Reson., **2008**. 192(1): p. 112-122.

7. Cavadini, S., A. Abraham, and G. Bodenhausen, *Proton-detected nitrogen-14 NMR by recoupling of heteronuclear dipolar interactions using symmetry-based sequences.* Chemical Physics Letters, **2007**. 445(1-3): p. 1-5.

8. Bak, M., J.T. Rasmussen, and N.C. Nielsen, *SIMPSON: A general simulation program for solid-state NMR spectroscopy.* Journal of Magnetic Resonance, **2000**. 147(2): p. 296-330.

9. Tosner, Z., et al., *Computer-intensive simulation of solid-state NMR experiments using SIMPSON.* Journal of Magnetic Resonance, 2014. 246: p. 79-93.

10. Tosner, Z., et al., *Optimal control in NMR spectroscopy: Numerical implementation in SIMPSON.* Journal of Magnetic Resonance, **2009**. 197(2): p. 120-134.

11. van Meerten, S.G.J., W.M.J. Franssen, and A.P.M. Kentgens, *ssNake: A cross-platform open-source NMR data processing and fitting application.* Journal of Magnetic Resonance, **2019**. 301: p. 56-66.

CHAPTER 4. GENERAL CONCLUSION

This thesis demonstrates the use of fast magic angle spinning solid-state NMR spectroscopy to characterize pure and formulated pharmaceuticals. In chapter 2, fast MAS ^{1}H SSNMR is used to look at pure and commercial drug products. Here, 1D and 2D NMR experiments are used to identify the solid forms of dilute API within formulations. The ^{1}H SSNMR experiments are compared with ^{13}C SSNMR, which is the workhorse method to characterize pharmaceuticals. The sensitivity of the ^{1}H NMR greatly exceeds that of ^{13}C and enables a 1-3 order reduction in the experiment time. Diagnostic ^{1}H SSNMR spectra of dilute APIs within formulations and commercial drug products can typically be obtained in minutes, even when the API has unfavorable T_1 relaxation times and low API loading, whereas ^{13}C SSNMR spectra would require hours or days of signal averaging to obtain NMR spectra of similar SNR. Also, the use of fast MAS ^{1}H SSNMR to distinguish different polymorphs of APIs within mixtures of APIs and excipients is presented. For the polymorphic forms of APIs, theophylline and mexiletine the ^{1}H SSNMR spectra of different crystalline forms are distinct, allowing polymorphic forms to be identified and detected based on ^{1}H chemical shifts or based on different responses to saturation and excitation pulses. Experiments on theophylline mixtures demonstrate that ^{1}H SSNMR spectra are quantitative after calibration on the individual components of the formulation.

Chapter 3 discusses the use of fast MAS FS HMQC experiments which function analogously to solution SOFAST HMQC NMR experiments. Dipolar and scalar ^{1}H{^{14}N} FS HMQC SSNMR experiments routinely provide 4- to 9-fold reductions in experiment times as compared to conventional HMQC SSNMR experiments. ^{1}H{^{14}N} FS RESPDOR allowed dipolar dephasing curves to be obtained in minutes, enabling the rapid determination of NH dipolar

coupling constants and inter-nuclear distances. $^{1}H\{^{14}N\}$ FS RESPDOR was used to assign multicomponent active pharmaceutical ingredients (APIs) as salts or cocrystals. FS HMQC also provided enhanced sensitivity for $^{1}H\{^{17}O\}$ and $^{1}H\{^{35}Cl\}$ HMQC experiments on ^{17}O labeled Fmoc-alanine and histidine hydrochloride monohydrate, respectively. While the focus of the current work has been on pharmaceuticals, the methods described here should also be applicable to study other complex mixtures of organic solids and the FS HMQC and FS RESPDOR experiments will provide access to valuable structural constraints from materials that are challenging to study due to unfavorable relaxation times or dilution of the nuclei of interest.